CHARACTERIZATION AND MITIGATION OF TRANSCEIVER PHASE NOISE FOR JOINT MAP CHANNEL ESTIMATION / DATA DETECTION IN OFDM / OFDMA

Ph.D. Thesis

KAMAYANI SHRIVASTAV

ID No. 2014REC9012

DEPARTMENT OF ELECTRONICS AND COMMUNICATION ENGINEERING

MALAVIYA NATIONAL INSTITUTE OF TECHNOLOGY JAIPUR

July 2019

Characterization and Mitigation of Transceiver Phase Noise for Joint MAP Channel Estimation / Data Detection in OFDM / OFDMA

Submitted in

fulfillment of the requirements for the degree of

Doctor of Philosophy

by

Kamayani Shrivastav

ID: 2014REC9012

Under Supervision of

Prof. R. P. Yadav

Professor - HAG, Dept. of ECE, MNIT, Jaipur

Prof. K. C. Jain

Retd. Professor, Dept. of Mathematics, MNIT, Jaipur

DEPARTMENT OF ELECTRONICS AND COMMUNICATION ENGINEERING

MALAVIYA NATIONAL INSTITUTE OF TECHNOLOGY JAIPUR

July 2019

Certificate

This is to certify that the thesis entitled "**Characterization and Mitigation of Transceiver Phase Noise for Joint MAP Channel Estimation / Data Detection in OFDM / OFDMA**" being submitted by **Kamayani Shrivastav (2014REC9012)** is a bona fide research work carried out under my supervision and guidance in fulfillment of the requirement for the award of the degree of **Doctor of Philosophy** in the Department of Electronics and Communication Engineering, Malaviya National Institute of Technology, Jaipur, India. The matter embodied in this thesis is original and has not been submitted to any other University or Institute for the award of any other degree.

Place: Jaipur

Date:

Prof. R. P. Yadav

Professor-HAG, Dept. of Electronics and Communication Engineering

MNIT Jaipur

Prof. K. C. Jain

Retd. Professor, Dept. of Mathematics

MNIT, Jaipur

Declaration

I, **Kamayani Shrivastav**, declare that this thesis titled, "**Characterization and Mitigation of Transceiver Phase Noise for Joint MAP Channel Estimation / Data Detection in OFDM / OFDMA**" and the work presented in it are my own. I confirm that:

- This work was done wholly or mainly while in candidature for a research degree at this university.

- Where any part of this thesis has previously been submitted for a degree or any other qualification at this university or any other institution, this has been clearly stated.

- Where I have consulted the published work of others, this is always clearly attributed.

- Where I have quoted from the work of others, the source is always given. With the exception of such quotations, this thesis is entirely my own work.

- I have acknowledged all main sources of help.

- Where the thesis is based on work done by myself, jointly with others, I have made clear exactly what was done by others and what I have contributed myself.

Date: Kamayani Shrivastav

(2014REC9012)

ब्रह्माण्ड की सारी शक्तियां हमारे भीतर ही हैं | मस्तिष्क की शक्तियां सूर्य की किरणों के समान हैं, जब वो केन्द्रित होती हैं चमक उठती हैं | उसी प्रकार हमारी नैतिक प्रकृति जितनी उन्नत होती है उतना ही उच्च हमारा प्रत्यक्ष अनुभव होता है और उतनी ही हमारी इच्छा शक्ति अधिक बलवती होती है | स्वतंत्र होने का साहस करो, जहाँ तक तुम्हारे विचार जाते हैं वहां तक जाने का साहस करो क्योंकि संभव की सीमा जानने का केवल एक ही तरीका है, असंभव से भी आगे निकल जाना | अत: उठो जागो और तब तक नहीं रूको जब तक लक्ष्य ना प्राप्त हो जाये |

स्वामी विवेकानंद

मेरे पिता जी ***"स्व. श्री शंकर लाल श्रीवास्तव"*** *को समर्पित |*

धुम्मा

Acknowledgement

"All of our technology is completely unnecessary to a happy life"

Tom Hodagkinson

As the journey of research continues for the life span, I pause and pay my gracious thank to all of those who made my research work possible, concerning to this doctoral thesis. The research work was conducted at the **Department of Electronics and Communication, Malaviya National Institute of Technology, Jaipur, India** and was supervised and guided by **Prof. R. P. Yadav**, who always steps towards destination of continuous research in the area of wireless communications. Sir, thanks for encouraging and accepting me as a PhD student and then heading me towards my ambitious dreams by filtering out all of my stupid mistakes at each of my frivolous turn without being judgmental. Special thanks to **Prof. K. C. Jain**, the co-supervisor, for his all offered guidance to hone my mathematical skills. I have been benefitted a lot by the advices given by these two during our brainstorming sessions not only on the technology and research but also on the life and living.

I would like to thank, **Prof. Vijay Janyani**, **Prof. Mohammad Salim**, **Prof. Ghanshyam Singh** and **Dr. S.J. Nanda**, DREC members, for their rich and vivid discussions, which we have had on the captivatating ideas at the time of reserch presentations. My gratitude to **Prof. Love Bhargava**, **Prof. D. Boolchandani**, and **Prof. Ghanshyam Singh**, DPGC Convener, for their continuos support to travel along the rules and regulations of the PhD programme. Special thanks to **Prof. K. K. Sharma**, heading the department and **Prof. K. R. Niyazi**, Dean Academics, to offer us immense work enviornment to produce effectively and creatively. I thank all my valued collegues and seniars, at the department and institute for having good times together at the workplace everyday, specially **Dr. S. A. Siddiqui**, for his valuable time which he spent in reading my research papers to guide me towards perfection in writing.

The most precious person to me, my soulmate-**Atul**, I love you for all your love and support through all my thick and thin in this journey. I always admire you for your diverse skill set for solving mathematical problems and handling my downs as well.

No amount of apology and appriciation can equalize the desolation of a child hood. My honey-**Chikoo**, I can see how tears have left so many stains and I promise to never hurt you again. From my deep heart I love you and wish for success to be there with you in every walk of your life. Special gratitude to **Mummy** and **Papa** for the values driving me here and toast to all those delight and hard times which I have in my heart with **Jiji** and **Chhunnu**, my siblings.

End? No, the journey doesn't end here. As success is a journey not the destintaion, I keep all the inspiring people in my heart who share the journey with me.....

Kamayani Shrivastav

India, 2018

Abstract

Orthogonal frequency division multiplexing/multiple access technique provides high data rate with high spectral efficiency for operating close to the Shannon capacity bounds. With the advantages of simple channel equalization, robustness against frequency selectivity of the channel and efficient implementation, this is a widely deployed technique for information presentation at the back-end of digital wireless communication systems. The efficient information processing at the digital back-end stands on the linear and noiseless information transmission and reception at the analogue front-end. In the real scenario, the imperfection of devices, those contribute to the analogue front-end, turns in the inaccuracy of the digital processing algorithms, involved in information processing. The inaccurate working of front-end devices, results in transceiver's impairments, such as phase noise, carrier frequency offset and in-quadrature phase imbalance effect. Besides all the advantages, orthogonal frequency division multiplexing/multiple access is very susceptible to transceiver's impairments.

This thesis addresses the orthogonal frequency division multiplexing/multiple access system performance under the impact of transceiver oscillator phase noise, which arises because of imperfect frequency up/down conversion of baseband signal to/from radio frequency at the analogue front-end. The random perturbation of the phase noise is characterized and analyzed quantitatively in terms of signal-to-interference+noise ratio for both of the systems. A closed form expression for the signal-to-interference+noise ratio is derived without the assumptions of complex Gaussian distribution of inter carrier interference and multi user interference.

With regards to the mathematical modeling of phase noise, both Wiener phase noise model for free running oscillator and Ornstein-Uhlenbeck phase noise model for phase locked loop oscillator are presented. A new joint maximum a posteriori algorithm in frequency domain is proposed for channel transfer function estimation in presence of phase noise in orthogonal frequency division multiplexing system. Further a cyclic gradient descent algorithm is proposed for optimization of the joint estimation.

A new alternative of iterative receiver design, for statistically optimal data detection in presence of phase noise is proposed. The maximum a posteriori cost function for the joint data detection and phase noise estimation in orthogonal frequency division multiplexing system is derived and optimized with proposed cyclic gradient descent optimization.

Simulation results demonstrate that the proposed algorithm shows significant improvement over the conventional methods of channel estimation and data detection. Simulation results are also showing that the proposed algorithm approaches the optimum mean square error in channel estimation and optimum symbol error rate in data detection. The performance of proposed algorithm maintains its significance even in multipath channel fading, precisely when phase noise is very high.

List of Publications

International Journals

P1 Kamayani Shrivastav, R. P. Yadav and K. C. Jain, "Joint MAP Detection for OFDM in presence of Phase Noise from Free Running and Phase Locked Loop Oscillator", *Wireless Personal Communications*, DOI 10.1007/s11277-019-06579-5.

P2 Kamayani Shrivastav, R. P. Yadav and K. C. Jain, "Cyclic Gradient Descent Optimization for Joint MAP Estimation of Channel and Phase Noise in OFDM", *IET Communications*, DOI: 10.1049/iet-com.2017.0732.

P3 Kamayani Shrivastav and R. P. Yadav, "Characterization of MUI for OFDMA Uplink in presence of Transceiver Phase Noise", *International Journal of Future Generation Communication and Networking*, vol. 10, no. 6, pp. 23-32, 2017.

International Conferences

P4 Kamayani Shrivastav and R. P. Yadav, "Analytical study of SINR for OFDMA Uplink in presence of Transceiver Phase Noise", in *Proc. International Conference on. Computer, Communications and Electronics*, Jaipur, 2017.

P5 Kamayani Shrivastav, Bhukya Chanti and R. P. Yadav, "Characterization of Phase Noise in Multicarrier Transmission: A Review", in *Proc. International Conference on Innovations in Electronics and Communication Engineering*, Hyderabad, 2015.

Contents

List of Figures

List of Tables

List of Abbreviations

1D	One dimensional
2D	Two dimensional
A/D	Analogue to digital
ADC	Analogue to digital conversion
AFE	Analogue front-end
AGC	Automatic gain controller
AR (1)	Autoregressive process of order one
AWGN	Additive white Gaussian Noise
BEM	Basis expansion model
BER	Bit error rate
BPF	Band pass filter
CFO	Carrier frequency offset
CFR	Channel frequency response
CIR	Channel impulse response
CP	Cyclic prefix
CPE	Common phase error
CRLB	Cramer-Rao lower bound
CTF	Channel transfer function
D/A	Digital to analogue

DAC	Digital to analogue conversion
DC	Direct current
DCR	Direct conversion receiver
DFT	Discrete Fourier transform
DPSK	Differential phase shift keying
DSP	Digital signal processing
DVB-T	Digital video broadcasting-terrestrial
EM	Expectation minimization
FDE	Frequency domain equalization
FDMA	Frequency division multiple access
FFT	Fast Fourier transform
FM	Frequency modulated
FRO	Free running oscillator
HPA	High power amplifier
ICI	Inter carrier interference
IDFT	Inverse DFT
IF	Intermediate frequency
IFFT	Inverse FFT
IQ	In-quadrature phase
ISI	Inter symbol interference
LMMSE	Linear MMSE

LNA	Low noise amplifier
LO	Local oscillator
LS	Least square
LTE	Long term evolution
MAP	Maximum a posteriori
MC	Multi carrier
MC-CDMA	Multi carrier-code division multiple access
MIMO	Multiple input-multiple output
ML	Maximum likelihood
MMSE	Minimum mean square error
MSE	Mean square error
MUI	Multi user interference
O-U	Ornstein-Uhlenbeck
OFDM	Orthogonal frequency division multiplexing
OFDMA	Orthogonal frequency division multiple access
OLR-MMSE	Optimal low rank-MMSE
PAPR	Peak-to-average power ratio
PCMB	Parametric channel modelling based
PDF	Probability density function
PHN	Phase noise
PLL	Phase locked loop

PSD	Power spectral density
PSK	Phase shift keying
QAM	Quadrature amplitude modulation
RF	Radio frequency
SC	Single carrier
SC-FDMA	Single carrier-frequency division multiple access
SER	Symbol error rate
SHR	Super heterodyne receiver
SINR	Signal-to-interference+noise ratio
SI	Self interference
SNR	Signal-to-noise ratio
SSB	Single side band
SVD MMSE	Singular value decomposition MMSE
TDMA	Time division multiple access
VCO	Voltage controlled oscillator
WLAN	Wireless local area network

1. Introduction

The requirement of high data rate and high spectral efficiency in wireless communication has led to a significant interest worldwide in the development of multi carrier transmission systems. Orthogonal frequency division multiplexing/multiple access (OFDM/A) has been widely accepted as the key technique for multi carrier transmission and rolled out in different flavours of communications standards like Wireless MAN-Advanced, 3GPP2 long term evolution (LTE) Advanced, wireless local area network (WLAN) and digital video broadcasting-terrestrial (DVB-T).

OFDM is a multi carrier modulation technique to represent the information, which reduces the complexity of receiver digital processing unit while combating the deleterious effects of the channel with simple correction algorithms. It enables one-tap equalization by cyclic prefix (CP) insertion even in frequency selective channel and the use of discrete Fourier transform (DFT) and its extremely efficient and well established fast Fourier transform (FFT) algorithm for implementation has made it amenable in terms of cost also [1-11]. OFDMA has the great potential for providing high spectral efficiency due to its integrated space-frequency and multi-user diversity [12-17]. However some of the immediate consequences of these compelling benefits in OFDM/A are: limiting the spectral efficiency because of CP insertion, deleterious impact of high peak-to-average power ratio (PAPR) and serious sensitivity towards transceivers' impairments [18]. The transceivers' impairments, such as phase noise (PHN), carrier frequency offset (CFO) and in-quadrature phase (IQ) imbalance effect, need to be addressed significantly to make the best possible use of limited radio spectrum to further increase throughput as well as user capacity.

The frequency difference between the receiver and transmitter local oscillators produces the CFO. The OFDM standards, such as IEEE 802.11a/g or DVB-T, use preambles to estimate and compensate the CFO [19-20]. Even after CFO estimation and compensation, the residual CFO impairs the orthogonality of the received OFDM signal and corrupts the channel estimate which further worsens the performance of OFDM system during equalization process. The solution for this is provided in [21-22] with adaptive algorithm design. IQ imbalance arises when a front end component does not respect the power balance or orthogonality between I and Q branch of the receiver and so the amplitude imbalance and phase orthogonality mismatch arises.

Whereas some previous IQ imbalance solutions were based either on offline calibration or online estimation [23], the current estimation schemes exhibit fast convergence and consider PHN [24-25].

While there are many transceivers' impairments that are to be taken in to consideration in designing a digital communication system, there is a convincing reason to focus on the PHN precisely. While CFO and IQ imbalance are deterministic, PHN on the other hand is random perturbations in the phase of the carrier signal generated by the transceiver oscillators [26-36]. Moreover the multi carrier systems, such as OFDM, suffer a much loss in signal-to-noise ratio (SNR) due to PHN than single carrier systems. This is the result of longer duration of multi carrier symbol and the loss of orthogonality between the subcarriers. Further, PHN severely limits the performance of systems that employ dense constellations and degradation gets more pronounced in high carrier frequency systems.

Thus being especially sensitive to transceivers' impairments, OFDM imposes high demands for the quality of used devices for radio implementation side. The radio transmitters and receivers need to be accurate and more energy efficient. The super heterodyne receiver (SHR) architecture [37] is selective and respective selective for radio frequency (RF) and intermediate frequency (IF) filters respectively. This needs the integration of the SHR to a single circuit which is very demanding or even very challenging because of image frequency and huge amount of analogue components. So in modern receiver architecture the main goal is to design flexible and as heavily integrated receiver as possible by minimising the number of analogue components and thus minimizing the power consumption, size and cost of the receiver.

In wireless mobile environment the low power consumption and high integrability is even more essential for compact mobile terminals with long battery life. Currently, when many transceivers, or parts of the transceivers, must be operating simultaneously as a single device, as in multiple input-multiple output (MIMO) transmission [38-40], even higher demands for the accuracy of radio devices has been set. Direct conversion receiver (DCR) is a strong contender of modern transceiver architecture [41] to be used in OFDM with high integrability and low power consumption. The direct conversion architecture (Figure 1.1) is applicable for multi-carrier, multi-standard and multi-mode operations.

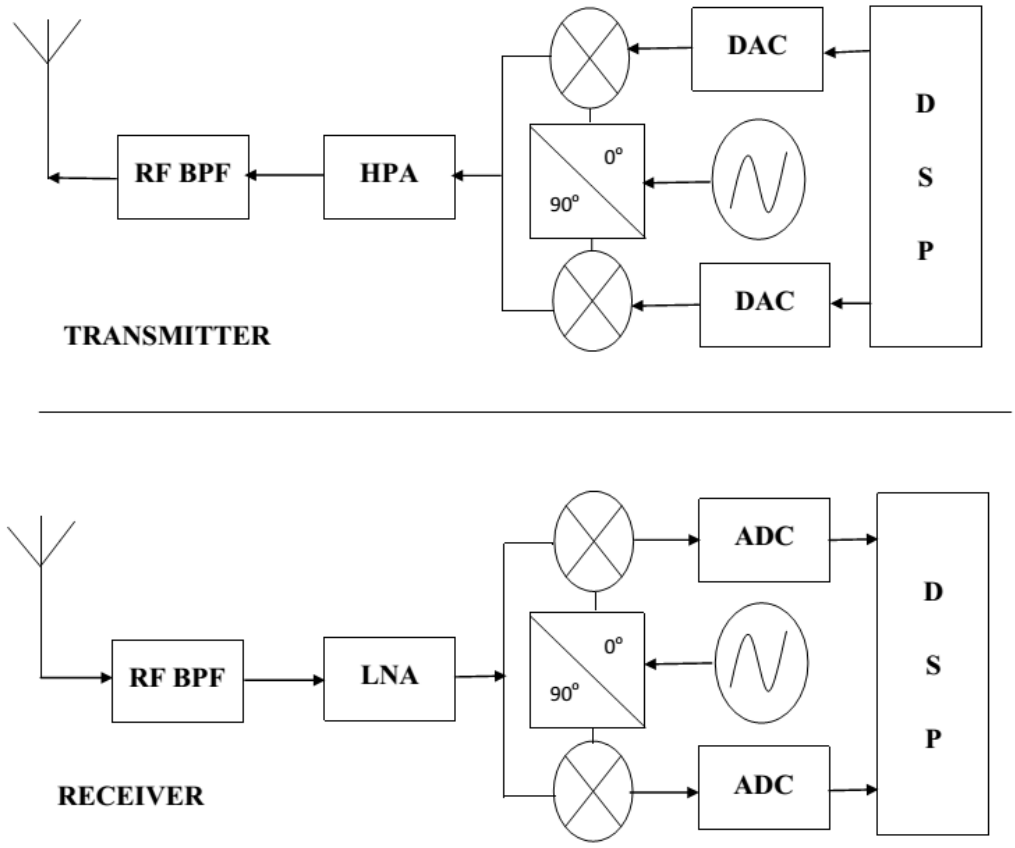

Figure 1.1 Direct Conversion Transceiver Architecture.

In single carrier communication system, the PHN transceiver impairment produces the random rotation to the symbol constellation called common phase error (CPE). In OFDM, in addition to the CPE, PHN also causes leakage of DFT, which subsequently produces inter carrier interference (ICI), serious 'in-band' effect of PHN. This impairs the orthogonality of the subcarriers by spreading their energies on top of each other's. CPE is the random error to the whole OFDM symbol whereas the stochastic ICI behaves like additive noise producing subcarrier wise random errors in OFDM symbol. CPE is dominating in higher order modulation schemes whereas the ICI becomes catastrophic for high PHN levels.

The 'out-of-band' effect comes into play in the multiple access scheme of the OFDM, which is OFDMA, causing multi user interference (MUI). This interference is induced by the spectral spread of the energy of each user's subcarriers on the top of other users' subcarriers [42-46]. A user in dominating CPE regime will not create MUI for

others but lying in the dominating ICI regime will be a great problem for others and the severity will increase with high PHN levels. In case of OFDM/A uplink, the transmitter CPE is not same for all the users and the ICI is not only because of the higher order components of PHN. The loss of the cyclic nature of the transmitted signal also causes the ICI and thus the mitigation techniques need to consider the whole PHN sequence of the length including CP [45].

1.1 Motivation and Objectives

This thesis addresses the OFDM/A system performance under the impact of transceiver oscillator PHN and contributes to improve it at the channel estimation and data detection stage. The first step towards the improvisation is to ascertain how badly PHN is affecting the OFDM/A system performance. The performance metric for this analysis, conducted over last twenty years, has been either signal-to-interference+noise ratio (SINR) or symbol error rate (SER)/ bit error rate (BER) [26-36, 42-46]. However, the evaluation was approximated with assumption of complex Gaussian distributed ICI and the MUI which surpasses the ICI in case of OFDMA, was also not incorporated. So a prominent motivation of this thesis is to characterize and analyze the SINR accurately with these two significant adaptations.

To improve the system performance, two possible approaches are either to fabricate the high quality, low powered and spectrally fine analogue devices for analogue front-end (AFE) or to design the digital signal processing algorithms to combat the impairments at the back-end. The first approach increases the cost and complexity whereas the later one adds the delay but still tolerable. The advancement of wireless communication engineering has attracted many of the researchers and academicians for the extensive research to produce many sound conclusions for estimating and compensating the PHN in OFDM systems [47-62]. One of the objectives of this thesis is to design a new algorithm, with lower computational complexity, to estimate the channel and detect the data in presence of PHN jointly with improved system performance over state-of-art results, by first estimating the PHN and then removing it from the OFDM signal.

1.2 Contribution of the Thesis

This thesis contributes in the area of characterization & analysis of OFDM/A system performance in presence of transceiver PHN and then improving it by estimating and removing the PHN for channel estimation and data detection with proposed algorithm and optimization.

First contribution does the statistical analysis of transceiver PHN effect on OFDM/A uplink system performance for arbitrary subcarrier mapping. A closed form expression for the SINR is derived without the assumption of complex Gaussian distribution of ICI and then analysed as a function of critical system parameters. This improved evaluation stringently specifies the plausible acceptable PHN characteristics for a certain OFDM/A uplink system and explains the serious under specification of local oscillator (LO) with Gaussian approximation [26-31].

Characterization of the MUI as an impact of transceiver PHN on the OFDMA uplink system performance for arbitrary subcarrier mapping, and different powers and PHN levels for different users is the **second contribution**. The MUI, accompanied with power and PHN level differences among the users at the transmitter, causes further performance degradation for users with low signal powers and high PHN. This efficient characterization will allow the design of oscillators to meet the necessary PHN requirements and tends to improve the performance of techniques designed to perform sub-channelization and resource allocation with PHN in OFDMA systems [63-65].

The joint estimation of channel transfer function (CTF) in presence of receiver PHN is the area of **third contribution** by employing the maximum a posteriori (MAP) criterion. The joint estimation utilizes the prior statistical knowledge of PHN spectral components without the assumption of small PHN. An iterative cyclic gradient descent optimization algorithm is also derived to minimize the cost function over the unknown CTF and PHN. Mathematically analysed Cramer-Rao lower bound (CRLB) and simulation results show that mean square error (MSE) of the channel estimation achieves near CRLB performance.

For **forth contribution**, an iterative receiver for statistically optimal data detection in presence of PHN is designed with the MAP cost function for the joint data detection and PHN estimation. Above mentioned cyclic gradient descent optimization algorithm

is used to minimize the cost function over the unknown data and PHN. Simulation results show that joint estimation and iterative cyclic gradient descent optimization, achieves near "No PHN" SER performance for both of the PHN modeling, i.e., Wiener process by free running oscillator (FRO) and Ornstein-Uhlenbeck (O-U) process by phase locked loop (PLL) oscillator.

1.3 Thesis Outline

The thesis is organised in 8 chapters. **Chapter 2** is devoted to study the state-of-art results and discusses the outcomes of recent research works. The chapter is also finding the research gap to decide upon the objectives of the thesis and related motivations. **Chapter 3** is to present the two different time varying models of oscillator PHN. Working principle of both the oscillators, i.e. FRO and PLL oscillator, is explained in context of PHN generation. The generated PHN is described under the topic of PHN profile and PHN modeling. **Chapter 4** discusses the principle of OFDM and its advantages & challenges. The impact of transceivers' impairments, specifically of PHN is presented. The OFDM system performance in terms of BER is simulated and OFDM system modeling with PHN impairment is derived in the last section. In **Chapter 5** the principle of OFDMA is presented with its advantages & challenges. The impact of transceiver PHN is characterised and analysed in terms of MUI and SINR respectively. The theoretical analysis is then verified with the corresponding simulation results. **Chapter 6** is about estimating the CTF in presence of receiver PHN in joint. After a brief on the channel estimation methods the chapter derives the joint MAP cost function for channel estimation in presence of receiver PHN which is further minimized with proposed cyclic gradient descent optimization algorithm. The proposed joint estimator is simulated for near optimum results even in frequency selective fading channel. In **Chapter 7** the joint data detection and PHN estimation is presented with cyclic gradient descent optimization. The proposed iterative OFDM receiver is implemented for both of the PHN modeling, i.e., Wiener and O-U process, to achieve near optimum SER performance. **Chapter 8** concludes the thesis with abstract discussion on all the produced results and proposed methods. The chapter also states the future scope of the presented research work.

2. Literature Review

The widely deployed systems with OFDM are following the basic technique of multi carrier transmission of [6-7], whereas the pioneer idea of multicarrier transmission with overlapped orthogonal subcarriers was given by [1] in 1967 and studied by [2] in 1968. Authors in [4] have shown that for realization of frequency division multiplexing, inverse DFT (IDFT)/DFT is computed for modulation and demodulation process. Thus in OFDM the modulators and demodulators can be implemented with digital inverse FFT (IFFT) and FFT respectively. In [5] cyclic extension of OFDM symbol was used as null guard interval and this new technique of CP insertion was shown to reduce the inter symbol interference (ISI) to a great extent in fading channels. With all these outcomes the OFDM became the potential technique for multi carrier transmission to implement the digital communication systems [8-10] with high data rate and capacity but also placed many challenges to face and recover [11], including transceivers' impairments.

Though many researchers have been studying the transceivers' impairments, the PHN is studied more than the others because of its highly degrading impact on the system performance. Moreover an OFDM system is much more vulnerable to PHN than single carrier system. In single carrier system, the PHN merely causes rotation in the symbol constellation, whereas in OFDM system, in addition to the rotational effect called CPE, PHN also causes ICI. CPE is a multiplication by the same complex number to that of all the subcarriers' symbols within an OFDM symbol. CPE estimation techniques therefore merely estimate the common complex multiplier for all the subcarriers of an OFDM symbol [26-30]. Such estimation techniques used the similar approach and solved the problem of CPE estimation with averaging the estimated CPE values on pilot subcarriers using either least square (LS) or maximum likelihood (ML) estimation [27-28].

The ICI is more complex part of the PHN effect and thus its estimation is also more complex than the estimation of the CPE. When CPE has been mitigated from the signal the remaining time domain PHN contribution, for individual OFDM symbol, is just the same as the original with only one exception that the mean of the remaining PHN is approximately zero. This zero mean PHN causes the ICI. The problem of estimation and mitigation of ICI have been widely studied in the literature [31-36]. A

linear interpolation based tail estimation technique was proposed in [36] to mitigate ICI while using CPE and ICI estimations one after one. Instead of other more complex interpolators, linear interpolation is used as the main tool to emphasize on computational simplicity. After obtaining the final estimate for the time domain PHN within the processed OFDM symbol, the actual mitigation of the ICI is done by de-convolving the corresponding received signal block with the FFT of the estimated PHN waveform.

As in OFDMA transmission, simultaneously transmitted user signals give rise to multiple PHN, the conventional PHN correction methods cannot be directly applied since they target at single PHN. Earlier PHN mitigation techniques for OFDMA transmission involve the estimation of multiuser CPE only [42], while the other more advanced mitigation techniques involve the estimation of ICI and MUI [43, 45-46] as well. In [46] the data symbols are detected after estimation and mitigation of CPE and channel effect. Further these detected symbols are used to estimate the ICI's spectral components to improve over MUI estimation technique.

ICI, which is a dominating factor over CPE, because of larger pass band cut off frequencies of low pass filter, is assumed to be complex Gaussian distributed in majority of the literature available [27-31]. In contrast for 'Slow' PHN model, where PHN does not change within one OFDM symbol, the relative PHN bandwidth, $\Delta_{PN} = \frac{2\,(PHN\ 3dB - BW)}{\Delta f(subcarrier\ spacing)}$ should be as low as possible to incorporate the advantages of OFDM transmission over single carrier transmission [45]. With low of this ratio, the assumption of complex Gaussian distribution of the ICI becomes false and even with higher number of subcarriers, the ICI is limit distributed with thicker tails [32-34].

In OFDMA system, MUI is also an important factor, which is considered marginally in previous analytical methods [42, 44]. As MUI takes in to account the significance of the power level of users as well the transmitter $2(PHN\ 3 - dB\ BW)$ the distribution of MUI in OFDMA cannot be taken same as ICI in OFDM system. Further in OFDMA uplink system these two will be precisely different for different users. Secondly a higher $2(PHN\ 3 - dB\ BW)$ of the PHN process can also lead to more energy in the MUI factor of ICI term. Considering these two facts and the OFDMA uplink scenario, not all the other users will produce the same MUI for the intended user.

A reliable estimation of channel and transmitted symbols incorporate the functionality of PHN estimation either in isolation or joint. The independent function of channel estimation, PHN estimation and symbol estimation, in case of isolated approach, may results in poor channel estimates which effectively will produce poor symbol estimates. In [31-32, 35-36] PHN estimation and mitigation techniques are proposed but the channel frequency response is assumed to be known in prior to the suppression which is not statistically optimal. In frequency selective environment, the joint approach of [47-52] produces the statistically optimal estimates by combining the PHN estimation with channel estimation.

In [47], on the criterion of MAP cost function, a joint channel, PHN and CFO estimation is proposed in time domain with high computational complexity. The estimation of channel impulse response (CIR) needs a priori knowledge of channel length which is not required in estimating CTF. In [48], minimum mean square error (MMSE) channel estimation is done in two successive stages. After joint CPE estimation the decision directed ICI reduction is performed which is not fully joint in true sense. The ICI is treated as additive receiver noise with known second order statistics and the parametric model of PHN realization is considered in [48]. The MAP based joint estimator of [49], utilizes a priori information on the PHN process to estimate CTF. Here the CTF is estimated in time domain which makes the method more complex than estimation in frequency domain. The ML based joint estimator of [50] utilizes the approach of forward and backward substitution in the frequency domain to estimate the channel. The method described in [50] proves its competency in the reduced computational complexity because of the frequency domain estimation but on the cost of performance degradation as a priori information on the PHN process is not used and the ML cost function is minimized with the constraint of small PHN approximation. In [51-52], Monte Carlo methods based on expectation minimization (EM) for channel estimation are proposed. The EM algorithm is an iterative method of obtaining ML estimates of parameters in the presence of hidden variables with very high computational complexity. In EM channel estimation, the non Gaussianity of the posterior probability density function (PDF) of the hidden variables, which are random parameters without direct observance, is the main problem. This has been solved in [51] with particle filtering technique and in [52] by considering point density estimation.

The emerging technique of massive MIMO renewed the possibility of further performance improvement and computational complexity reduction with the aid of spatial diversity [59-60]. In [59], basis expansion model (BEM) coefficients are jointly estimated in time domain with very high computational complexity, while the joint covariance matrix of phase and channel is already known. The two stage time domain MAP estimation of CPE corrupted CIR in [60] is not fully joint in channel estimation stage.

In regards of symbol estimation in OFDM system, some initial methods used the approach of isolated estimation [35-36], whereas recently with high carrier frequency and dense constellations, a reliable detection of transmitted symbols incorporates the functionality of PHN estimation in joint [53-58]. In [35] the estimated PHN is compensated in received signal before next iteration of channel equalization and symbol detection, without performing any optimization. In the LS approach of [36], the ICI is simply treated as added noise without utilizing any a priori knowledge. The method of [36] only deals with the discontinuities at the edges of consecutive symbols in block based OFDM transmission.

In [53-54] the authors presented a time domain approach to jointly estimate the symbol and PHN. The variational inference, approximation of Bayesian inference is used with the assumption of continuous distributed a-prior density of symbols. The joint estimation of data and PHN of [55] optimizes the minimum mean square prediction error of PHN with some extra numerical complexity. The blind compensation of PHN is proposed in [56] with data detection where time averaged PHN is approximated over sub blocks. In frequency selective fading this type of estimation is not optimal as the fading within N samples corrupts the PHN realization. In [57], PHN DFT coefficient matrix is approximated with one of the entries of codebook with assumption of equal probability. With joint ML approach the method shows some performance degradation as compare to MAP and is also constrained by the air interface. In [58] the time domain joint MAP approach to detect the data in presence of PHN is presented with the aid of amplify and forward relaying strategy.

Further, the performance improvement in joint symbol detection is shown in literature [61-62], with MIMO OFDM while using channel coding and spatial diversity. With high computation complexity, the frequency domain joint MAP approach of [61]

obeys the deterministic restriction with the assumption of small PHN and considers a-prior known statistics of PHN and data both. The joint MAP technique of [62] is code aided synchronization with EM framework.

3. Oscillator Phase Noise

Sending the electrical or electromagnetic signals from transmitter to the receiver for conveying the information is telecommunication. The transmission of signal may happen in two distinct ways, either as baseband transmission or as band pass transmission. In baseband transmission the signal is around the direct current (DC) frequency whereas in a band pass transmission, information signal is up converted to a particular frequency, known as carrier frequency (f_c). This up conversion is known as modulation and the modulated signal is spread around carrier frequency even having the spectrum same as information bearing baseband signal. Usually a baseband transmission happens through a baseband channel over wires and cables while the wireless transmission is essentially band pass but not vice versa [66].

Further the band pass transmission can be categorized as single carrier (SC), i.e. information signal is asserted on a single carrier frequency, or multicarrier (MC), i.e. information signal is embedded on many parallel carrier frequencies. Whether the SC or MC transmission is there, the modulation is done for frequency up conversion of baseband signal to radio frequency (RF) and demodulation is done for frequency down conversion of RF signal to baseband frequency [66].

3.1 Transceivers' RF Impairments

As the most applicable modern transceiver hardware used for wireless mobile communication is the direct conversion architecture, Figure 3.1 shows the up/down conversion operation with this architecture. The architecture consists of analogue and digital part. The analogue part processes the continuous time signal at RF for signal transmission and reception and is known as RF front-end. The digital part known as back-end, deals with the signal in digital domain for information representation and processing. Unfortunately, the RF front-end devices, made up of electronics, are not ideal and producing the noise and distortion in the signal at the time of transmission/ reception. This undesirable noise further introduces inaccuracy of digital processing algorithms at the back-end and degrades the overall system performance. This problem of non ideal RF devices which are performing digital to analogue (DAC) &

analogue to digital (ADC) conversion, frequency up/down conversion and amplification, is known as transceivers' RF impairments.

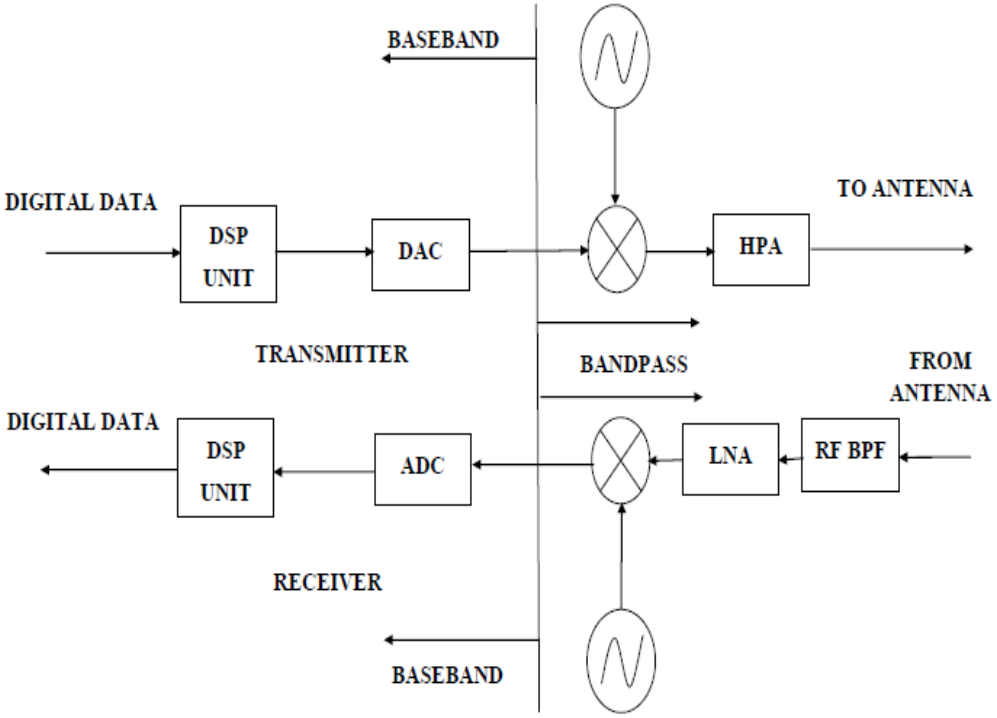

Figure 3.1 Baseband to Band pass Modulation and Band pass to Baseband Demodulation.

The amplification of the signal is done with high power amplifier (HPA) at the transmitter side and with the low noise amplifier (LNA) at the receiver side. The non ideal amplification leads to the in-band and out-of-band distortion because of the non linearity which further causes interference to the adjacent channels, especially in MC communication. As the OFDM signal is having high PAPR, it will drive the high power amplifier in saturation region and result will be the signal distortion. In case of mobile communication it will further cause higher heat dissipation and poor battery life as the amplifier efficiency is inversely proportional to the PAPR. Many of the researchers have produces the sound results to overcome this problem of high PAPR and non linearity of the power amplifiers [67-70].

ADC & DAC, operating at few GHz for mobile transceivers face the challenges of high sampling rate and high resolution. With these two necessities, ADC & DAC further need to deal with the challenge of achieving low power dissipation with

efficient on chip integrability. With all these challenges to overcome, the ADC & DAC directly lend in the various noise sources including jitter noise, quantization noise, thermal noise and non linearity's. A detailed survey of analysing these noise sources and then combating with these can be found in the literature [71-73].

At the stage of frequency up/down conversion which is achieved by the mixers (multiplication in time domain and convolution in frequency domain) and oscillators, three types of transceivers' RF impairments can take place, i.e. CFO, IQ imbalance and PHN. At the time of frequency conversion in direct conversion architecture the RF signal is split into I and Q branches which is mixed with the LO signals having the phase difference of 90^0. Unfortunately in the real scenario this difference is not exactly 90^0 and it results in some correlation between the LO signals that feed the mixers. This mismatch in the phase differences is known as IQ imbalance and studied by many authors in [23-25]. Difference in the LO frequencies of the transmitter and receiver, produces the CFO which is estimated and mitigated in the training phase of the communication [19-22].

In the frequency conversion stage a periodic co-sinusoidal signal known as information carrier is generated by LO and mixed with information signal. Unfortunately being the part of analogue front end, both the devices, mixer and oscillator, are not ideal though in this research work we will take mixer with ideal characteristics and will address the oscillator imperfections only. The non ideal LO produces the spectral spread of the carrier signal which is the attribute of PHN and amplitude noise. Here we will keep the amplitude noise in control with the mean of automatic gain controller (AGC) and will consider the PHN as the solo contribution of spectral spread.

3.2 Oscillators

The autonomous system, oscillator provides a periodic co-sinusoidal reference signal used for up/down conversion of the baseband/RF signal to/from RF/baseband frequency. Oscillator in isolation, known as FRO (Figure 3.2), consist of an amplifier composed of diodes and/or transistors and a positive feedback network which is a resonator circuit.

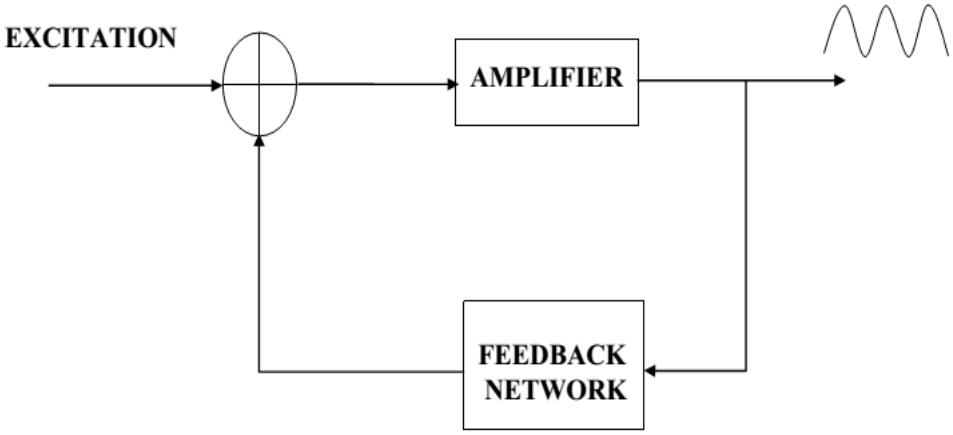

Figure 3.2 Free Running Oscillator.

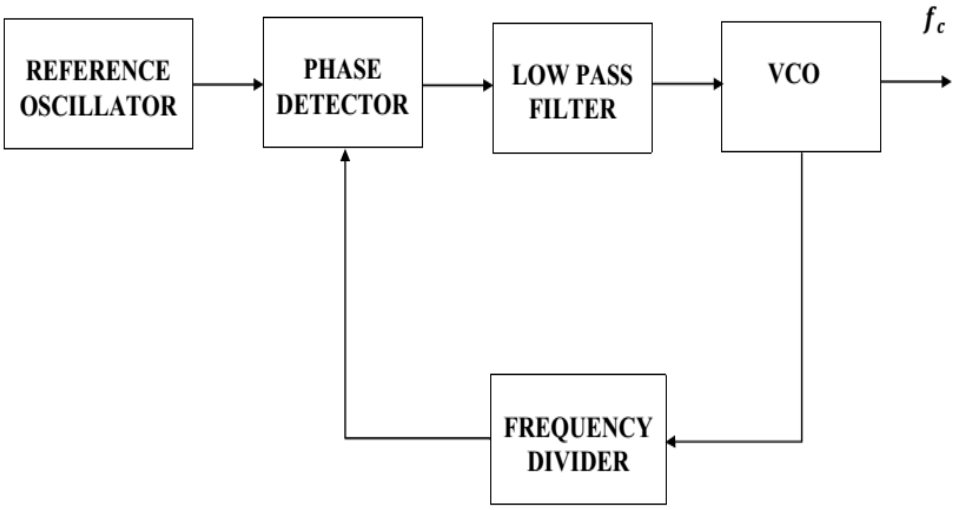

Figure 3.3 Phase Locked Loop Oscillator.

In practice wireless digital communication systems use PLL oscillator because of its high stability and easy control. As shown in Figure 3.3 the error signal generated by phase detector, after comparison of two input signals, is passed through the low pass filter and then is used to drive a voltage controlled oscillator (VCO) to produce an output frequency signal. Through a frequency divider this frequency is feedback to the system input. Any drift in the output frequency will increase the error signal to drive the frequency of VCO in opposite to reduce the error. Thus the output frequency is

locked to the input frequency or to some integer multiple of input frequency which is the frequency of reference oscillator.

Either FRO or PLL VCO, in an ideal oscillator for a perfect periodic signal the transition of phase over a time interval should be constant whereas practically this phase increment is a random variable. This random variation of phase is phase jitter and its instantaneous deviation is called PHN [74-77]. Thus the output of a practical oscillator is noisy and can be written as:

$$s(t) = [A + a(t)] \sin[\omega_c t + \theta(t)] \tag{3.1}$$

where A and $\omega_c = 2\pi f_c$ are amplitude and angular frequency respectively and $a(t)$ is amplitude fluctuation which can be kept in limit by using an AGC. $\theta(t)$, the phase fluctuation (time varying PHN), is very difficult to mitigate and can have major impact on system performance. In Figure 3.4 the output of a noisy oscillator is compared with the ideal one and we can observe that because of PHN the zero crossing time is changing randomly in case of noisy oscillator.

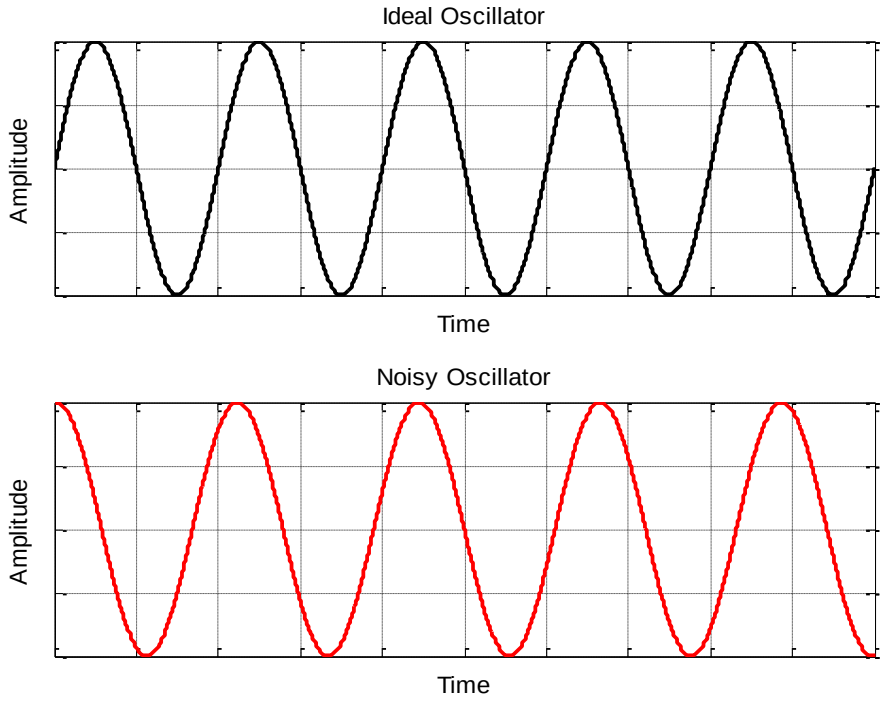

Figure 3.4 Output Signal from Ideal and Noisy Oscillator.

In frequency domain, in case of ideal oscillator power is concentrated at the central frequency, i.e. power spectral density is Dirac delta function. This signal is mixed with the information bearing signal (centred on zero frequency) also known as baseband signal. This embedding process (Figure 3.5) translates the base band frequency content to the bandanas region which is centred on high frequency f_c.

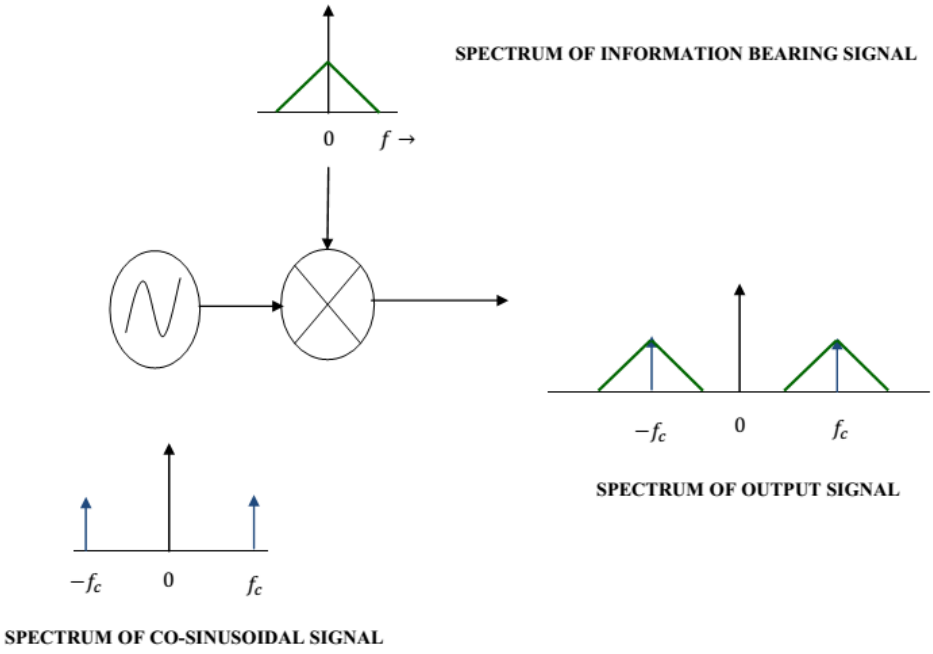

Figure 3.5 Modulation with Ideal Oscillator.

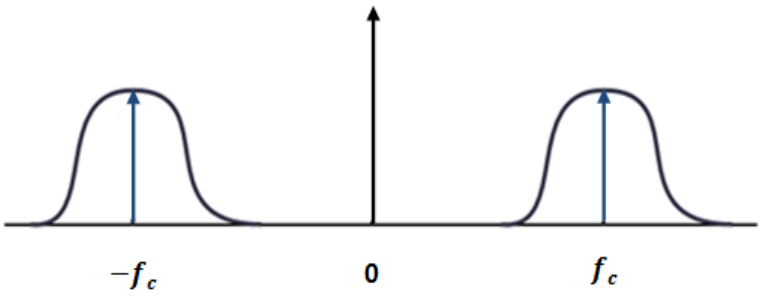

Figure 3.6 Spectral Spreading in the Noisy Oscillator.

As the LO used for this process (FRO or PLL VCO) is not perfectly ideal it shows the spectral spreading around the f_c (Figure 3.6) and when the information bearing signal spectrum is convolved with this spectrum the output signal is totally distorted.

3.3 Sources of Noise in an Oscillator

Phase fluctuations, resulting in the random shifting of oscillator frequency have its origin in the noise sources present in the internal circuitry of an oscillator. These noise sources may be thermal noise i.e. caused by Brownian motion of electrons, shot noise i.e. caused by small fluctuations in current due to the random electron emission and flicker noise i.e. cause by active device characteristics. These noise sources can be further categorized in white (uncorrelated) and color (correlated) noise sources [75]. Thermal and shot are white whereas flicker is colour noise source.

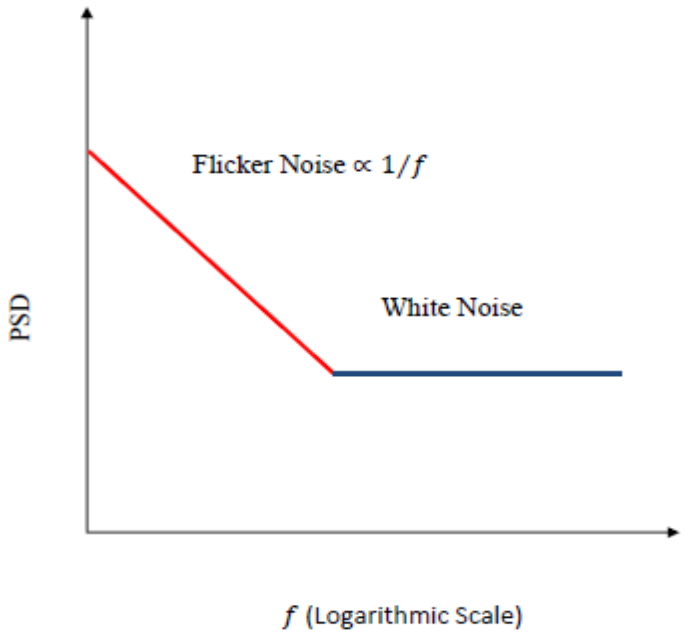

Figure 3.7 PSD of Noise Sources in the Oscillator Circuitry.

The white noise has the flat power spectral density (PSD) given by [74-76]:

$$S_{white}(f) = K_{white} \tag{3.2}$$

where K_{white} is the constant for particular device. The PSD of color noise is given by:

$$S_{1/f}(f) = K_{1/f}\frac{I^a}{f} \tag{3.3}$$

where $K_{1/f}$ is the constant for particular device. I is the current through device and a is the constant in the range of .5 to 2. Figure 3.7 is showing the total PSD of the white and color noise sources present in the oscillator circuitry.

The PHN generation mechanism is based on two different phenomenons. First is the direct amplification/attenuation of the white and color noise sources resulting in the white PHN and flicker PHN with PSD:

$$S_{PHN\ white}(f) = K_{PHN\ white} \tag{3.4}$$

where $K_{PHN\ white}$ is again a constant for particular device and:

$$S_{PHN\ 1/f}(f) \propto \frac{1}{f} \tag{3.5}$$

respectively. The second mechanism is based on the frequency modulation of the noise sources present in the oscillator circuit. This is equivalent to the integration process in the time domain. According to [72] the PSD of the frequency modulated (FM) PHN is given by:

$$S_{PHN\ FM}(f) \propto A^2\frac{{f_c}^2}{f^2}\,S_{source}(f) \tag{3.6}$$

where $S_{source}(f)$ is PSD of noise source present in the system. Thus with the Equations (3.2) and (3.3) the resulting white FM PHN has PSD proportional to $1/f^2$ and flicker FM PHN has PSD proportional to $1/f^3$. This mechanism is shown in the Figure 3.8 and Table 3.1. The oscillator PHN spectrum having white PHN (flat) & white FM PHN ($1/f^2$) spectra because of white noise sources and flicker PHN ($1/f$) & flicker FM PHN ($1/f^3$) spectra because of color noise sources is shown in Figure 3.9.

The short term frequency instability resulting in the random phase variation of a signal ($s(t)$) generated by the noisy oscillator is characterized by single-side-band (SSB) PHN spectrum, having unit of decibels below the carrier per hertz (dBc/Hz) in frequency domain as [76-77]:

$$L(f) = \frac{P_{SSB}(f_c + f)}{P_s} \tag{3.7}$$

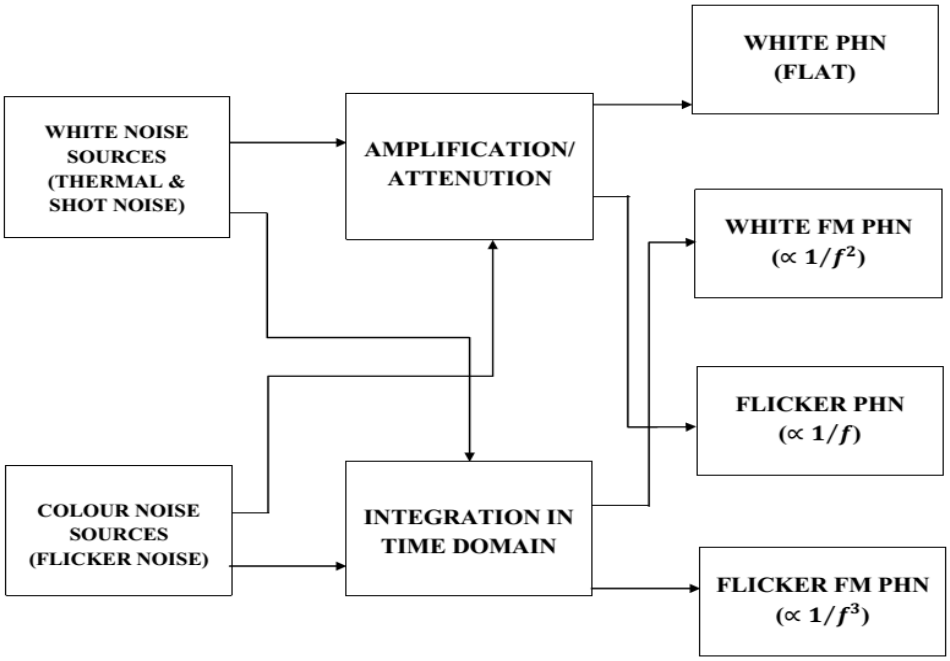

Figure 3.8 PHN Generation.

Source of Noise	Resulting PHN	Spectra	dBc/Hz
Thermal & Shot Noise	White PHN	Flat	-0
	White FM PHN	$\propto {}^{1}/_{f^2}$	-20
Flicker Noise	Flicker PHN	$\propto {}^{1}/_{f}$	-10
	Flicker FM PHN	$\propto {}^{1}/_{f^3}$	-30

Table 3.1 PHN Generation.

where f_c and f are oscillation and offset frequencies respectively and P_s is the total signal power around centre frequency. $P_{SSB}(f_c + f)$, represents the single side band power at a frequency offset of f from the carrier f_c with a measurement bandwidth of 1 Hz.

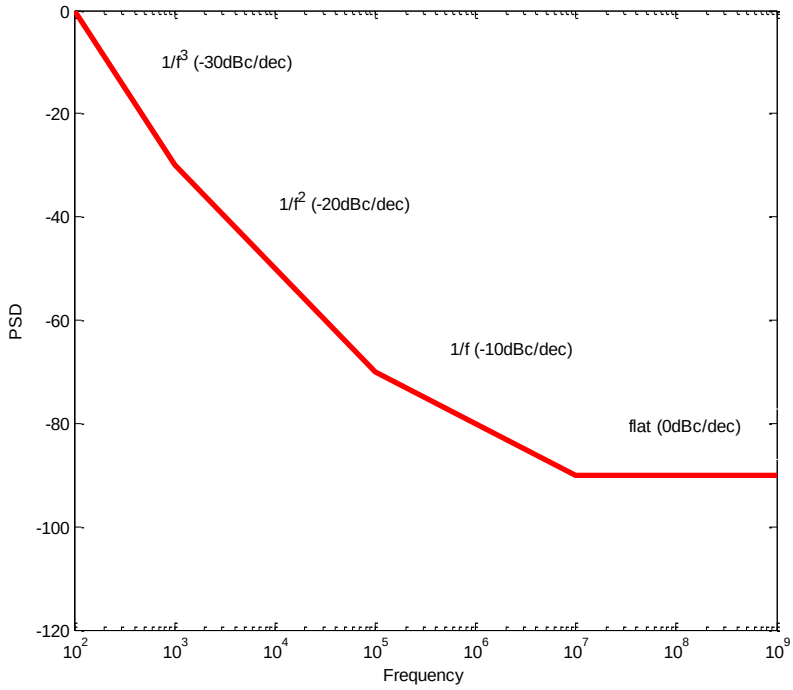

Figure 3.9 PSD of PHN in Oscillator Output.

For FRO, PHN is result of internal noise sources where in case of PLL oscillator internal noise sources of each block contribute in the output PHN spectrum. According to the analysis done in [78-79], in case of PLL oscillator, output PHN spectrum follows the reference oscillator below a particular frequency and is identical to VCO above that.

3.4 Phase Noise Modeling

To understand the impact of PHN in either SC or MC communication system it is essential to model the PHN process accurately. This section focuses on the PHN modeling for simple FRO model [74, 76] and more complex PLL VCO model [78-79]. Though the FRO model is easy to simulate mathematically, PLL is widely used in practice for digital communication systems.

In general, time varying PHN process ($\theta(t)$), can be written as following stochastic differential equation:

$$d\theta(t) = \varphi(\mu - \theta(t))dt + \sigma dB(t) \tag{3.8}$$

where $\theta(t)$, and $B(t)$ are continues time Ornstein- Uhlenbeck (O-U) process and Brownian process respectively. μ is asymptotic mean, φ is the drift and σ^2 is the variance of the noise present in the system which is white noise in our case. Solution for Equation (3.8) with the initial condition $\theta(0)$ is [80]:

$$\theta(t) = \theta(0)\, e^{-\varphi t} + \mu(1 - e^{-\varphi t}) + \sigma \int_0^t e^{-\varphi(t-s)} dB_s. \tag{3.9}$$

If $\theta(t)$ is sampled with the sampling interval T_s/N, means $\theta_n = \theta(nT_s/N)$ where $n = 0, 1, 2, \ldots, N-1$ then:

$$\theta_{n+1} = \theta_n e^{-\varphi\frac{T_S}{N}} + \mu\left(1 - e^{-\varphi\frac{T_S}{N}}\right) + \phi_n\ . \tag{3.10}$$

Equation (3.10) represents the autoregressive process of order one (AR (1)) where ϕ_n is a sequence of identically and independently distributed (iid) random variables with mean zero and variance, ${\sigma_{\phi_n}}^2$ such that:

$$\phi_n = \sigma_{\phi_n}\epsilon_n \tag{3.11}$$

where $\epsilon_n \sim iid\mathcal{N}(0,1)$ and $\phi_n \sim iid\mathcal{N}(0,\ {\sigma_{\phi_n}}^2)$. In this case, Equation (3.10) is known as discrete time regular O-U process with:

$${\sigma_{\phi_n}}^2 = \frac{\sigma^2}{2\varphi}(1 - e^{-2\varphi\frac{T_S}{N}}). \tag{3.12}$$

3.4.1 Free Running Oscillators

If we take no drift in the process, $\varphi = 0,$ then Equation (3.10) is:

$$\theta_{n+1} = \theta_n + \phi_n \tag{3.13}$$

which is Wiener process [76] with mean zero and variance, ${\sigma_{\phi_n}}^2 = \sigma^2$. PHN from the FRO follows the Wiener process of Equation (3.13) with probability density function (PDF), $Pr(\phi_n) = \mathcal{N}(0, {\sigma_{\phi_n}}^2)$. Further with the PHN process of a FRO, modelled as Wiener (also known as random walk) process or Brownian motion:

$$\alpha(t) = \sqrt{c}\, B(t) \tag{3.14}$$

where c is the diffusion rate of the particular oscillator describing its quality, $\alpha(t)$ is random time shift in the carrier and $B(t)$ is the standard Brownian motion. The carrier

phase shift and time shift are related as $\theta(t) = 2\pi f_c \alpha(t)$. For a discrete time Brownian motion process, the sampled version of Equation (3.9) can be written as:

$$\alpha_n = \sqrt{c}\, B(nT_s/N) \tag{3.15}$$

where T_s/N is the sampling interval. For a standard Brownian motion:

$$B(nT_s/N) - B((n+1)T_s/N) \sim \mathcal{N}(0, T_s/N). \tag{3.16}$$

Which means that α_n is an accumulated Gaussian random variable with zero mean and variance cT_s/N and so the discrete time phase shift θ_n is having the variance:

$$\sigma^2 = {\sigma_{\phi_n}}^2 = 4\pi^2 f_c^2\, cT_s/N. \tag{3.17}$$

The frequency domain characterization of PHN process is done with its PSD, $S_\theta(f)$. In case of FRO, $S_\theta(f)$ is Lorentzian PSD [77] which is squared magnitude of a first order low pass filter transfer function and is given as:

$$S_\theta(f) = \frac{1}{\pi} \frac{\pi f_c^2 c}{(\pi f_c^2 c)^2 + f^2}\,. \tag{3.18}$$

Figure 3.10 illustrate the FRO output PHN PSD for Wenzel standard 100 MHz-ultra low noise crystal oscillator. Data points for the intended mask are directly taken from [81].

It is well established conclusion [76-77] that at high offset frequencies $S_\theta(f)$ is approximated as SSB PHN spectrum, $L(f)$, which means:

$$L(f) \approx S_\theta(f) \quad for\ large\ f \tag{3.19}$$

Now we use a parameter, PHN 3-dB Bandwidth (Δf_{3dB}), to characterise the oscillator PHN property. Δf_{3dB} is a measure of the point where the $S_\theta(f)$ has decayed by half of its maximum value. The relation between c and Δf_{3dB} is:

$$c = \frac{\Delta f_{3dB}}{\pi f_c^2}. \tag{3.20}$$

Thus the variance of PHN process is given by:

$$\sigma_\phi^2 = 4\pi^2 f_c^2\, cT_s/N = 2\pi\beta\, T_s/N \tag{3.21}$$

where $\beta = 2\Delta f_{3dB}$.

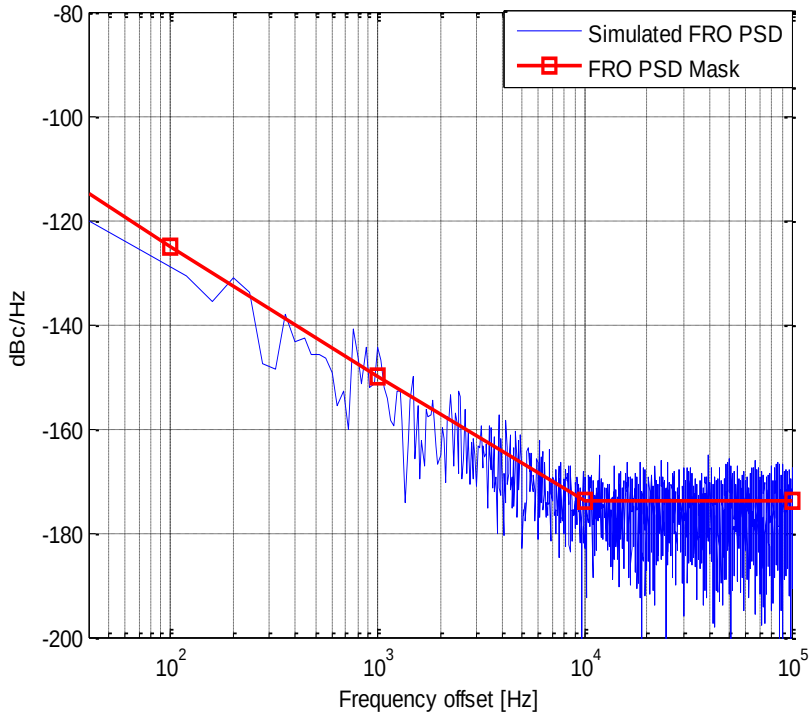

Figure 3.10 PHN PSD Out from FRO (Wenzel standard 100 MHz-ultra low noise crystal oscillator).

3.4.2 Phase Locked Loop Oscillators

Digital communication systems, requiring the low PHN oscillators, generally avoid the low noise dedicated crystal oscillators because of very high cost. Thus a PLL VCO is employed widely because of its high stability with ease of control and affordable cost. Though PHN from the PLL VCO follows the regular O-U process [80], but for wide sense stationary output from the PLL, asymptotic mean should be zero [78] and with that, Equation (3.8) results in:

$$d\theta(t) = -\varphi\theta(t)dt + \sigma dB(t) \tag{3.22}$$

with the solution:

$$\theta(t) = \theta(0)\, e^{-\varphi t} + \sigma \int_0^t e^{-\varphi(t-s)} dB_s \tag{3.23}$$

which is celebrated O-U process [80]. The discrete time sampled version of Equation (3.23) is:

$$\theta_{n+1} = \theta_n e^{-\varphi\frac{T_S}{N}} + \phi_{PLL_n} \tag{3.24}$$

where ϕ_{PLL_n} is a sequence of identically and independently distributed (iid) random variables with mean zero and variance:

$$\sigma_{\phi_{PLL_n}}{}^2 = \frac{\sigma^2}{\varphi}\left(1 - e^{-\varphi\frac{T_S}{N}}\right). \tag{3.25}$$

In literature, [79] has solved the Equation (3.22) for the PLL VCO with loop filter of order one (Figure 3.3) resulting in zero mean and variance:

$$\sigma_{\phi_{PLL_n}}{}^2 = 4\pi^2 {f_c}^2 \left(C_{RO}\frac{T_S}{N} + 2\sum_{i=1}^{2}(\xi_i + \zeta_i)(1 - e^{-\lambda_i\frac{T_S}{N}})\right). \tag{3.26}$$

where:

$$\lambda_{1,2} = \frac{\omega_{lpf} \pm \sqrt{({\omega_{lpf}}^2 - 4\omega_{lpf}\sqrt{C_{PLL}})}}{2},$$

$$\xi_1 = \frac{C_{RO}\lambda_2}{(\lambda_1 - \lambda_2)\lambda_1}, \qquad \xi_2 = \frac{-C_{RO}\lambda_1}{(\lambda_1 - \lambda_2)\lambda_2},$$

$$\zeta_1 = \frac{C_{RO} + C_{VCO}}{(\lambda_1 - \lambda_2)^2}\left(\frac{{\lambda_2}^2}{2\lambda_1} - \frac{\lambda_1\lambda_2}{2(\lambda_1 + \lambda_2)}\right),$$

and

$$\zeta_2 = \frac{C_{RO} + C_{VCO}}{(\lambda_1 - \lambda_2)^2}\left(\frac{{\lambda_1}^2}{2\lambda_2} - \frac{\lambda_1\lambda_2}{2(\lambda_1 + \lambda_2)}\right)$$

where f_c is the centre frequency of VCO in Hz , ω_{lpf} is the angular corner frequency of the low pass filter in rad/sec and $\sqrt{C_{PLL}}$ is the PLL bandwidth in Hz. C_{RO} and C_{VCO} are diffusion rates of the reference oscillator (RO) and VCO respectively.

While considering the white noise sources only, in both, RO and VCO, in case of PLL VCO PSD, $S_{\theta_{PLL}}(f)$ is:

$$S_{\theta_{PLL}}(f) =$$

$$e^{-4\pi^2 f_c^2\{(\xi_1+\zeta_1)(\xi_2+\zeta_2)\}} \sum_{\vartheta_1,\vartheta_2=0}^{+\infty} \frac{\left[\left(4\pi^2 {f_c}^2\right)^2 (\xi_1 + \zeta_1)^{\vartheta_1}(\xi_2 + \zeta_2)^{\vartheta_2}\right](4\pi^2 {f_c}^2 C_{RO} + \vartheta_1\lambda_1 + \vartheta_2\lambda_2)}{(\vartheta_1!\,\vartheta_2!)\left[\left(\frac{4\pi^2 {f_c}^2 C_{RO}}{2} + \vartheta_1\lambda_1 + \vartheta_2\lambda_2\right)^2 + 4\pi^2 f^2\right]}$$

(3.27)

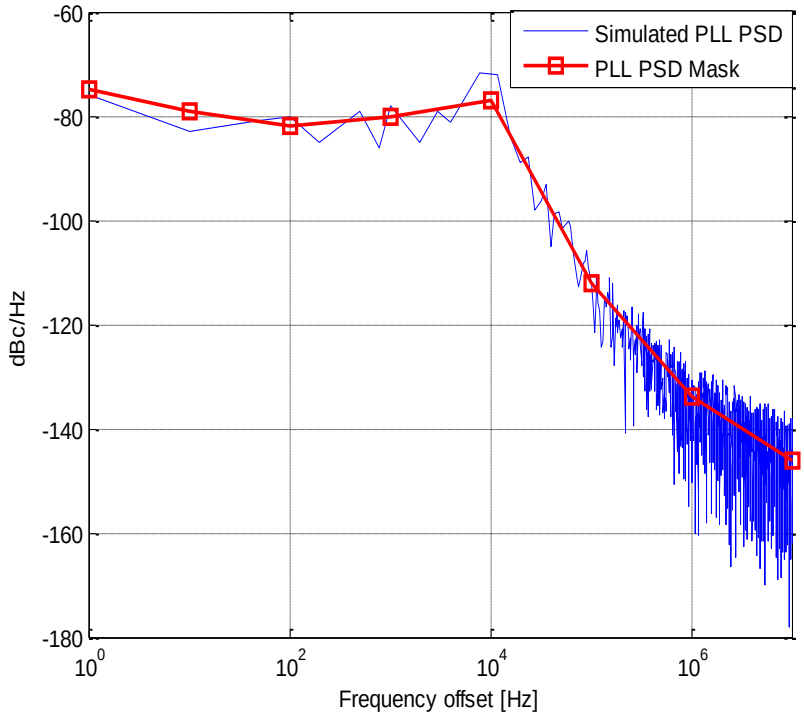

Figure 3.11 PHN PSD Out from PLL VCO (ADF4360-1).

Figure 3.11 illustrate the PLL output PHN PSD for ADF4360-1, 2.25GHz with loop bandwidth of $10kHz$. Data points for the intended mask are directly taken from [81].

The simulated samples of PHN modelled as Wiener process and celebrated O-U process, for FRO and PLL VCO respectively, are shown in Figure 3.12. Though the time varying PHN process of FRO can be characterized with β only, PLL VCO requires more parameter to characterize such as given in Table 3.2, assuming that the VCO is noisier than reference oscillator.

f_c	$5GHz$
β	$20kHz$
f_{lpf}	$20kHz$
C_{RO}	$10^{-25}s$
C_{VCO}	$10^{-19}s$
C_{PLL}	$4 * 10^{8}\ /s^2$

Table 3.2 PHN Modeling Parameters.

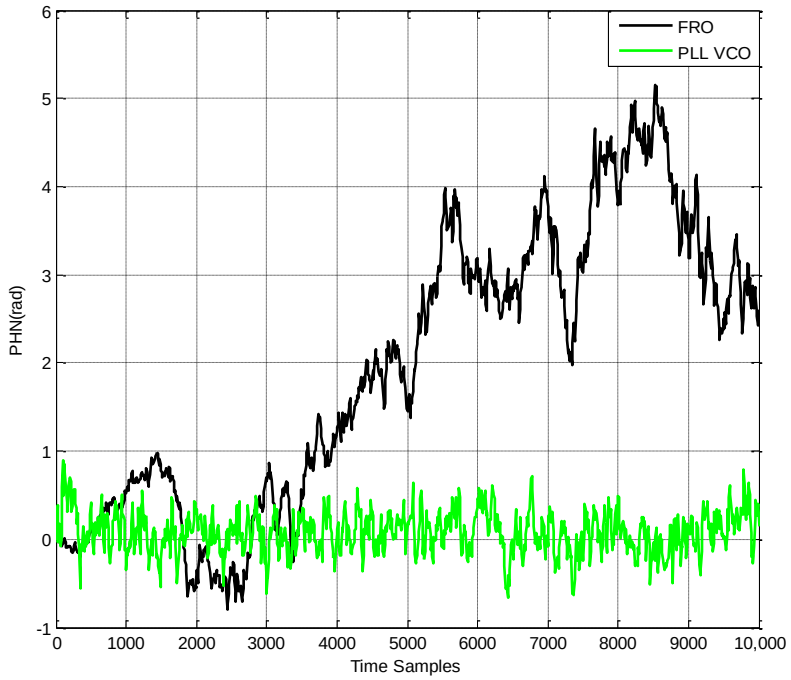

Figure 3.12 Simulated PHN Time Samples for FRO and PLL VCO.

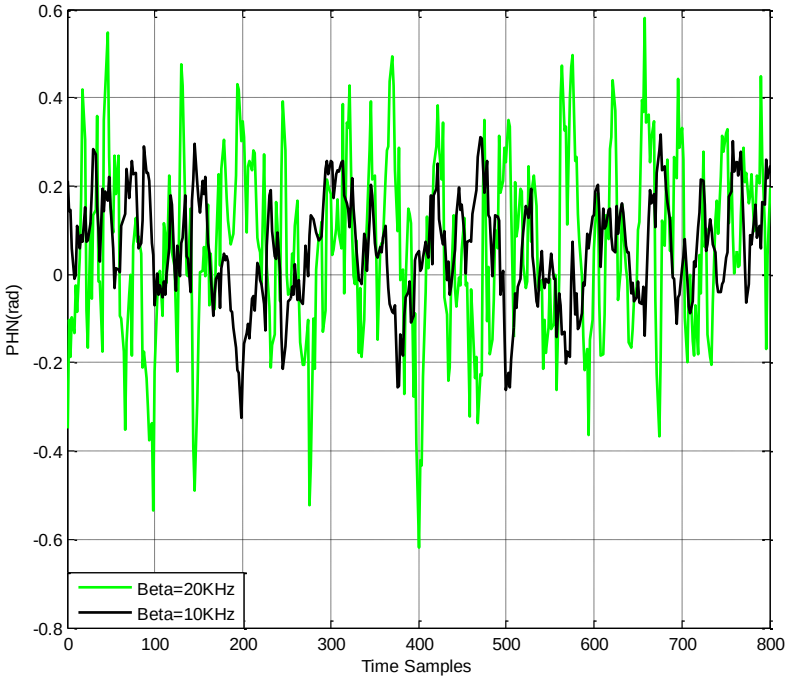

Figure 3.13 Simulated PHN Time Samples for FRO after CPE Removal.

The simulated samples of PHN, modeled as Wiener process for FRO with β =20 KHz and 10 KHz are shown in Figure 3.13 after CPE removal.

3.5 Conclusion

Analyzing and mitigating the impact of transceiver PHN by means of digital signal processing algorithms necessitates the accurate mathematical modeling of generated PHN. As the FRO model is easy to simulate mathematically and PLL is widely used in practice for digital communication systems, the PHN modeling for both of the oscillators are presented. With the white noise sources in the oscillator circuitry, the PHN is modelled as Wiener process and celebrated O-U process, for FRO and PLL VCO respectively. The frequency domain characterization in terms of PSD is done for both the PHN processes and time samples are simulated.

4. Orthogonal Frequency Division Multiplexing

Tremendous growth in the demand of high data rate at minimal cost for as many users with smart flexibility and great reliability of multimedia wireless communication systems, have attracted many academicians and researchers to develop the communication technique which is spectral efficient and robust to the fading environment, and the result is MC transmission. Either in urban or indoor wireless communication, multipath fading is the main cause of performance degradation. In multipath environment, the resultant signal at the receiver antenna is the combination of multipath waves and can vary in amplitude and phase. This results in the rapid amplitude fluctuation of the received signal within a time interval or distance, known as fading. Fading is the function of the transmitted signal bandwidth, the intensity distribution of the waves and relative propagation time. With the channel parameters i.e., delay spread, coherence time, Doppler spread and coherence bandwidth, fading can be classified as [82]:

Flat Fading

If the channel is not time dispersive i.e. BW of signal < coherence BW of channel or delay spread < symbol period, the channel is flat and there does not exist the inter symbol interference (ISI) at the receiver.

Frequency Selective Fading

If the channel is time dispersive i.e. BW of signal > coherence BW of channel or delay spread > symbol period, the channel is frequency selective and there exists the ISI at the receiver.

Slow Fading

If the channel is not frequency dispersive i.e. coherence time > symbol period or the channel is having low Doppler spread, the channel is slow i.e. the channel impulse response does not change within the symbol duration and signal does not get frequency dispersion at the receiver.

Fast Fading

If the channel is frequency dispersive i.e. coherence time < symbol period or the channel is having high Doppler spread, the channel is fast i.e. the channel impulse

response changes rapidly within the symbol duration and signal goes under frequency dispersion at the receiver.

It is clear from the above classification that to combat the frequency selective multipath fading the use of narrowband signals is a potential solution and this evolved the idea of MC communication. Various kind of MC communication includes multi carrier code division multiple access (MC-CDMA) and OFDM.

In case of MC-CDMA, serial chips (Pseudo Random Codes) of direct sequence spread data symbols are converted in parallel stream and are asserted on each orthogonal sub carriers [83]. This parallel conversion increases the bit duration and so reduces the signal bandwidth. These narrowband signals are transmitted through the channel and are not sensitive to frequency selective fading of the channel. Within a time period, orthogonal subcarriers allow the efficient accommodation of many users as they do not interfere to each other, i.e. no ICI.

In late 1950s, classical multicarrier modulation systems were used to transmit the data over non overlapped band limited orthogonal signals in military with high frequency radio links. Since these systems demanded for high précised front-end devices to recover the each sub carrier without inter carrier interference, this concept did not get much attention that time. In January 1970, an U. S. patent gave the name of OFDM to this concept [3]. In 1971 [4] suggested the use of IDFT (inverse DFT)/DFT to generate/recover orthogonal subcarriers which eliminated the requirement of high précised front-end devices at the transmitter and receiver.

The invention of FFT, simplified the OFDM modem even more with fast DFT algorithm. In last two decades OFDM is the one of the MC technique which have become part of new emerging communication standards like Wireless MAN-Advanced, 3GPP2 Long Term Evolution (LTE) Advanced, Wireless Local Area Network (WLAN) and Digital Video Broadcasting - Terrestrial (DVB-T).

4.1 Principle of OFDM

The goal for designing a MC transmission scheme for a mobile wireless channel is that the channel is slow during one symbol duration and the fading over subcarriers is frequency non selective means flat [82]. For that the symbol duration should be

greater than the maximum delay spread of the channel and the subcarrier spacing should lesser than the coherence bandwidth of the channel. Thus the principle of MC communication is to convert a high rate serial data stream to the many low rate parallel data sub streams. Each of these sub streams is modulated on one of the subcarriers. Figure 4.1 shows an example of multi carrier communication with 4 sub carriers. As the symbol duration is increased, the subcarrier symbol rate is very less than the serial data rate; the delay spread impact is reduced allowing the less complex equalization.

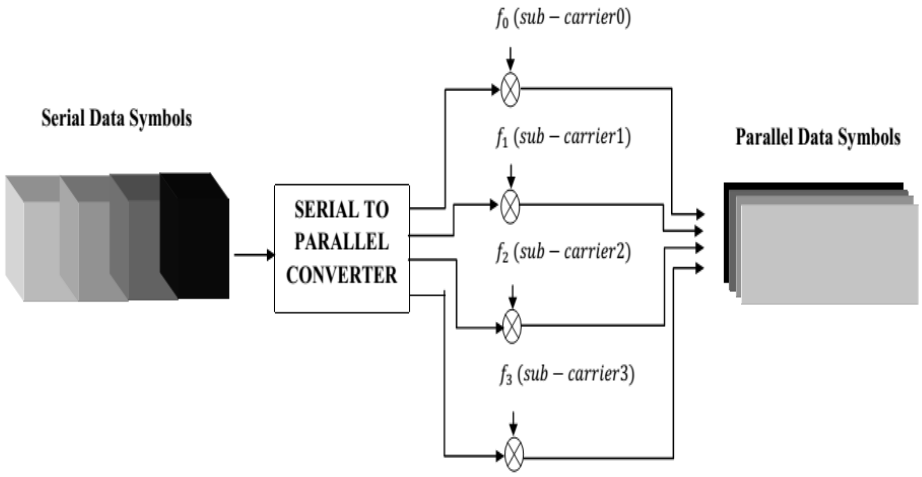

Figure 4.1 Multicarrier Modulation.

OFDM is a low complex modulation/multiplexing MC technique to modulate N orthogonal sub carriers with N complex valued source symbols $X_k,\ k = 0,1,\dots,N-1$, efficiently by using digital signal processing. The source symbol is achieved after source coding, interleaving, and channel coding if applicable. The source symbol duration T_d of the serial data symbol results in the OFDM symbol duration:

$$T_s = N\,T_d \tag{4.1}$$

after serial to parallel conversion. With rectangular pulse shaping, to achieve the orthogonality between the signals of N sub carriers, N sub carriers are having the sub carrier spacing:

$$\Delta f = \frac{1}{T_s}. \tag{4.2}$$

The N parrallel modulated source symbols $X_k, k = 0,1, \dots, N-1$ are referred as an OFDM symbol with T_s symbol duration and bandwidth $F_s = N\Delta f$. However OFDM follows the principle of frequency division multiplexing (FDM) to sent parallel data sub streams over a single radio channel but with the aid of orthogonal subcarriers OFDM is much spectral efficient than FDM. As shown in Figure 4.2 in conventional FDM, each transmitter uses a carrier frequency different than other and because of the non orthogonality a large band gap is required to eliminate the ICI, whereas in case of OFDM half of the bandwidth is saved because of the overlapped orthogonal sub carriers.

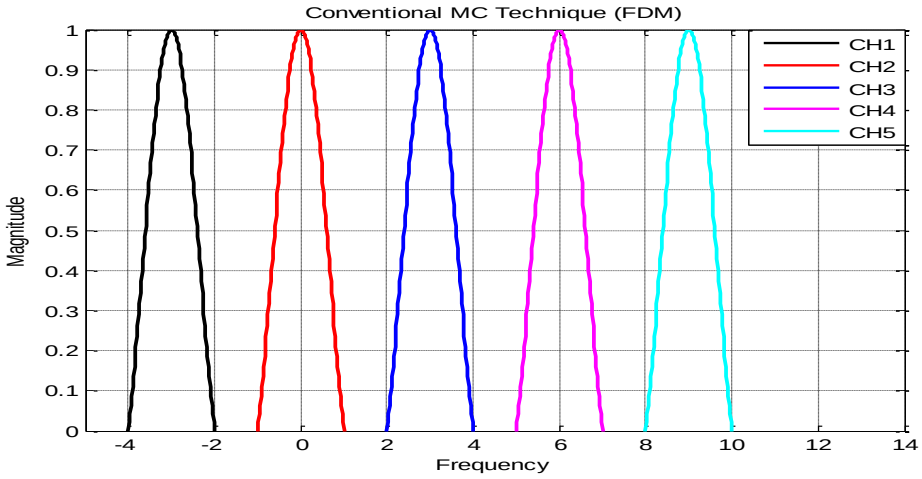

(a)

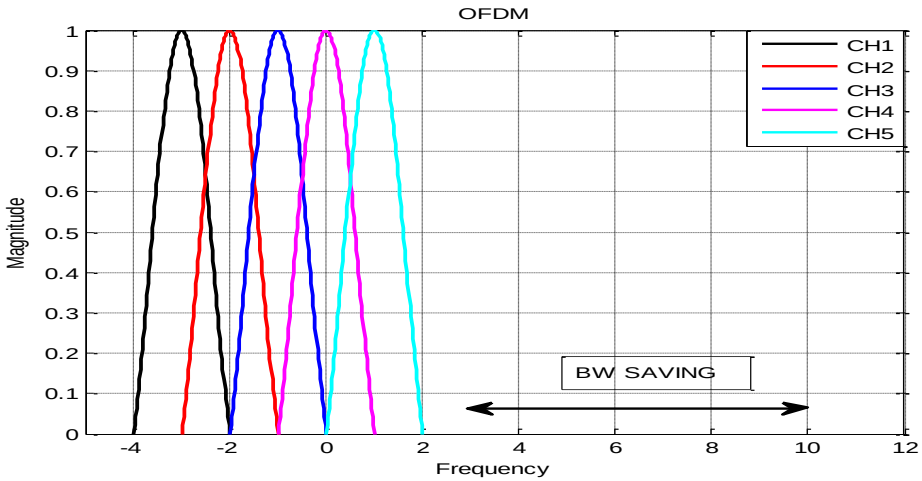

(b)

Figure 4.2 Comparison of Bandwidth Requirements in (a) Conventional FDM (b) OFDM.

Two signals which are mutually independent of each other are orthogonal signals and this orthogonality allows communication of multiple signals over a single radio channel with accurate detection. In context of the OFDM, orthogonality property can be described with its power density spectrum shown in Figure 4.3 for 5 orthogonal subcarriers. We can observe from Figure 4.3 that each sub carrier peak is coinciding with nulls of all others which validate the orthogonality in between the sub carriers of OFDM signal. Peaks are located at the center frequency with the gap of sub carrier spacing Δf.

As the number of subcarriers N increases, the spectrum approaches to single carrier modulation with ideal Nyquist filtering. As the symbol duration on each subcarrier increases, the time dispersion i.e. ISI, caused by frequency selective fading of the channel is reduced.

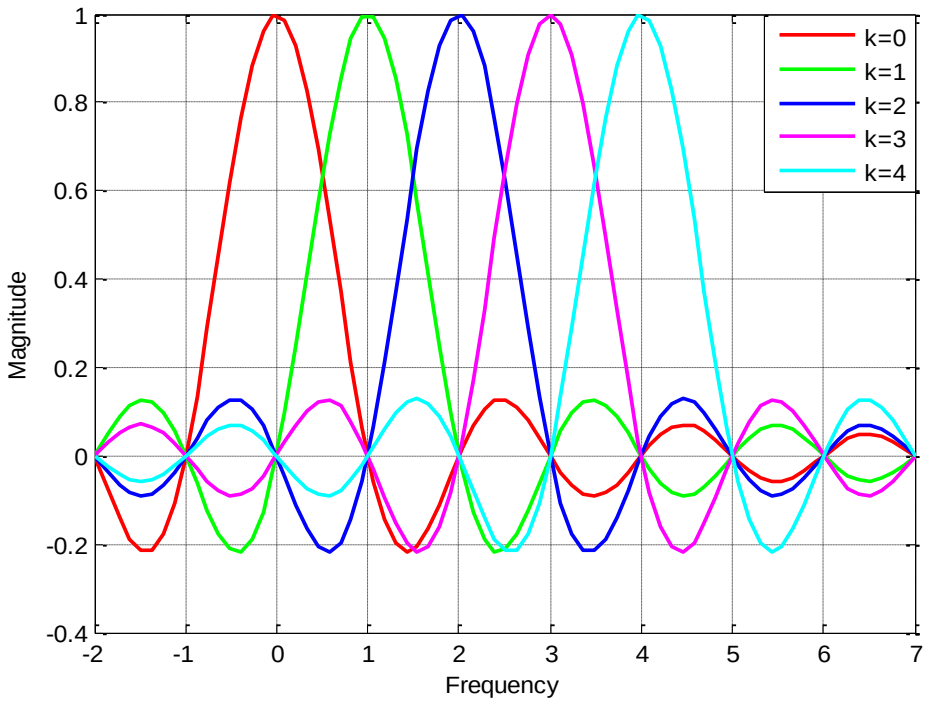

Figure 4.3 Spectrum of OFDM Signal with $N = 5$.

Though the parallel conversion increases the symbol duration T_d to $T_s = N\,T_d$ to reduce the ISI, but to completely eliminate the time depressiveness of the channel a guard time of duration:

$$T_{CP} \geq \tau_{max} \tag{4.3}$$

is inserted in between the consecutive OFDM symbols which enables the one tap low complex equalization at the receiver, where τ_{max} is the channel impulse response duration. The guard time is a cyclic prefix (CP) i.e. pre inserted cyclic extension of the OFDM symbol, to maintain the orthogonality and reduce the ICI, which extends the OFDM symbol duration:

$$T_s' = T_{CP} + T_s. \tag{4.4}$$

Figure 4.4 shows the time/frequency representation of an OFDM symbol and an OFDM frame. Block of N_S consecutive OFDM symbols is known as an OFDM frame where N_S is function of coding/spreading.

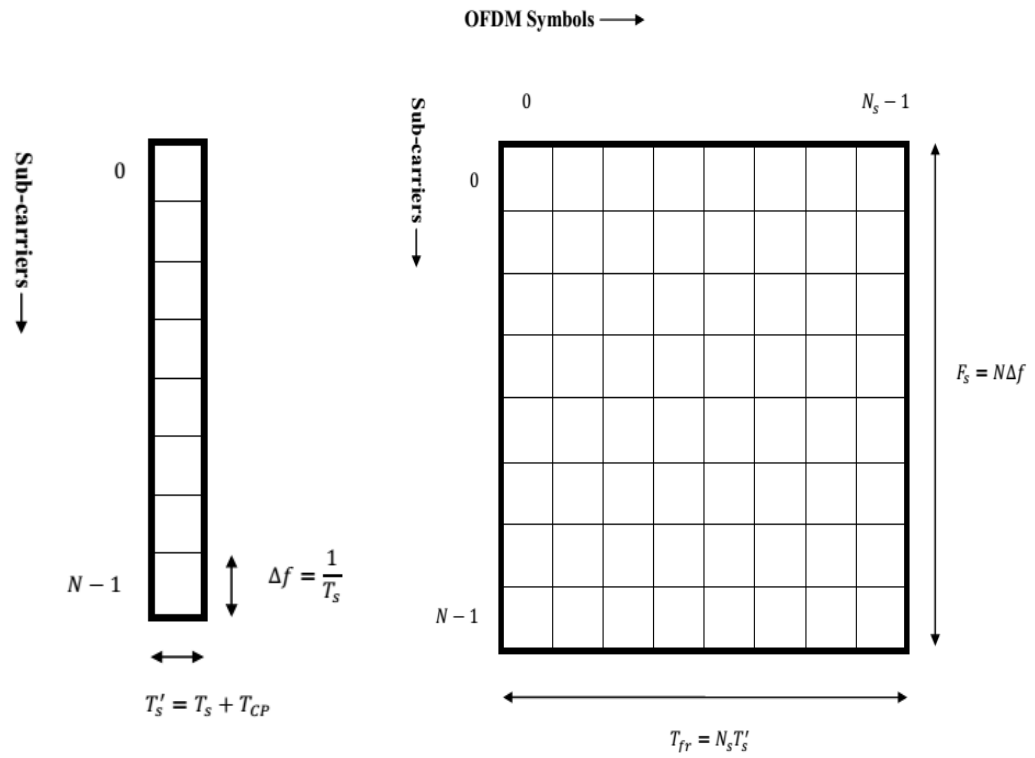

(a) (b)

Figure 4.4 OFDM (a) Symbol (b) Frame.

The main advantage of using OFDM as the multi carrier modulation technique lies in its implementation with IDFT and even more computationally efficient IFFT (inverse

FFT). If $X_k^m, k = 0,1, \dots, N-1$, is the frequency domain QAM modulated symbol on k^{th} subcarrier of m^{th} symbol then, $\mathrm{X}^m = [X_0^m, X_1^m, \dots, X_{N-1}^m]^T$ defines a symbol vector. Consequently the n^{th} sample of the discrete time baseband signal after taking IFFT is:

$$S_n^m = \frac{1}{N}\sum_{k=0}^{N-1} X_k^m e^{\frac{j2\pi kn}{N}}, \quad 0 \le n \le N-1. \tag{4.5}$$

The N_g discrete samples of the guard interval are inserted to prevent the ISI, where:

$$N_g = \left\lceil \frac{\tau_{max} N}{T_s} \right\rceil. \tag{4.6}$$

This results in:

$$S_n^m = \frac{1}{N}\sum_{k=0}^{N-1} X_k^m e^{\frac{j2\pi kn}{N}}, \quad -N_g \le n \le N-1. \tag{4.7}$$

This digital sequence is converted to analogue signal waveform $S^m(t)$ with duration T_S'. The $S^m(t)$ is up converted to the RF signal and transmitted over the channel. The channel can be additive white Gaussian Noise (AWGN) or multipath channel as applicable. Let the discrete time composite CIR with order L is denoted by $g(l)$ and the CTF on the k^{th} subcarrier is denoted by h_k, and then h_k can be given as:

$$h_k = \sum_{l=0}^{L-1} g(l) e^{\frac{-j2\pi kl}{N}}. \tag{4.8}$$

After RF down conversion, the received signal waveform, $r^m(t)$ is convolution of $S^m(t)$ with the continuous time CIR ($g(t,\tau)$) and addition of AWGN ($w^m(t)$). This received signal is passed through an A/D converter, where $r^m(t)$ is sampled with the rate N/T_s, which gives the output sequence $r_n^m, n = -N_g, \dots, N-1$. N_g Samples, in which ISI is present, are removed before OFDM demodulation. Denoting the discrete time AWGN impairment to the m^{th} symbol by w_n^m, the received OFDM signal after down & analogue to digital conversion and CP removal can be written as:

$$r_n^m = [S_n^m \otimes g(n)] + w_n^m, \qquad 0 \le n \le N-1 \tag{4.9}$$

where $\otimes$ denotes the circular convolution. Since the N_g samples of the received sequence are removed which only contains the ISI, after taking the FFT of r_n^m, the frequency domain received signal on the k^{th} subcarrier of the m^{th} symbol is without ISI and ICI and is given by:

$$y_k^m = X_k^m h_k + W_k^m \qquad 0 \le k \le N-1 \tag{4.10}$$

where X_k^m is k^{th} element of symbol vector X^m, h_k is the k^{th} element of channel vector $\mathrm{h} = [h_0, h_1, h_2, \dots, h_{N-1}]^T$, W_k^m is AWGN in frequency domain. It is preferable to represent the signal model in matrix form as:

$$\mathbf{Y}^m = \mathbf{D}^m \mathbf{F}\mathbf{g} + \mathbf{W}^m \tag{4.11}$$

where $\mathbf{Y}^m = [y_0^m, y_1^m, \dots, y_{N-1}^m]^T$, $\mathbf{F}$ is the $N \times L$ DFT matrix with $F(n,l) = exp\left(-\frac{j2\pi nl}{N}\right)$, $\mathbf{D}^m = diag[X_0^m, X_1^m, \dots, X_{N-1}^m]$ and $\mathbf{g} = [g(0), g(1), \dots, g(L-1)]^T$ is the time domain channel vector. $\mathbf{W}^m = [W_0^m, W_1^m, \dots, W_{N-1}^m]^T$, is an uncorrelated white noise vector distributed as, $\Pr(\mathbf{W}^m) = C\mathcal{N}(0, 2\sigma_\omega^2\mathbf{I})$ with mean zero and covariance matrix $2\sigma_\omega^2\mathbf{I}$, which says:

$$\Pr(\mathbf{W}^m) = \frac{1}{(2\pi)^N \sigma_\omega^{2N}} \exp\left(\frac{-1}{2\sigma_\omega^2} \mathbf{W}^{mH} \mathbf{W}^m\right). \tag{4.12}$$

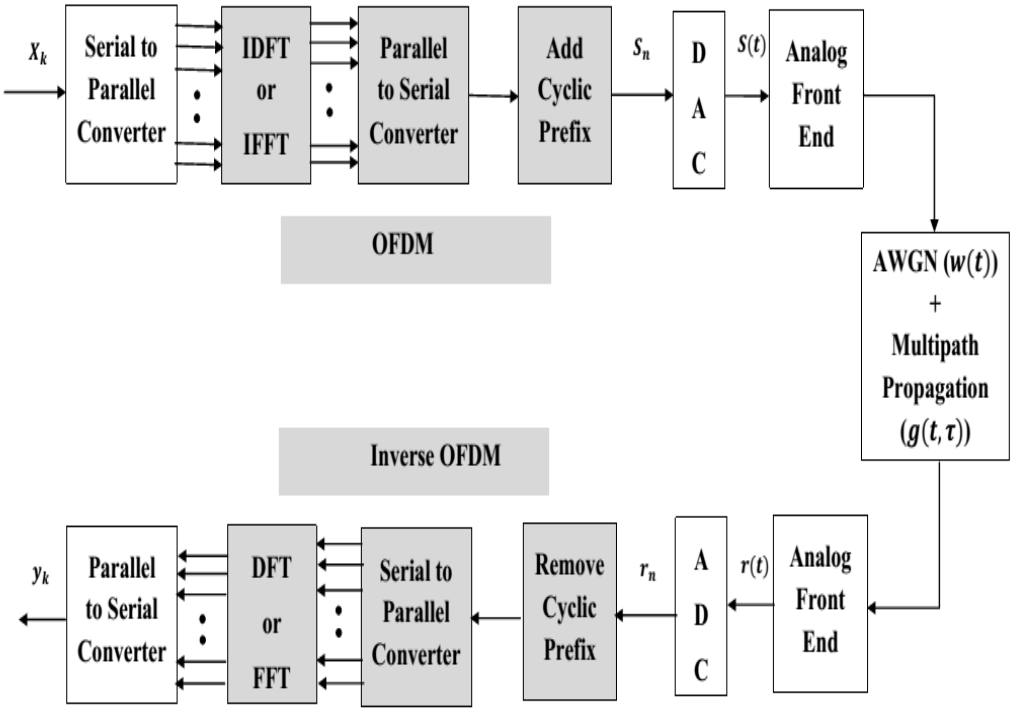

Figure 4.5 OFDM Modulation and Demodulation.

As $\mathbf{h} = \mathbf{Fg}$, Equation (4.11) can be rewritten as:

$$\mathbf{Y}^m = \mathbf{D}^m\mathbf{h} + \mathbf{W}^m \tag{4.13}$$

where $\mathbf{h} = [h_0, h_1, h_2, \dots, h_{N-1}]^T$.

Figure 4.5 illustrate the basic block diagram for multi carrier communication system with the OFDM modulation/Demodulation employing IDFT (IFFT)/ DFT (FFT).

Performance, in the term of SER, of the OFDM system is simulated in Figure 4.6, where each simulation point is conducted using 10,000 OFDM symbols in MATLAB. Simulation model is based on IEEE 802.11g like system with parameters given in Table 4.1.

OFDM symbols are generated using 16- quadrature amplitude modulation (QAM) and 64-point IFFT, and then prepended by CP of length 16 samples before transmitting over the channel. The channel is AWGN or multipath channel as applicable. For multipath channel the discrete sampled CIR is modelled as, $L = 10$ tapped delay lines having an exponentially decreasing power delay profile (PDP):

$$\alpha_l^2 = E\{|g(l)|^2\} = \frac{1}{\gamma} exp(-0.5l), l = 0,1,..,L-1 \tag{4.14}$$

where $\gamma = \sum_l exp(-0.5l)$, is choosen to normalise the PDP to unit energy. The 64-point FFT of the received signal is taken after CP removal.

F_s	20 MHz
N	64
FFT Size	64
N_g	16 Samples
Mapping	16-QAM

Table 4.1 OFDM Modeling Parameters.

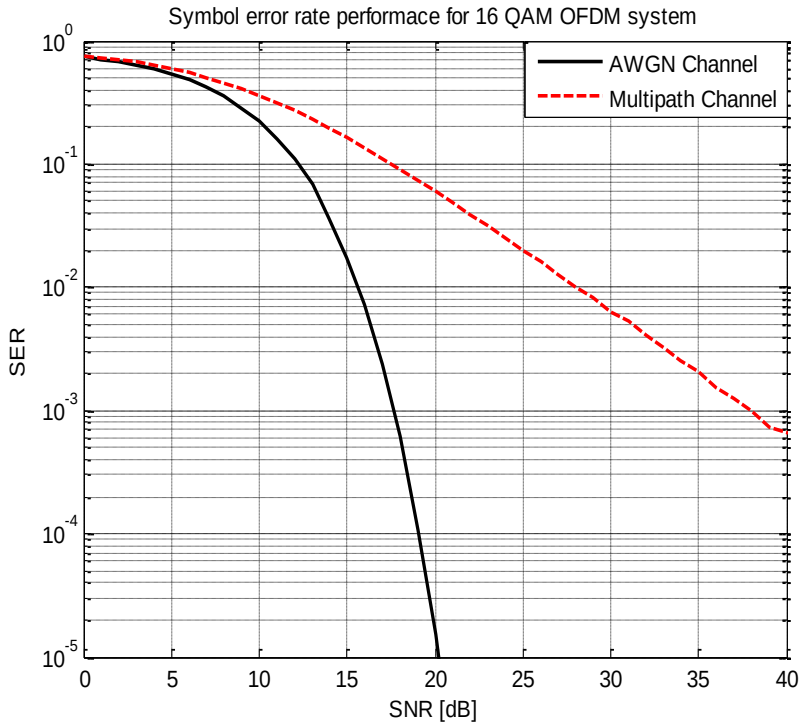

Figure 4.6 16-QAM OFDM SER Performance.

4.2 Advantages of OFDM

In OFDM the wideband wireless radio channel with frequency-selective fading is turned into a set of narrow-band channels (the subcarriers) with flat fading (NO ISI) which makes the data symbol resilient against multipath fading with **one tap easy frequency domain equalization** (FDE) at the receiver side.

The orthogonality between densely spaced subcarriers makes the system **resilient against the ICI** while abandoning the requirement of steep and precise band pass filters for detection and gives the **optimum spectrum utilization** too. **Efficient digital signal processing** with IFFT/FFT and FDE makes the OFDM a **low complex application for the MIMO principle**.

In OFDM each burst allocation can be changed from frame to frame as well as the modulation order. This allows the base station to **dynamically adjust the bandwidth** usage according to the current system requirements. The bandwidth of the operation can vary from country to country, depending upon the spectrum allocation. This tends to variations in the OFDM parameters like the subcarrier spacing and the OFDM symbol period which further needs the flexibility in hardware design.

Secondly with different subcarrier spacing the Doppler spread effect and frequency offset get change which demands for modifications in baseband algorithms. As to make the RF front-end flexible to accommodate difference in bandwidths is easier than changing the baseband algorithms which are applied to compensate the channel's deleterious impacts, bandwidth scalability is used. As shown in Figure 4.7, **bandwidth scalability** is easy to apply in case of OFDM by just adjusting the FFT size. This scaling of bandwidth, while maintaining the subcarrier bandwidth and symbol duration, produces minimal impact to higher layers.

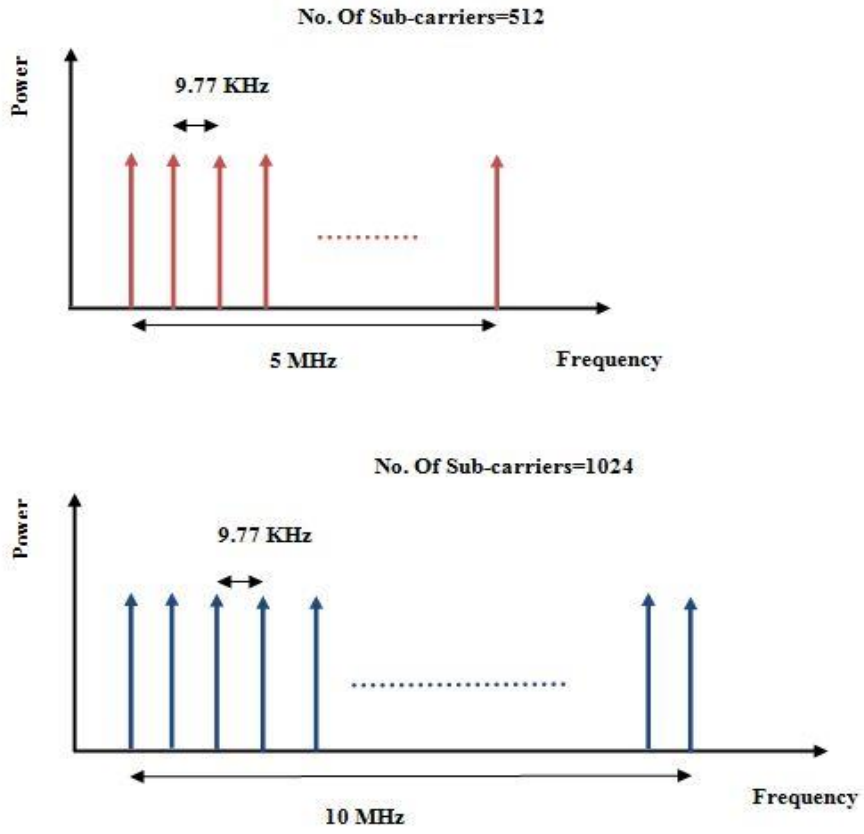

Figure 4.7 Bandwidth Scalability in OFDM.

The capacity increment by using **adaptive channel coding and modulation**, and **adaptive spreading**, are also the key advantages of OFDM technique.

4.3 Challenges of OFDM

With all the advantages of MC transmission to guarantee a high spectral efficiency with a low cost receiver a reliable and robust digital synchronization and channel estimation is mandatory in OFDM with IFFT/FFT operation. Especially in fading channel when high order modulation schemes are employed with coherent detection, synchronization is even critical.

The **synchronization** unit of OFDM demodulator (Figure 4.8) is including the time and frequency synchronization units. These synchronizations are performed with digital algorithms which are either based on blind synchronization (uses intrinsic redundancy of CP of each OFDM symbol) or pilot aided synchronization (uses dedicated data which are frequency/time multiplexed with transmitted data).

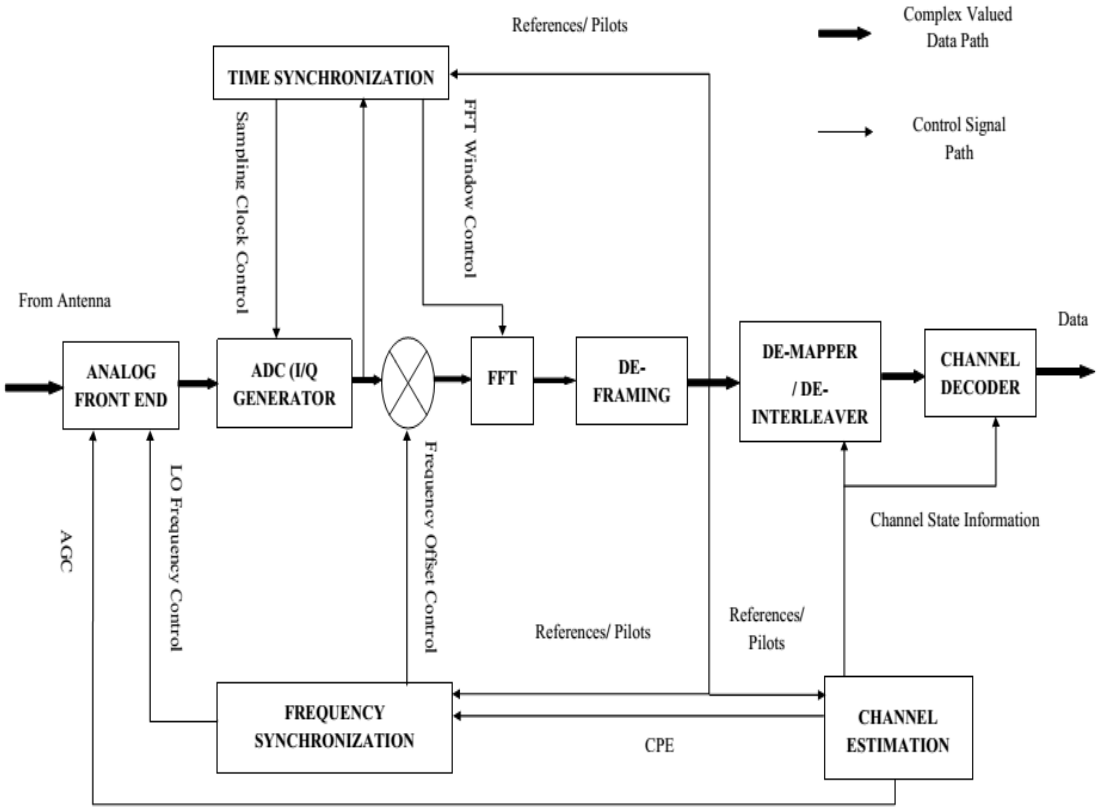

Figure 4.8 Synchronization Unit of OFDM Demodulator.

The main objective of **time synchronization** for OFDM systems is to know when a received OFDM symbol starts. By using the guard time, the timing requirements can be relaxed. If a timing error is small enough to keep the channel impulse response within the guard time, the orthogonality is maintained and a symbol timing delay can be viewed as a phase shift introduced by the channel which can be estimated and corrected at channel estimation stage. However, if a time shift is larger than the guard time, ISI and ICI occur and signal orthogonality is lost. The time synchronization is to estimate the FFT window positioning (OFDM symbol/frame synchronization) and sampling rate for analogue to digital conversion control (I/Q balance). The operation of time synchronization can be carried out in two steps: coarse and fine symbol timing.

As a MC system is much more sensitive than a SC system, to a carrier frequency offset (CFO), another essential function of an OFDM demodulator is the **frequency synchronization**. Difference in oscillator frequencies of the transmitter and receiver, Doppler shifts, and **PHN** produces the frequency offset. This frequency offset leads to a reduced amplitude signal and to a loss of orthogonality between sub-carriers which introduce ICI. Like time synchronization, frequency synchronization can be performed in two steps: coarse and fine frequency synchronization. An **automatic gain control** (AGC) signal for the incoming analogue signal is also needed to adjust the gain of the received signal to its desired values.

The simplified OFDM transmitter front end (Figure 4.9) consists of an I/Q generator with a local oscillator, low pass filters, channel band pass filters, mixers and high power amplifiers (HPAs). The receiver front end is also having the similar components. Unfortunately the HPAs are non linear devices and MC modulated systems using OFDM are more sensitive to HPA non linearity than SC modulated systems. Because of the superposition of N narrowband signals in time domain, OFDM signal have a **high peak-to-average power ratio (PAPR)**. This requires the higher output back-off values with HPAs to keep an acceptable performance, otherwise leading to severe clipping effects. At high carrier frequency the RF transmitter and receiver oscillators increase the infrastructure cost, so low cost transceivers ’oscillators are employed with the cost of higher **PHN**.

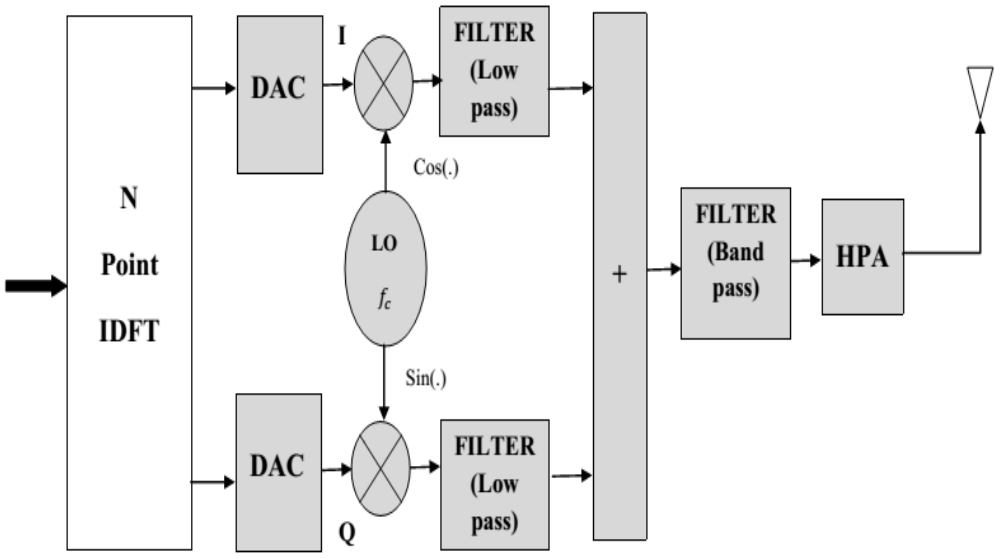

Figure 4.9 OFDM Transmitter Front End.

OFDM without guard time is an optimum spectrum utilizing system, and its optimum normalized efficiency approaches to 1 bit/s/Hz with large number of subcarrier. But in the digital implementation of OFDM (Figure 4.10), the guard time T_{CP} (or N_g samples) inserted after the IDFT operation at the transmitter side produces the loss in spectral efficiency and the spectral efficiency reduces to:

$$Eff_{sptr} = 1 - \frac{T_{CP}}{T_S + T_{CP}} \; for \; large \; N. \tag{4.15}$$

The number of the FFT points, N decides about the complexity of the operation which is of $\mathcal{O}(NlogN)$. Large value of N results in long T_S, and makes the system vulnerable to the time variant nature (Doppler spread) of the channel and more sensitive to the transceiver PHN. At the same time long T_S improves over spectrum utilization while reducing the loss due to T_{CP}. So a trade off is maintained in between spectrum utilization and sensitivity to Doppler spread and transceiver PHN.

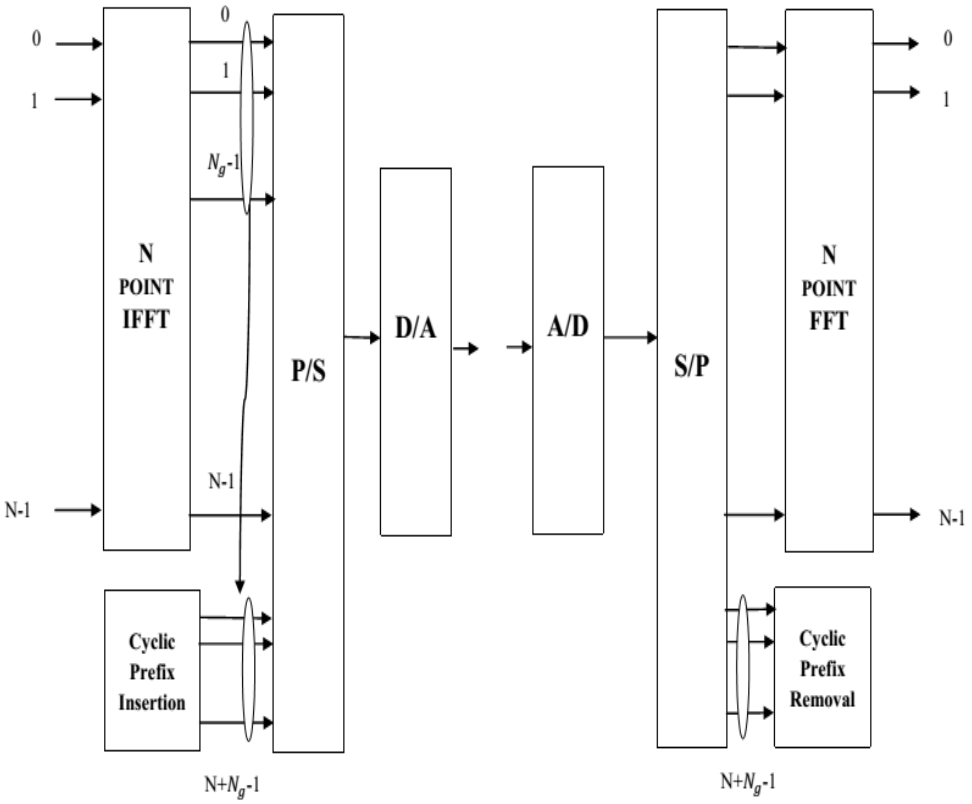

Figure 4.10 Digital Implementation of OFDM.

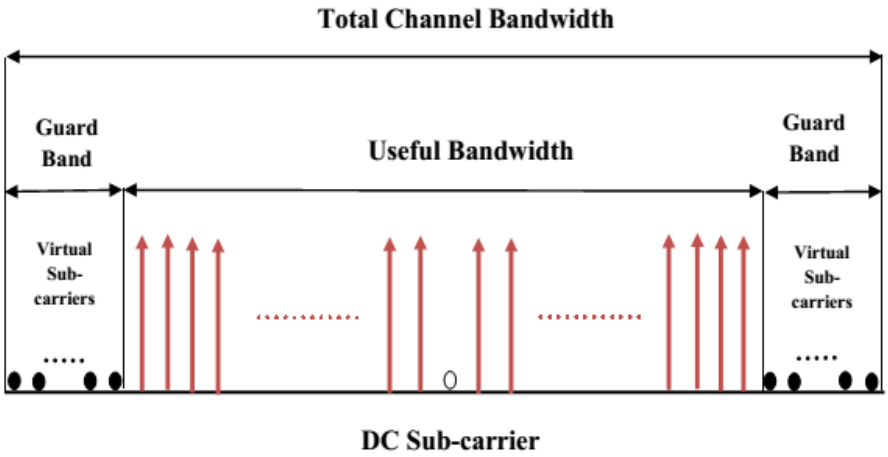

Figure 4.11 Virtual Subcarriers used for Filtering.

To simplify the design and implementation of filters while achieving the high frequency resolution in the channel bandwidth, slightly higher numbers of FFT points are employed than required data transmission subcarriers. This implementation facilitates with null subcarriers (guard band), also called virtual subcarriers at both sides of the spectrum (Figure 4.11). As the DC component creates a very low frequency which cannot be passed through a band pass filter a DC problem arises in OFDM too. To avoid this, a null subcarrier is put in the middle of the spectrum known as DC subcarrier and is not used for transmission.

The main advantage of an OFDM transmission and reception is the digital implementation of an OFDM system with FFT processing which makes it the preferable choice for wireless services. This necessitates that the digital signal after digital IFFT processing is converted back to the analogue domain with a digital to analogue (D/A) converter, for IF/RF up conversion at the transmission side and vice versa (A/D conversions) at the receiver side. The accuracy required for the used constellation, the difference between the receiver sensitivity and the maximum received power and the sampling rate are some of the prime parameters which decide about the number of bits reserved for the D/A and A/D conversions.

Further, at the receiver side, converter should be more accurate due to a higher disturbance. So practically to achieve satisfactory trade-offs between the performance and implementation complexity, for 16 to 64- quadrature amplitude modulation (QAM) transmission, 6-8 bits or higher should be used with D/A converters, and for the receiver A/D converters, 8-10 bits or higher are used. To avoid aliasing, the sampling rate is a crucial parameter. The sampling rate should be at least twice the maximum frequency of the signal which is theoretically maintained by choosing:

$$f_{samp} = F_s = \frac{1}{T_{samp}} = \frac{N}{T_s} \ . \tag{4.16}$$

Whereas practically in regards of adjacent channel interference, to achieve a better channel selectivity in the receiver, a higher sampling rate:

$$f_{samp} \geq \frac{N}{T_s} \tag{4.17}$$

which is greater than the channel bandwidth is recommended.

4.4 Phase Noise Impaired OFDM System Modeling

There are many transceivers' impairments that are to be taken in to consideration while designing an OFDM communication system. Still there is a convincing reason to focus on the PHN precisely as CFO and I/Q imbalance impairments are constant over time whereas the PHN is of time varying nature. Hence, one can measure CFO and I/Q imbalance in training phase and then can compensate these in data transmission stage. As such an approach cannot be adopted for PHN; it is likely to be most dominant impairment in data transmission stage. Since, in OFDM, very high quality transceiver oscillators are needed, which increase the cost, it is preferable to mitigate the effect of the PHN in digital domain to ensure the performance of system.

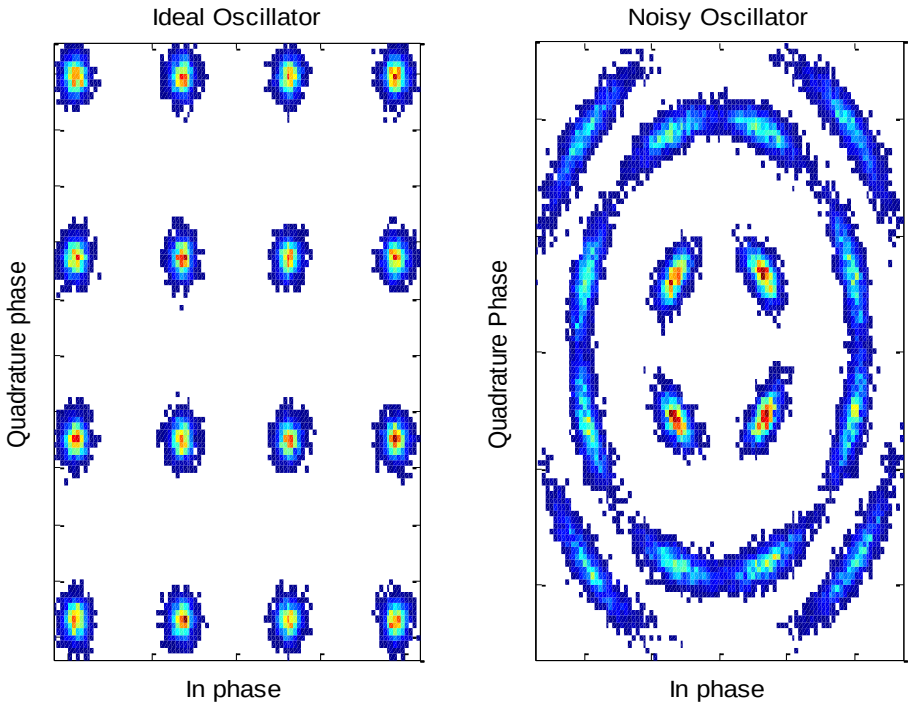

Figure 4.12 Effect of Phase Noise in SC Communication System (Random rotation in constellation).

OFDM is much more vulnerable to PHN than SC systems [84]. In SC systems, the phase noise merely causes simple random rotation in the symbol constellation known as CPE. Figure 4.12 (a) shows the received signal constellation of a SC, 16 -QAM modulation over an AWGN channel (SNR=30dB) whereas the effect of PHN from an

FRO (PHN variance=.06 rad^2), on received signal constellation is shown in Figure 4.12 (b).

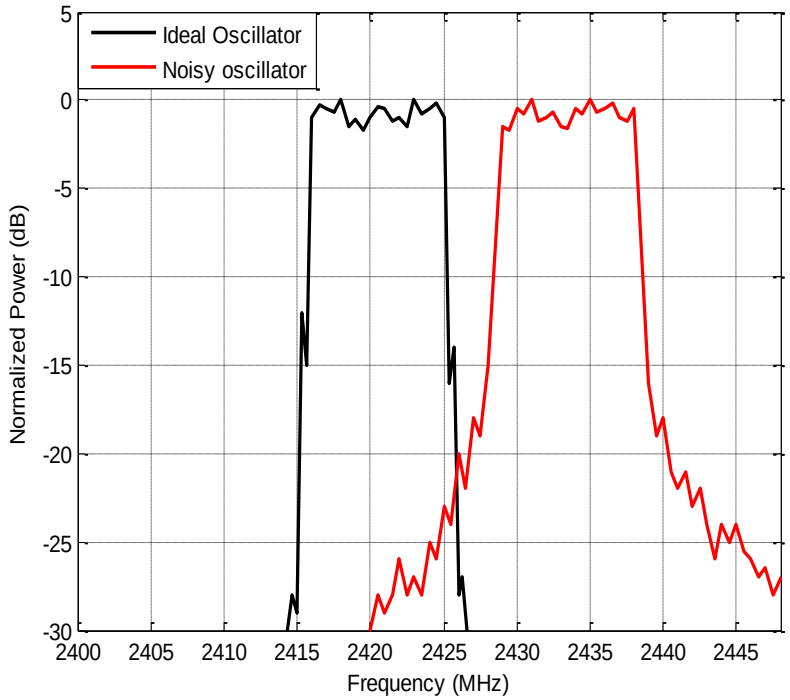

Figure 4.13 Effect of Phase Noise in MC Communication system (Spectral Re-growth (in-band-ICI) (out-of- band -MUI)).

In OFDM systems, in addition to the rotational effect, PHN also causes ICI. The ICI is present because PHN causes energy of individual subcarriers to spread on the top of all the other subcarriers [85-87]. Figure 4.13 shows two systems with the bandwidth of 22MHz where first system employs the ideal oscillator without PHN with carrier frequency 2420.5 MHz whereas second system uses a noisy FRO (PHN variance=.06 rad^2) with carrier frequency 2433.5 MHz, which cause spectral re-growth and results in power leakage to the first band, producing the ICI.

Figure 4.14 (a) shows the received signal constellation of an OFDM system with 64 subcarriers which are, 16 -QAM modulated whereas the impact of an AWGN channel (SNR=35dB) is shown in Figure 4.14 (b).

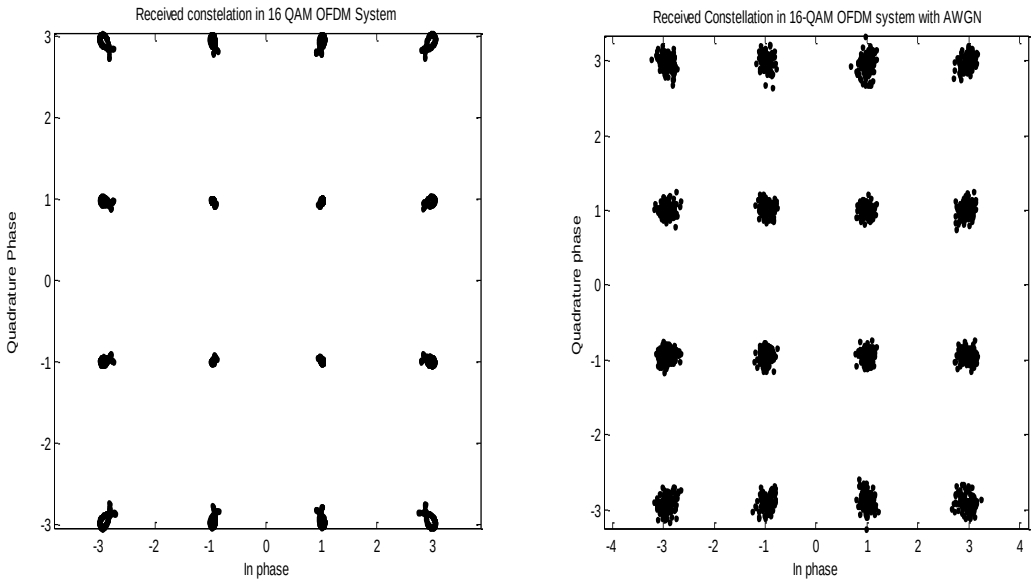

(a) (b)

Figure 4.14 Received Constellation in (a) 16-QAM OFDM System (b) with AWGN.

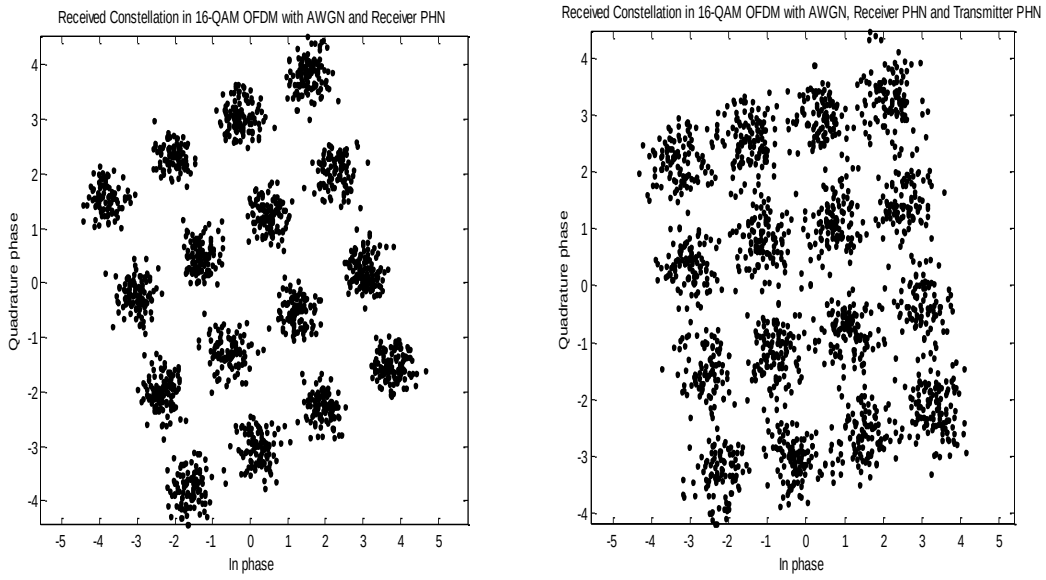

(a) (b)

Figure 4.15 Received Constellation in 16-QAM OFDM System with (a) Receiver Phase Noise (b) Transceiver Phase Noise.

Figure 4.15 (a) shows the received signal constellation of an OFDM system with 64 sub-carriers which are, 16 -QAM modulated over AWGN (SNR=35dB) with receiver PHN (both CPE and ICI) from an FRO (PHN variance=.06 rad^2) whereas the effect of receiver as well transmitter PHN from an FRO (PHN variance=.06 rad^2), on received

signal constellation is shown in Figure 4.15 (b). The constellation rotation is produced because of the CPE whereas the cloudy constellation is impact of ICI.

The effect of PHN on BER of the OFDM system (Table 4.1) before compensating it is shown in Figure 4.16 for receiver FRO PHN (PHN variance=.06 rad^2) only and for transceiver FRO PHN (PHN variance=.06 rad^2) and is compared against the BER of pure AWGN channel.

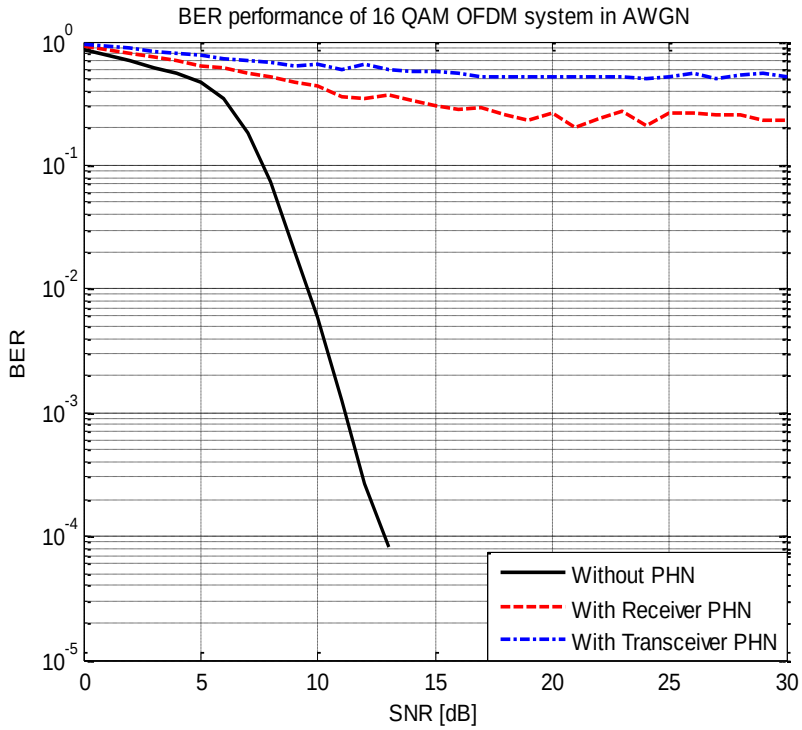

Figure 4.16 16-QAM OFDM BER Performance in AWGN Channel with Phase Noise.

In this work we are considering packet transmission of OFDM symbols in which a packet consists of several consecutive OFDM symbols. Few initial symbols are full pilot and followed by pay load. In payload symbols data and pilot subcarriers are multiplexed together.

At the receiver side, full pilot symbols are used for channel estimation while the data vector is assumed to be known. At the time of payload receiving channel is exactly known. Figure 4.17 is illustrating this packet structure.

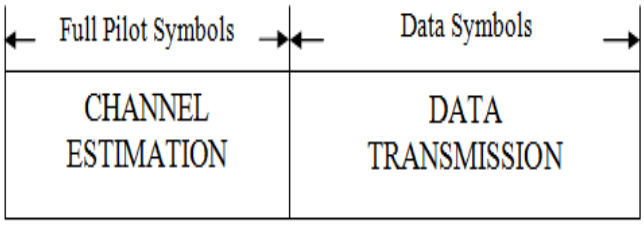

Figure 4.17 OFDM Packet Structure.

Further to model an OFDM system with receiver PHN consisting of N subcarriers with sampling instant T_s/N we denote the discrete time receiver PHN impairment to the n^{th} subcarrier of the m^{th} symbol by θ_n^m than the received OFDM signal after down conversion and CP removal can be written as:

$$r_n^m = [S_n^m \otimes g(n)]e^{j\theta_n^m} + w_n^m,\ 0 \le n \le N-1. \tag{4.18}$$

If $\theta^m = [\theta_0^m, \theta_1^m, \dots \theta_{N-1}^m]^T$, is the PHN vector for the m^{th} OFDM symbol, then:

$$\mathrm{P}^m = [p^m_{-\frac{N}{2}}, p^m_{-\frac{N}{2}+1}, \dots, p_0^m, \dots, p^m_{\frac{N}{2}-2}, p^m_{\frac{N}{2}-1}]^T \tag{4.19}$$

defines a vector of the DFT coefficients of one realization of $e^{j\theta_n}$ during m^{th} OFDM symbol where:

$$p_k^m = \frac{1}{N}\sum_{n=0}^{N-1} e^{j\theta_n^m} e^{\frac{-j2\pi nk}{N}},\ -\frac{N}{2} \le k \le \frac{N}{2}-1 \tag{4.20}$$

After taking the FFT of r_n^m, the frequency domain received signal on the k^{th} subcarrier of the m^{th} symbol is:

$$y_k^m = \sum_{q=0}^{N-1} X_q^m h_q p^m_{\langle k-q\rangle} + W_k^m, 0 \le k \le N-1 \tag{4.21}$$

where X_q^m is q^{th} element of symbol vector X^m, h_q is the q^{th} element of channel vector $\mathrm{h} = [h_0, h_1, h_2, \dots, h_{N-1}]^T$, W_k^m is AWGN in frequency domain and $p^m_{\langle k-q\rangle}$ is the $(k-q)^{th}$ spectral component of PHN spectral component vector, P^m, with modulo N indexing. Further note that with modulo N indexing, the lower order spectral components of PHN are given by $p_0, p_1, p_{N-1}, p_2, p_{N-2}$ etc. For convenience of the later analysis it is preferable to represent the signal model in matrix form as:

$$\mathbf{Y}^m = \mathbf{H}^m\mathbf{P}^m + \mathbf{W}^m \tag{4.22}$$

where

$\mathbf{Y}^m = [y_0^m, y_1^m, \dots, y_{N-1}^m]^T$, $\mathbf{P}^m = [p_0^m, p_1^m, \dots, p_{N-1}^m]^T$, $\mathbf{h} = [h_0, h_1, h_2, \dots, h_{N-1}]^T$,

$\mathbf{X}^m = [X_0^m, X_1^m, \dots, X_{N-1}^m]^T$ and $\mathbf{H}^m$ is a column wise circulant matrix whose first column is vector $[h_0X_0^m, h_1X_1^m, \dots, h_{N-1}X_{N-1}^m]^T$. $\mathbf{W}^m = [W_0^m, W_1^m, \dots, W_{N-1}^m]^T$, is an uncorrelated white noise vector distributed as, $\Pr(\mathbf{W}^m) = \mathcal{CN}(0, 2\sigma_\omega^2\mathbf{I})$ as given in Equation (4.12).

4.5 Conclusion

OFDM, as a low complex modulation technique, became the potential contender for MC transmission to combat the frequency selectivity of the channel. The synchronization unit (including the time and frequency synchronization units) of OFDM demodulator is performing the robust digital synchronization and channel estimation with digital algorithms. The presence of transceiver PHN degrades the OFDM system performance because of the rotational effect CPE and spectral re-growth ICI. Mathematical modeling for OFDM system, without and with PHN, is presented and system performance is simulated for packet transmission of OFDM symbols in AWGN and multipath channel.

5. Orthogonal Frequency Division Multiple Access

OFDM has established itself as a popular transmission technique for wireless mobile services in frequency selective fading environment. It can be used in combination with various multiple access schemes, such as OFDM combined with time division multiple access (TDMA) (OFDM-TDMA), OFDM combined with code division multiple access (CDMA)(MC-CDMA) and OFDMA [16].

In case of OFDM-TDMA, multiple users are handled by allocating the users with different time slots where multiple of symbols are separated in time but not in frequency grid. As shown in Figure 5.1 all the subcarriers are used by the one of the users for a finite number of OFDM symbol duration [13].

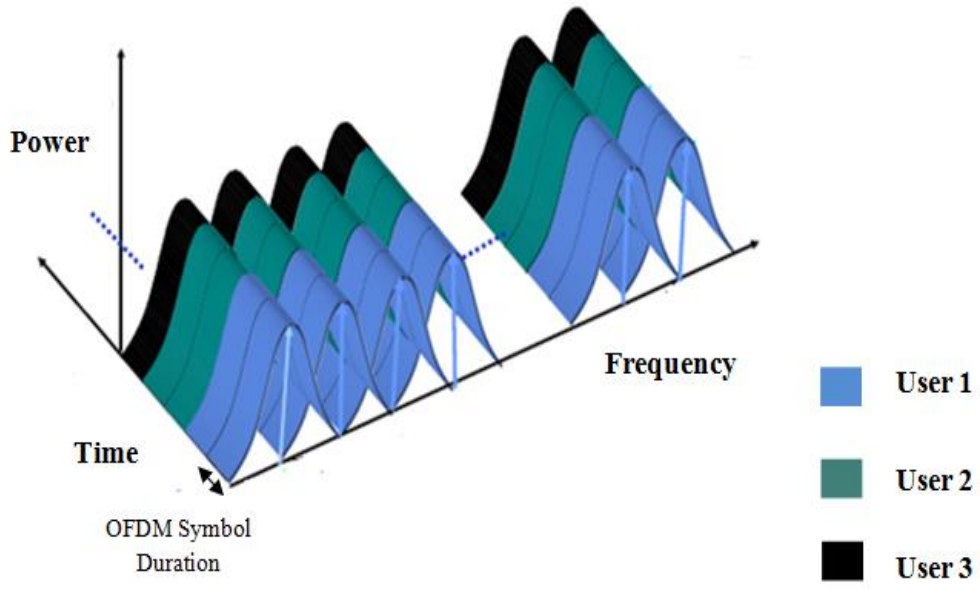

Figure 5.1 OFDM-TDMA Time-Frequency-Power Grids [13].

Combination of OFDM and CDMA known as MC- CDMA, handles the multiple users with different spreading codes. In this case the multiple signals of many users

do overlap in both time and frequency domain but can be separated with applying the right spreading code at the receiver side [83].

In OFDMA system, both the time and frequency resources are used to separate the multiple users. As OFDMA is typically used with burst transmission and a burst consists of many OFDM symbols. In an OFDM symbol there are many subcarriers. So, a subcarrier in frequency domain and symbol duration in time domain is the finest unit. The combination of a time unit and a frequency unit, i.e. a symbol period and a subcarrier is the finest slot which or group of which is allocated to one of the multiple users. Figure 5.2, is showing the time frequency and power grid of OFDMA [13, 15].

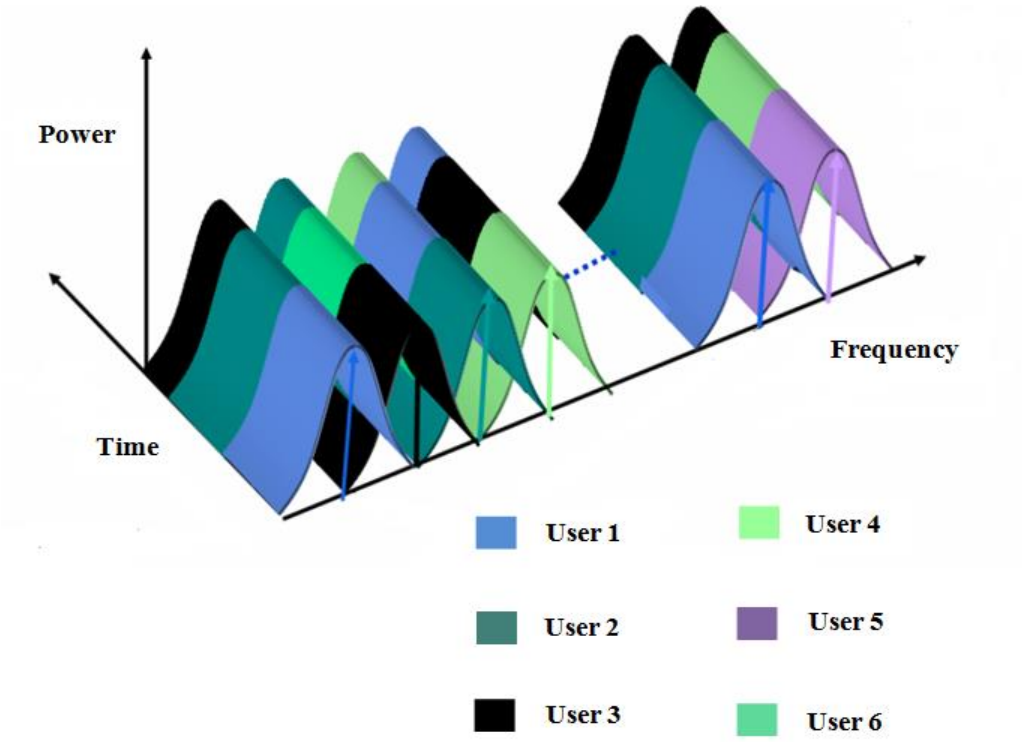

Figure 5.2 OFDMA Time-Frequency-Power Grids [13].

Practically, in frequency domain the allocation is not done at the level of subcarriers but on the group of subcarriers. This subcarriers' allocation is known as sub channelization and is discussed in the later section.

5.1 Principle of OFDMA

To explain the basic principle of OFDMA transceiver we are considering here that one user is using one subcarrier in the given time slot, i.e. number of users $(U) = N$. With this the simplest OFDMA uplink scheme is illustrated in Figure 5.3. At the transmitter side (mobile terminal) each user is having individual transmitters. At the receiver side (base station) the received signal is the sum of U users' signal which acts as an OFDM signal. Because of this in OFDMA receiver, a single MC-demodulator (OFDM demodulator) is required than U demodulators as in case of conventional frequency division multiple access (FDMA) system. At the transmitter side a single transmitter consists of symbol generator and OFDMA modulator. The symbol is generated with applicable channel coding and mapping. These symbols are then OFDMA modulated with sub channelization and SC modulator (in case of $U = N$) or OFDM modulator in case a single user is using group of the sub carriers.

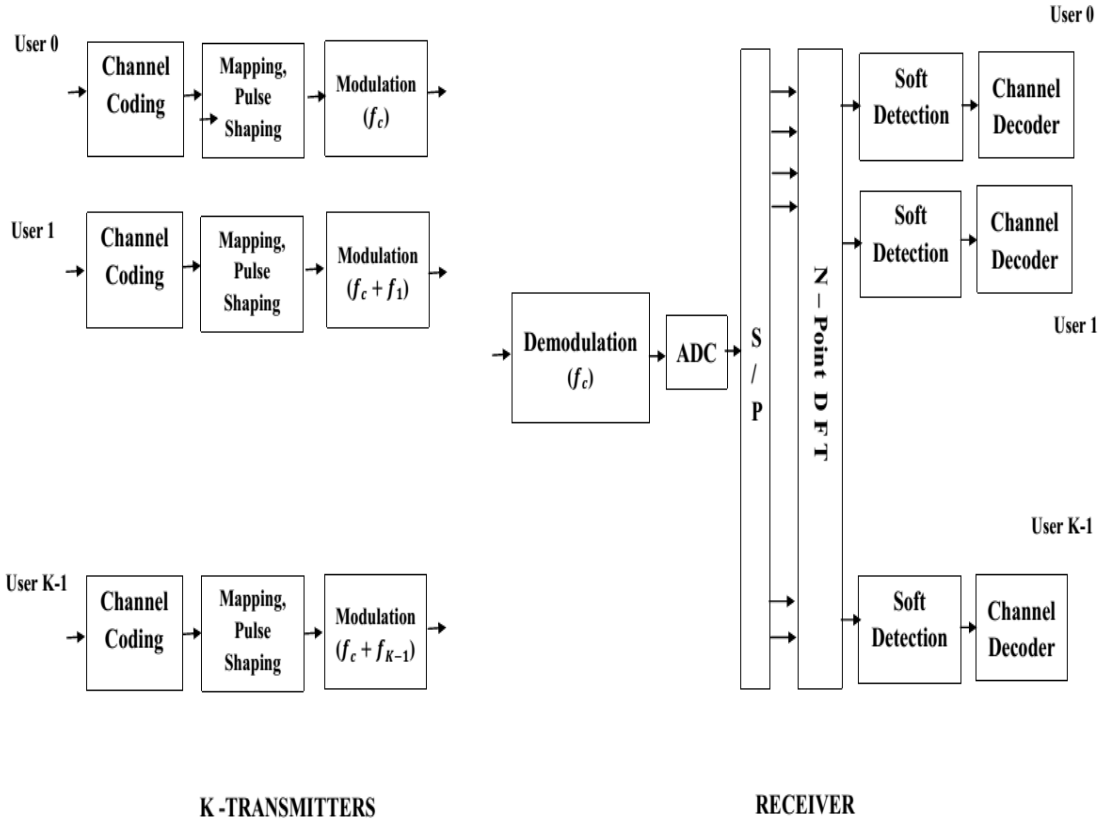

Figure 5.3 OFDMA Uplink.

An exact clock and carrier synchronization is must for an OFDMA system to ensure orthogonality between the U modulated signals from different mobile terminals. This is achieved by transmitting synchronization signals from the receiver to all mobile terminals instantly. Each terminal OFDM modulator drives the carrier frequency and clock signal from these downlink signals. In case of coherent detection, simple carrier and clock recovery circuits are sufficient in the demodulator to extract this information from the received signal as the clock and carrier frequencies are available at the base station. This factor simplifies the OFDMA demodulator.

5.2 Sub Channelization in OFDMA

In frequency domain the allocation is not done at the level of subcarriers but on the group of subcarriers known as sub channel. The sub channel is a group of subcarriers in same burst but might be in different time slots. This grouping of subcarriers can be done in two different ways: Contiguous mapping and Interleave mapping [13, 15-16].

In contiguous mapping a sub channel is group of adjacent subcarriers. Here the number of subcarriers in a sub channel is predefined. In figure 5.4, the time frequency grid of an OFDMA burst containing 4 symbols and 10 subcarriers is shown. One sub channel is group of 2 subcarriers. The contiguous mapping can be further divided in two categories depending on that how these sub channels are allocated to the different users within a time slot. If a user within a time slot is allocated with all the sub channels consecutively than it is called Consecutive contiguous mapping and if not consecutive sub channels than it is Block wise contiguous mapping. In Figure 5.4 the given burst is divided in 20 sub channels contiguously, where user 1and 2 are using 5-5 sub channels and user 3 and 4 are using 6 and 4 sub channels respectively. Figure 5.4 (a) is showing the above resource allocation in consecutive contiguous mapping where the Figure 5.4 (b) is using the Block wise contiguous mapping. Contiguous mapping is also known as Localized mapping. In contiguous mapping the channel frequency response is expected to be correlated very strongly within sub channel and this unit will have the same channel feedback for the adaptive modulation and coding and thus reducing the overhead. At the same time it will be very sensitive for the highly frequency selective fading environment. The block wise contiguous mapping

can overcome the problem of frequency selective fading sensitivity with the advantage of lesser overhead [88].

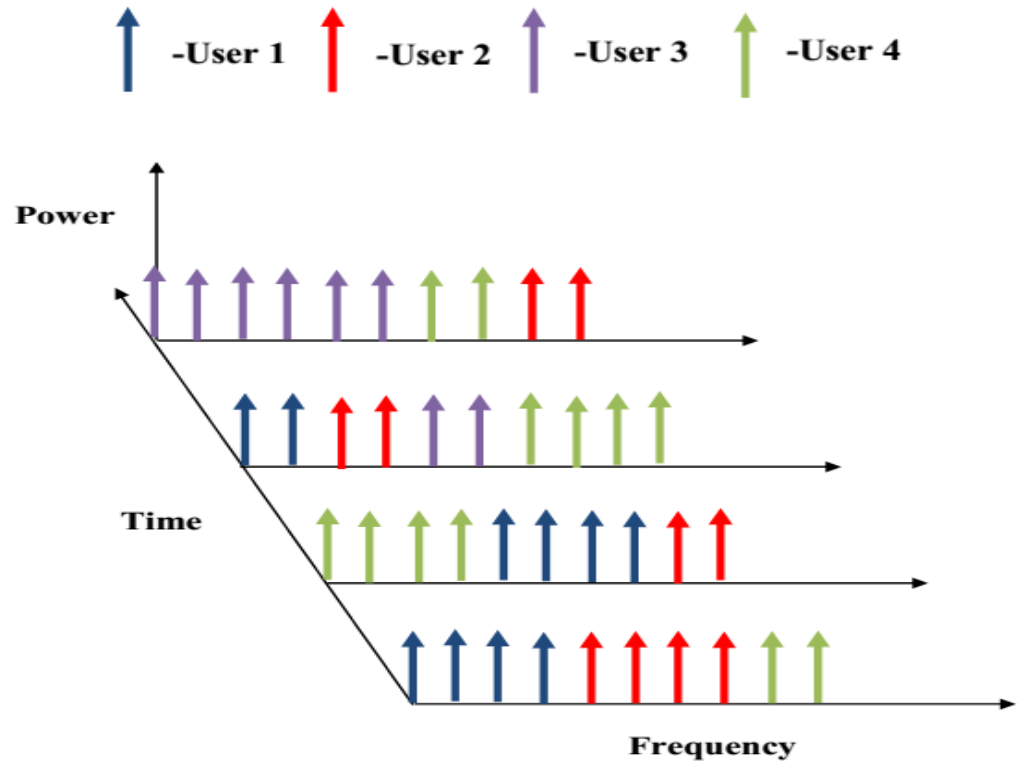

(a)

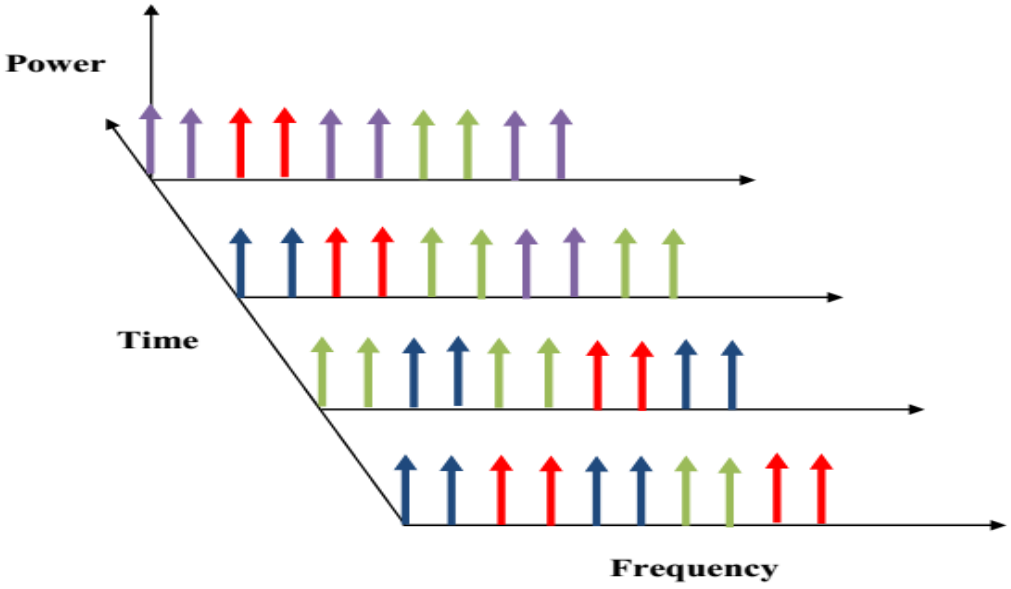

(b)

Figure 5.4 Contiguous Mapping (a) Consecutive (b) Block wise.

In interleave mapping a sub channel is group of distributed subcarriers across all the number of subcarriers in frequency domain. Here the number of subcarriers in a sub channel can be different depending on the resource requirement of different users. In Figure 5.5, the time frequency grid of an OFDMA burst containing 4 symbols and 10 subcarriers is shown. In Figure 5.5 the given burst is divided in 4 sub channels, where sub channel 1and 2 are using 12-12 sub carriers and sub channel 3 and 4 are using 6 and 10 sub carriers respectively. The interleave mapping is also known as Distributed mapping and is much more robust to frequency selective fading, while fully exploiting the channel's frequency diversity but highly sensitive for frequency synchronization [88].

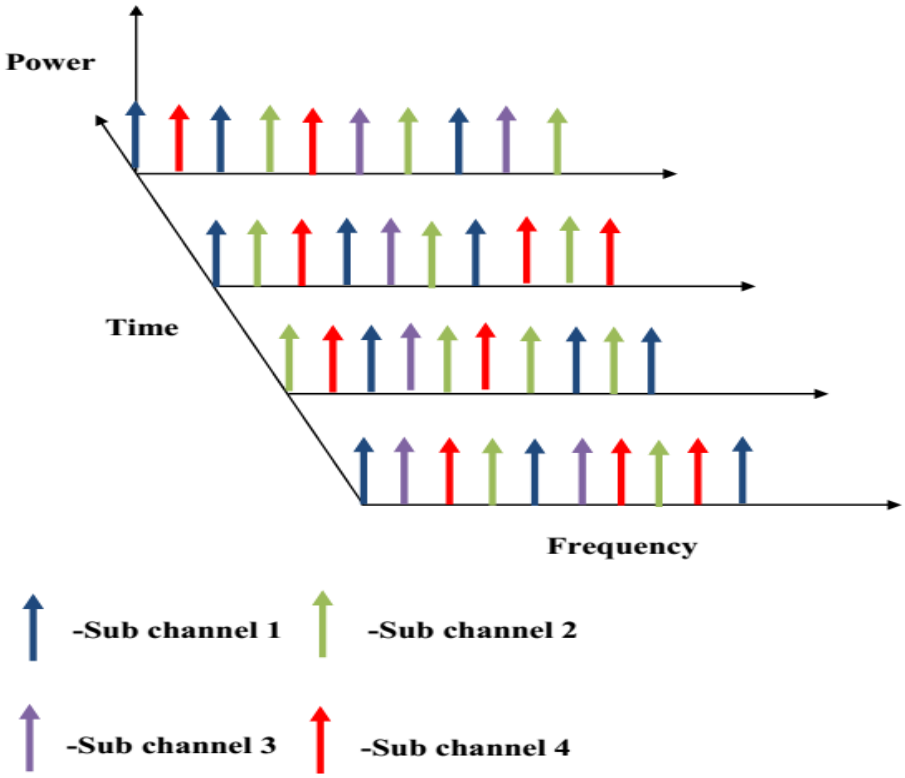

Figure 5.5 Interleave Mapping.

In context of the orthogonality, like OFDM in OFDMA also this can be described with its power density spectrum shown in Figure 5.6 and Figure 5.7 for contiguous and interleave mapping respectively. We can observe from Figure 5.6 and Figure 5.7 that each sub carrier peak is coinciding with nulls of all others which validate the

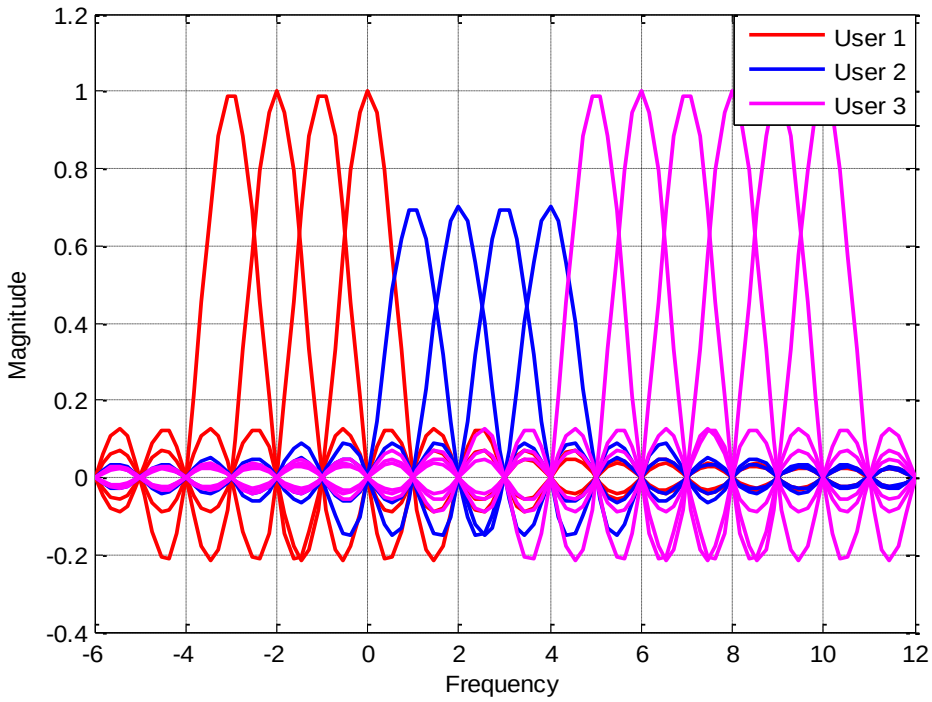

Figure 5.6 Spectrum of an OFDMA Symbol with Consecutive Contiguous Mapping.

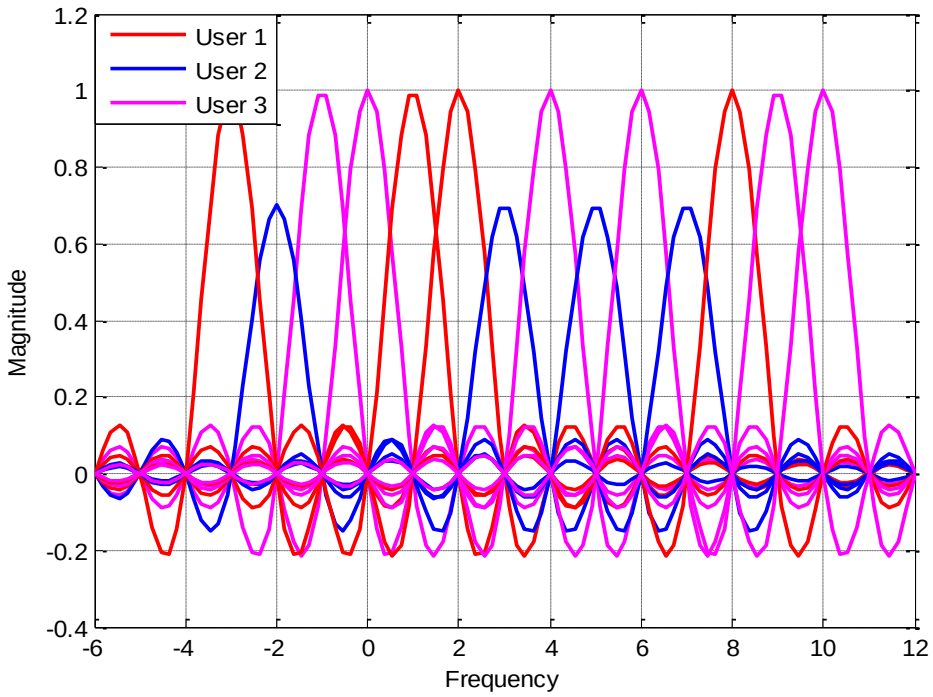

Figure 5.7 Spectrum of an OFDMA Symbol with Interleave Mapping.

Orthogonality in between the sub carriers of OFDMA signal. Peaks are located at the center frequency with the gap of sub carrier spacing $\Delta f = \frac{1}{T_s}$. In Figure 5.6 and 5.7, the resource of 14 orthogonal subcarriers is divided in 3 different users with different resource requirements. User 1 and 2 are using 4-4 subcarriers whereas the user 3 requires 6 subcarriers within a time slot.

Figure 5.6 is the example of consecutive contiguous mapping in which one sub channel is group of two contiguous subcarriers and user 1 and 2 are allocated with 2-2 sub channels and user 3 with 3 sub channels consecutively. In Figure 5.7 interleave mapping is done to allocate the same resource, where all the subcarriers of all the three users are distributed across the frequency grid.

5.3 DFT Spread OFDMA

As discussed in chapter 4, an OFDM signal suffers from a high PAPR because of superposition of N narrowband signals in time domain. At the transmitter side where HPAs are used, this necessitates the linear and with large back off operation of HPAs to avoid inter as well harmonics modulation. Moreover in the uplink where transmitter is a small mobile terminal this calls for major problem because of shorter battery life and higher power consumption with more expensive unit.

This calls for an alternative for the uplink OFDMA scheme which is single carrier frequency division multiple access (SC-FDMA), also known as DFT-spread OFDMA [89]. It is very similar to traditional OFDMA with the only difference that the resulting signal applied to the transmitter is behaving like a single carrier and consequently is with lower PAPR.

In Figure 5.8 the block diagram of OFDMA and SC-FDMA is compared where in case of SC-FDMA, the block of serial input time symbols after the applicable channel coding and constellation mapping, from u^{th} user is converted to parallel and an $\mathfrak{A}_u$ -point DFT is applied before transmitting it to the OFDMA modulator. $\mathfrak{A}_u$ is the number of subcarriers which are used by the u^{th} user. In this way all time symbols are spread over all allocated sub-carriers and become a frequency domain symbol. The subcarrier mapping can be both contiguous and interleaved after which N-point IDFT is applied. This will produce a new parallel time domain symbol which is converted to

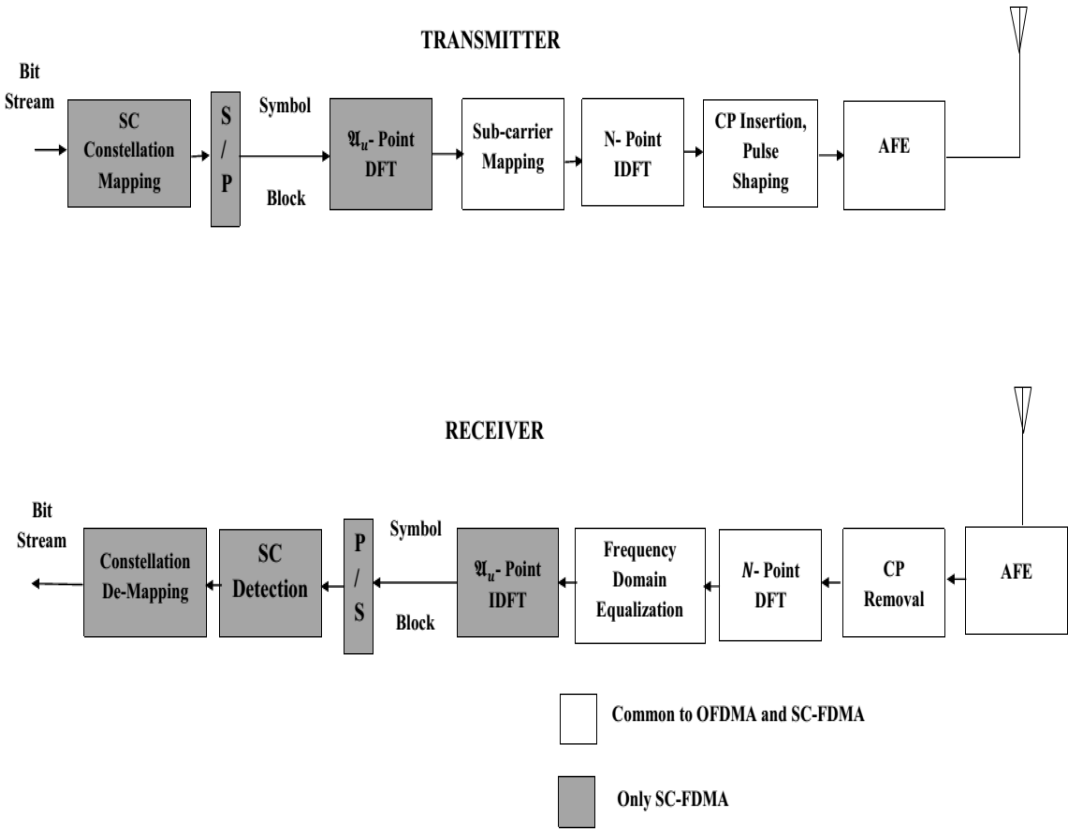

Figure 5.8 SC-FDMA Transceiver.

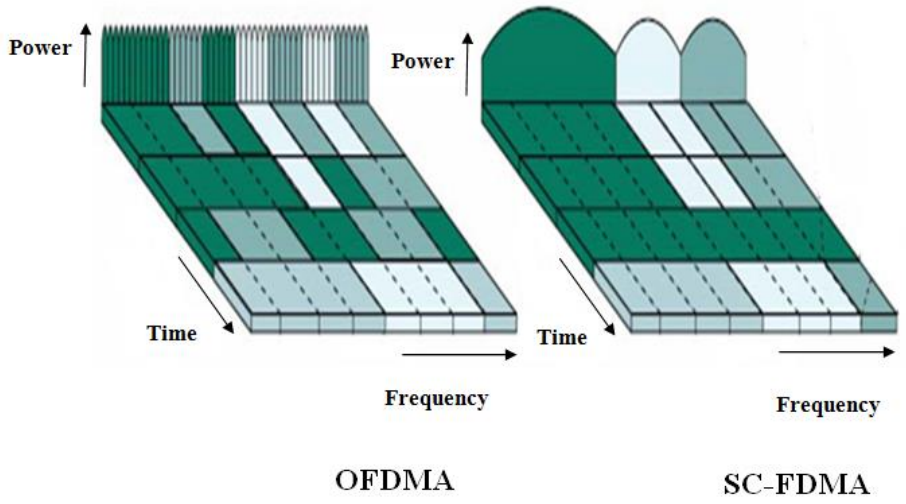

Figure 5.9 Resource Allocations in OFDMA and SC-FDMA [15].

serial and then to analogue signal. At the receiver side $\mathfrak{U}_u$- point IDFT is applied in extra than OFDMA demodulation to create the original symbols.

The resulting signal in case of SC-FDMA is a single carrier signal for a user [89], as shown in Figure 5.9. Either contiguous or interleave sub channelization is applied; in both the cases the reduction in PAPR holds [90]. Reducing the PAPR being the upside also causes the performance degradation in fading channel. As in case of DFT spreading PAPR is moved to frequency domain, this leads to high out-of-band emission for the instant [91].

5.4 Frequency Hopping OFDMA

Both the block wise contiguous and Interleave mapping can be combined with frequency hopping such that the sub channels assigned to a user and subcarriers assigned to a sub channel respectively, are not in the same order for all the time slots in a burst [92].

The hopping pattern is decided by the base station and may be periodic and non-periodic at the same time uniformly and non- uniformly distributed over the signal bandwidth. With this a method for re-scheduling resources in the time domain must also be employed. This opens the way for adaptive sub channelization schemes. Figure 5.4 (b) and 5.5 are the examples of non- uniformly distributed frequency hopped block wise contiguous and interleave OFDMA respectively.

Frequency hopping OFDMA approaches the basic principle of MC-CDMA [93]. In MC-CDMA spreading of the signal bandwidth is done using direct sequence spreading with processing gain P_G. In OFDMA, frequency assignments can be further specified with radio resource management resulting to a better BER performance than MC-CDMA in a cellular environment even at the boundaries of cells where the maximum interference is experienced [94-95]. This improvement over MC-CDMA increases with resource load because the whole diversity use of MC-CDMA causes higher MUI at higher resource load. Even for a fully loaded system the OFDMA without any radio resource management outperforms the MC-CDMA.

5.5 Diversity in OFDMA

Besides all the advantages of OFDM, i.e. one tap easy frequency domain equalization, resilient against the ICI, abandoning the requirement of steep and precise band pass filters, optimum spectrum utilization, efficient digital signal processing, suitability for MIMO principle, dynamically adjusting the bandwidth, adaptive channel coding and modulation, adaptive spreading and bandwidth scalability, OFDMA possess the advantage of multi user diversity and interference diversity with higher gains as the signaling in case of OFDMA is managed over sub channel level whereas in the other multiple access schemes such as MC-CDMA this is done over sub carrier level.

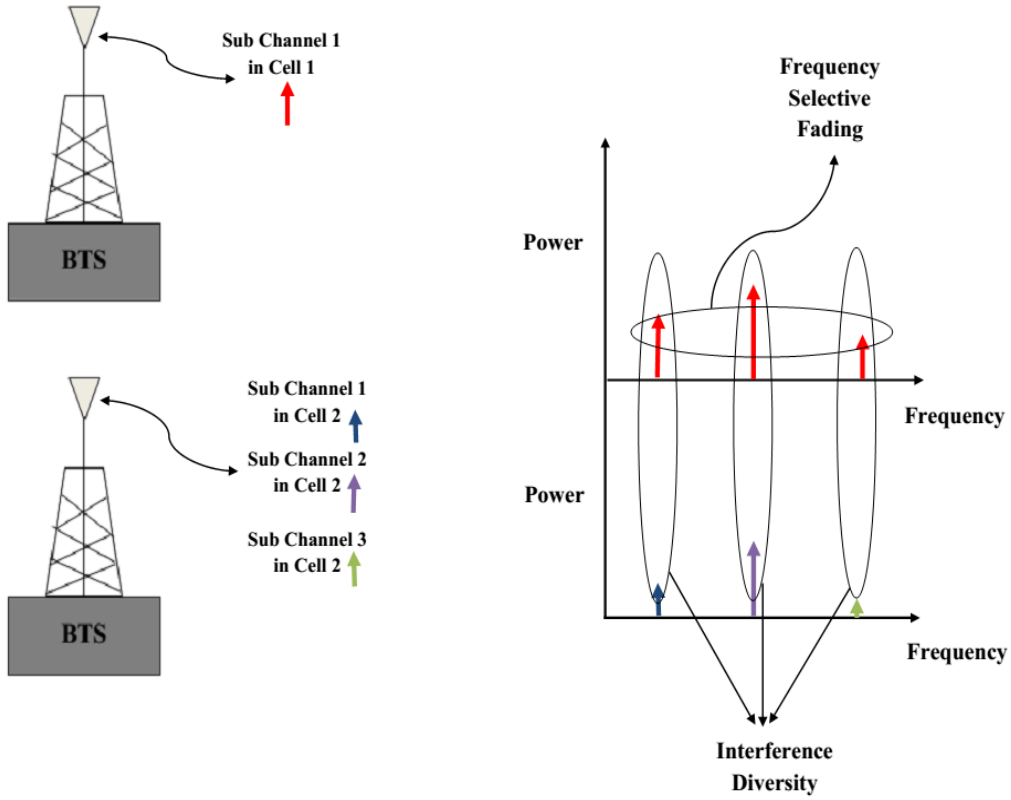

Figure 5.10 Interference Diversity in OFDMA.

Typically in the multi cellular environment the deployment of any multiple accesses scheme faces the challenge of tight frequency reuse. At the sub channelization stage the OFDMA accepts this challenge by exploiting **interference diversity** and approaches to the frequency reuse factor of 1 in fully loaded system with different

mapping (interleave only) of subcarriers to sub channel in different but adjacent cells without co channel interference. As shown in figure 5.10, the intended user of the intended cell is using a group of sub carriers with sub channel 1. The sub carriers of this sub channel are assigned to different users in the adjacent cells. As the co channel interfering users in the adjacent cells are on different location the incoming interference will be diversified.

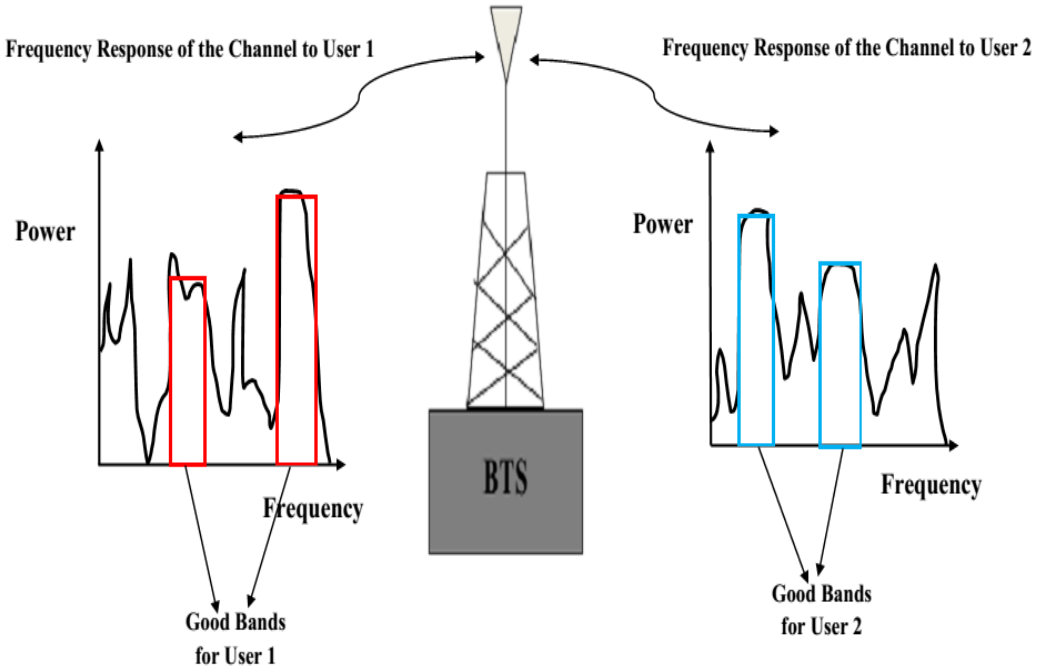

Figure 5.11 Multi User Diversity in OFDMA.

In case of OFDMA the scheduling of the resources can be done by exploring both the frequency and time domain responses of the channel. As the frequency responses of the channel will be different on the same frequencies for the different users (Figure 5.11), the good and bad bands of the corresponding users will be different. The sub channelization allocated as per these bands can lead to have higher bit rates for the corresponding user without fading effects while using the **multi user diversity**. Contiguous sub channelization supports the use of multi user diversity in OFDMA as the channel frequency response is highly correlated in contiguous sub carriers and the allocation of good and bad bands is easy.

5.6 Comparison of Sub Channelization Schemes

With many of the advantages provided by the different sub channelization schemes in the OFDMA, we can compare these schemes for different concepts.

Concept	Contiguous Mapping	Interleave Mapping
Frequency Reuse	Cannot approach to unit frequency reuse	Unit Frequency reuse is possible
Multi user diversity	Uses multi user diversity in frequency domain	Cannot use multi user diversity
Interference Diversity	Cannot use frequency diversity on averaging	Uses frequency diversity on averaging
Channel State Information	Required	Not required
Scheduling	Complex schedulers are needed at the base station	No complex scheduling
Terminal Mobility	Fixed deployment	Both fixed and mobile deployment
Gain	Loading gain	Diversity Gain
Compatibility	Suitable to combine with beam forming	Suitable to combine with MIMO

Table 5.1 Comparison of Sub Channelization Schemes.

5.7 Phase Noise Impaired OFDMA System Modeling

Like all other challenges of OFDM, i.e., time and frequency synchronization, high PAPR, CFO and IQ imbalance, OFDMA also faces the challenge of transceiver RF impairment because of time varying PHN. In OFDMA, CPE and in-band ICI is not the only source of interference that should be considered. The multiplexing of several users in an OFDMA scenario introduces out-of-band interference from one user on another in the OFDMA symbol. This MUI is induced by the spectral spread of the energy of each user's subcarriers on the top of other users' subcarriers. The spread is more severe in case of uplink, when there are unequal power levels as well unequal

transmitter 2(PHN 3-dB BW) for different users due to different path loss effects and different oscillator non idealities respectively, in an uplink scenario. Additionally, in the case of transmitter PHN, ICI results not only from the higher order components of PHN but also because of the loss of the cyclic nature and so the orthogonality is destroyed of the transmitted signal as the transmitter PHN affects the samples of the CP differently than the corresponding samples in the actual OFDMA signal part. Further, the transmitter PHN impairing the CP also tend to produce ICI and hence not only $N-1$ but $N+N_g-1$ samples of PHN realization should be considered for PHN mitigation.

In regards of PHN impaired OFDMA modeling, we consider the uplink of an OFDMA with $U(u = 1,2,3,\dots,U)$ users and $\mathcal{U}$ represents the index set of use full subcarriers with size $\mathfrak{A}$, means that among N subcarriers, the u^{th} user is assigned to a subset of $\mathfrak{A}_u$ subcarriers with index set: $\mathcal{U}_u = \{\mathcal{U}_1^u\, \mathcal{U}_2^u\, \mathcal{U}_3^u \dots \mathcal{U}_{\mathfrak{A}_u}^u\}$, either contiguous or interleaved where $(.)^u$ denotes the u^{th} user. If $x^{m,u}$ is the m^{th} frequency domain symbols sent by the u^{th} user, then k^{th} entry of it, say $X_k^{m,u}$ is nonzero if $k \in \mathcal{U}_u$. Thereupon discrete time baseband signal of the u^{th} user using IFFT can be represented as:

$$S_{k,n}^{m,u} = \frac{1}{N}\sum_{k \in \mathcal{U}_u} X_k^{m,u}\, e^{j2\pi\frac{kn}{N}}, 0 \le n \le N-1\,. \tag{5.1}$$

As there is no ISI in between the windows of N samples, and that the whole processing can be done in a symbol to symbol manner, we drop the OFDMA symbol index m hereafter. After this the signal is transformed back to the serial form and is up converted to RF with noisy transmitter oscillator and finally is sent over the channel. Let the discrete time composite channel impulse response with order L^u between the u^{th} user and the uplink receiver be denoted by $g^u(l)$ and the channel frequency response on the k^{th} subcarrier of u^{th} user's channel be denoted by h_k^u, then we have:

$$h_k^u = \sum_{l=0}^{L_k-1} g^u(l) e^{-j2\pi\frac{kl}{N}}\,. \tag{5.2}$$

Denoting the discrete time transmitter PHN process, receiver PHN process and AWGN impairing to the u^{th} user by $\theta_{T,n}^u$, $\theta_{R,n}^u$ and w_n respectively, the received OFDMA symbol after down conversion and CP removal can be written as:

$$r_n = \sum_{u=1}^{U}[(S_{k,n}^{u} e^{j\theta_{T,n}^{u}}) \otimes g^{u}(l)]\, e^{j\theta_{R,n}^{u}} + w_n. \quad (5.3)$$

After taking the FFT, the frequency domain received symbol on the k^{th} subcarrier is:

$$y_k = p_0^u h_k^u X_k^u + \sum_{i=1}^{U} \sum_{\substack{q \in \mathcal{U}_i \\ q \neq k}} p_{k-q}^{i} h_q^i X_q^i + W_k. \quad (5.4)$$

As h is a circulant matrix we can effectively map the transmitter PHN as receiver PHN, and by writing $\theta_{T,n}^{u} + \theta_{R,n}^{u} = \theta_n^u$, we have $p_q^u = \frac{1}{N}\sum_{n=0}^{N-1} e^{j\theta_n^u} e^{-j\frac{2\pi nq}{N}}$ and W_k is the AWGN noise in frequency domain.

From Equation (5.4), we find the effect of phase noise in OFDMA to be different from that of single user OFDM. First of it the CPE term (p_0^u) varies according to the index u, means that each user suffers from different CPE and they need to be consider separately for each user to estimate and mitigate.

Secondly, the summative term, called ICI, includes the user's 'in-band' ICI (Self Interference (SI)) and ICI caused by MUI. While including the frequency domain dummy symbols transmitted by each active user in Equation (5.4) a unified frequency domain signal model can be given by:

$$y_k = \sum_{u=1}^{U} \sum_{q=0}^{N-1} p_{k-q}^{u} h_q^u X_q^u + W_k\ . \quad (5.5)$$

Splitting the summative (ICI) term is important for our analysis purpose , as MUI takes in to account the significance of the power level of users as well the transmitter 2(PHN 3-dB BW) as these two will be significantly different for different users precisely in case of OFDMA uplink. So the signal for u^{th} user, on his k^{th} subcarrier is given as:

$$y_k = p_0^u h_k^u X_k^u + \sum_{\substack{q \in \mathcal{U}_u \\ q \neq k}} p_{k-q}^{u} h_q^u X_q^u + \sum_{\substack{i=1 \\ i \neq u}}^{U} \sum_{\substack{q \in \mathcal{U}_i \\ q \neq k}} p_{k-q}^{i} h_q^i X_q^i + W_k. \quad (5.6)$$

First to characterize the Phase Noise strength in OFDMA transmission, we adopt a parameter widely used in literature which is the relative PHN Bandwidth, $\Delta_{PN} = \frac{2(PHN\ 3dB-BW)}{\Delta f(subcarrier\ spacing)}$. Having the desired advantages of OFDM transmission over single carrier transmission with 'slow' PHN model, restricts to have low of this ratio which makes the assumption of complex Gaussian distribution of the ICI false, even with higher number of subcarriers. Secondly a higher $2(\ PHN\ 3dB - BW)$ of the PHN process and the higher value of power level can also lead to more energy in the

MUI factor of ICI terms. Considering these two facts and the OFDMA uplink scenario, not all the $U-1$ users will produce the MUI for u^{th} user but only those who will satisfy the following inequality will be the disruptive users for u^{th}user:

$$\sum_{a=1}^{N-1} E[|p_a^u|^2] < \sum_{a=1}^{N-1} E\left[\left|p_a^j\right|^2\right] \; for\; j = 1\; to\; U\; and\; j \neq u\,. \tag{5.7}$$

Here we define a subset of users for the u^{th} user I_u, $\forall j \in I_u$ with size I_u. Since the PSD of phase noise tapers off rapidly beyond the loop bandwidth, most of the energy in a phase noise sequence is contained in the frequency components corresponding to the first few orders. Hence, the largest contribution to interference on a particular sub-carrier is likely to come from users occupying adjacent sub-carriers. As a result, disruptive users who are occupying sub-carriers adjacent to the u^{th} user are likely to be most disruptive users. Keeping this valid, the Equation (5.6) can be rewritten while using Equation (5.7) as:

$$y_k = p_0^u h_k^u X_k^u + \sum_{\substack{q \in u_u \\ q \neq k}} p_{k-q}^u h_q^u X_q^u + \sum_{i \in I_u} \sum_{\substack{q \in u_i \\ q \neq k}} p_{k-q}^i h_q^i X_q^i + W_k \tag{5.8}$$

where the second term is SI and third term is MUI. From Equation (5.7) and (5.8) the SINR of k^{th} subcarrier is given by (using modulo $N-1$ indexing):

$$SINR_k = \sum_{u=1}^{U} \frac{E\left[\left|X_k^u h_k^u p_0^u\right|^2\right]}{E\left[\left|W_k + \sum_{q=1}^{N-1} X_{k-q}^u h_{k-q}^u p_q^u + \sum_{i \in I_u} \sum_{q=1}^{N-1} X_{k-q}^i h_{k-q}^i p_q^i\right|^2\right]}\,. \tag{5.9}$$

With reasonable assumptions that, h_k^u , X_k^u , and p_k^u are mutually independent and stationary, and that $\forall k, \forall u : X_k^u$ are mutually independent random variables with zero mean and variance ${\sigma^2}_k^u$, we can write ${\sigma^2}_k^u = \mathrm{E}\,[|X_k^u|^2]$, ${\sigma_h}^2{}_k^u = \mathrm{E}\,[|h_k^u|^2]$ and $\sigma_w^2 = \mathrm{E}\,[|W_k|^2]$ so:

$$SINR_k = \sum_{u=1}^{U} \frac{{\sigma^2}_k^u {\sigma_h}^2{}_k^u E[|p_0^u|^2]}{\sigma_w^2 + \sum_{q=1}^{N-1} {\sigma^2}_{k-q}^u {\sigma_h}^2{}_{k-q}^u E\left[\left|p_q^u\right|^2\right] + \sum_{i \in I_u} \sum_{q=1}^{N-1} {\sigma^2}_{k-q}^i {\sigma_h}^2{}_{k-q}^i E\left[\left|p_q^i\right|^2\right]}\,. \tag{5.10}$$

By using derivation of PHN variance from [43], $SINR_k$ is given in Equation (5.11) as its final form to analyze.

$$SINR_k = \sum_{u=1}^{U} \mathbb{S} \tag{5.11}$$

where:

$$\mathbb{S} = \frac{{\sigma^2}_k^u {\sigma_h}^2{}_k^u \left[-\frac{1}{N} + \frac{2}{N^2}\sum_{n=0}^{N-1}(N-n)e^{-\frac{j2\pi\beta^u T_s n}{N}}\right]}{\sigma_w^2 + \sum_{q=1}^{N-1} {\sigma^2}_{k-q}^u {\sigma_h}^2{}_{k-q}^u \left[-\frac{1}{N} + \frac{2}{N^2}\sum_{n=0}^{N-1}(N-n)e^{-\frac{j2\pi\beta^u T_s n}{N}}\cos\left(\frac{2\pi kn}{N}\right)\right] + \mathbb{M}}$$

and

$$\mathbb{M} = \sum_{i\in I_u}\sum_{q=1}^{N-1} {\sigma^2}_{k-q}^i {\sigma_h}^2{}_{k-q}^i \left[-\tfrac{1}{N} + \tfrac{2}{N^2}\sum_{n=0}^{N-1}(N-n)e^{-\frac{j2\pi\beta^i T_s n}{N}}\cos\left(\tfrac{2\pi kn}{N}\right)\right].$$

This is the closed form solution to efficiently compute the effect of ICI (SI and MUI) on OFDMA signal in either contiguous or interleaved multiuser configuration.

5.8 Analysis of Signal to Interference + Noise Ratio

In presence of PHN, Equation (5.11) indicates that SINR is a function of various system parameters like, $\beta, N, N/T_s(sampling\ frequency(F_s)), SNR = \frac{\sigma^2}{\sigma_w^2}$ and their corresponding ratios. The system performance in terms of SINR is analyzed in this section and depicted in Figures 5.12-5.16, for AWGN channel.

OFDM system performance with imperfect oscillator is strongly dependent on 2(PHN 3-dB BW): β and so for OFDMA system too. As shown in Figure 5.12, the larger β is the worse the SINR is. But unlike OFDM, in case of OFDMA, the shown range of β can be bifurcated in three areas: No PHN/ CPE area, ICI/ non Gaussian distribution area, and ICI overwhelm/ Gaussian distribution area. First is explained by the fact that as number of subcarriers is increased, PHN impact gets worsen due to the shorter subcarrier spacing, hence more sensitive to PHN. Singularity of the following area says that as PHN increases, ICI gets dominance over CPE and non-Gaussian distribution of ICI terms make the negligence of correlation between these terms false and heavier tails of the limit distribution makes the degradation independent to the number of subcarriers [33-35]. In Gaussian distribution area where power of DC value spills more into other spectral components, ICI overwhelms. With higher N, degradation is higher, since with higher value of N Gaussianity is reached faster because as the number of summands increases, the sum becomes a Gaussian random variable.

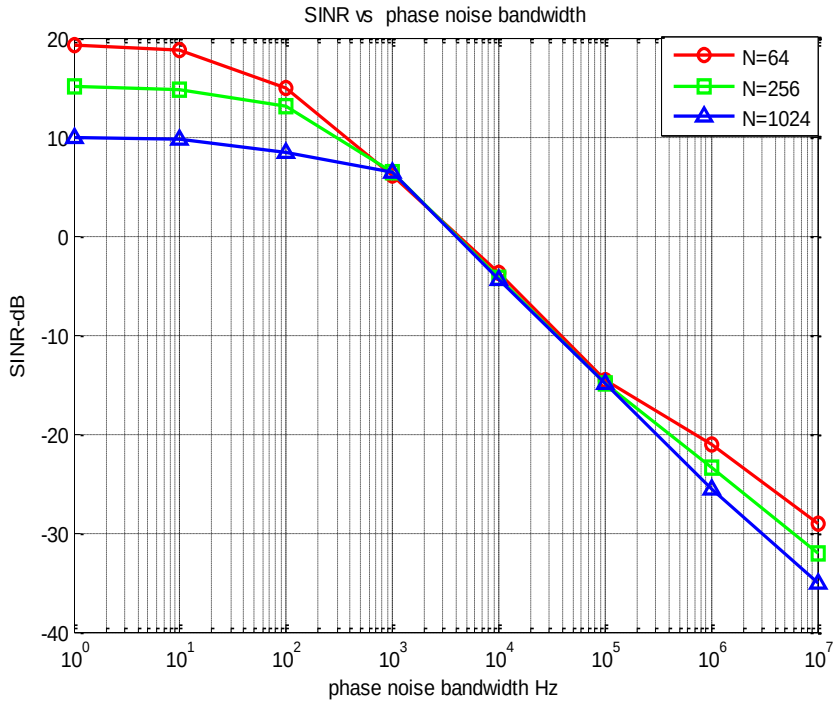

Figure 5.12 Effect of β on SINR Performance for Different No. of Subcarriers (N), with SNR=20dB and F_s=20 MHz.

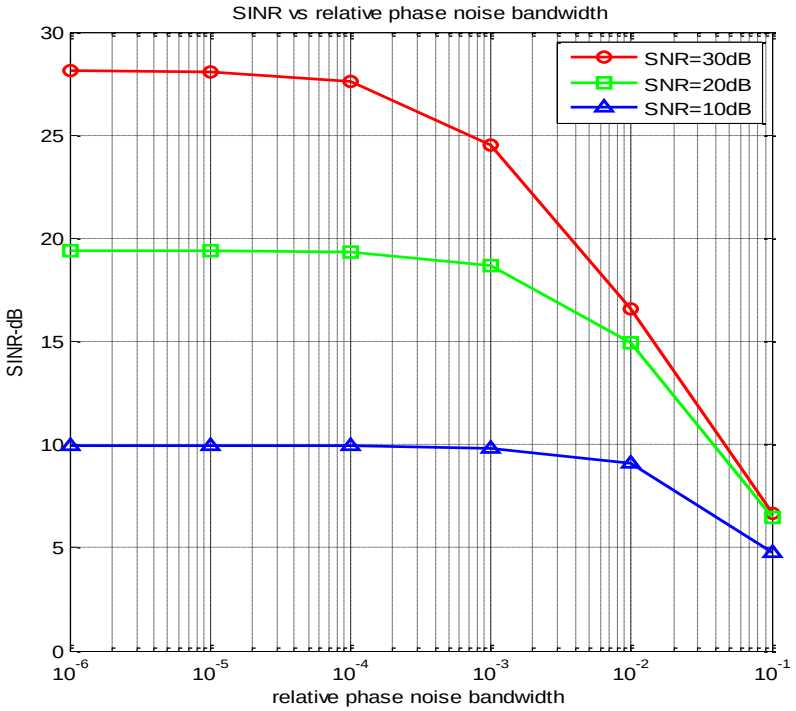

Figure 5.13 Effect of Δ_{PN} on SINR Performance for Different SNR Levels.

It can be observed from Figure 5.13 that for higher transmission data rate $R = F_s$, when β is very small in comparison to the subcarrier spacing (Δf), i.e., Relative PHN 3-dB BW ((Δ_{PN}) is of the order of 10^{-4} or less, PHN becomes negligible, and it is equivalent to the no PHN/ CPE case. When Δ_{PN} is between 10^{-4} and 10^{-2}, non-Gaussian ICI can be mitigated with application of effective ICI correction schemes. Now we compare the intended range of Δ_{PN} (10^{-4} to 10^{-2}) with its peer range in OFDM system [31], i.e., 10^{-5} to 10^{-2} and find that in case of OFDMA the range gets restricted, as 'out- of-band' effect is also included with 'in-band' effect of OFDM case. The overwhelmed ICI area makes the degradation a logarithmically linear function of Δ_{PN} which is not the practical range as 'small' PHN approximation does not hold anymore. With Figure 5.13 we can also observe that higher SNR leads to better performance in the presence of PHN but at the same time systems with high SNR are more sensitive to PHN.

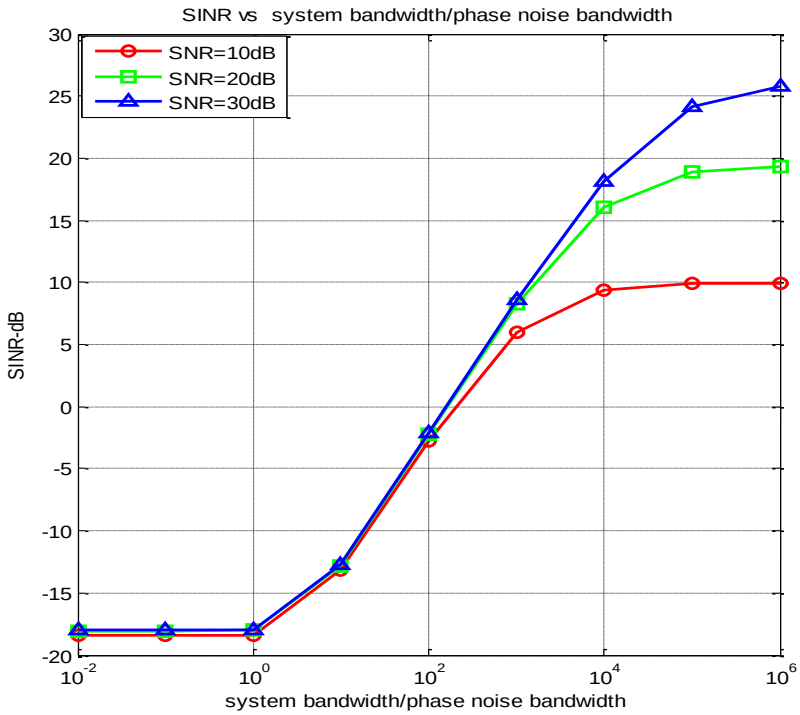

Figure 5.14 Effect of R/β on SINR Performance for Different SNR Levels, with N=256.

It is shown in Figure 5.14, that higher transmission data rate R, results in a better system performance but at the same time SINR has a limiting low value for small

R/β, regardless of the SNR value. This can be proved by letting R/β approach zero in Equation (5.11), which gives:

$$SINR_{k\frac{R}{\beta}=0} = \frac{SNR}{SNR(N-1)-N}. \tag{5.12}$$

As $N \gg 1$ always, this limit can be approximated to $\frac{1}{N-1}$, which says that, for large PHN (thus, low R/β), a high SNR does not improve the performance. Therefore, a well designed system must have a reasonable R/β ratio in order to achieve adequate performance. Further, Equation (5.11) shows that SINR becomes SNR when R/β approaches to infinity:

$$SINR_{k\frac{R}{\beta}=\infty} = SNR. \tag{5.13}$$

This can be proved directly from Equation (5.11) that when R/β goes to infinity, the system is equivalent to a normal one without PHN.

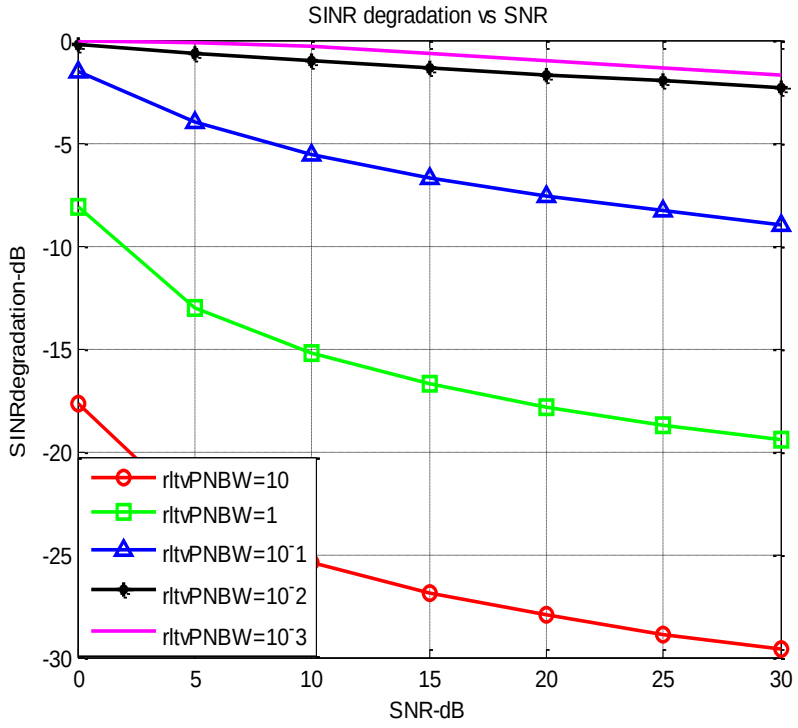

Figure 5.15 SINR Degradation as a Function of SNR with Different Δ_{PN} Settings.

As stated earlier, the Figure 5.15 shows that for high PHN levels with $\Delta_{PN} \geq 1$, SINR degradation exceeds the value of SNR itself. This implies that the ICI

overwhelms the desired signal. We also observe that, when $10^{-2} \leq \Delta_{PN} \leq 1$, though system loss does not exceed the value of the SNR, it is considerably high, e.g., the SINR degrades with 7.58 dB for $\Delta_{PN} = 10^{-1}$, when the SNR equals 20 dB. This happens, as high PHN levels are catastrophic here. In particular if, $10^{-4} \leq \Delta_{PN} \leq 10^{-2}$, all PHN correction schemes which are based on CPE estimation, does not improve or even makes the performance worse with these high PHN levels and we need to go beyond the standard approach to compensate the CPE, and that is to have effective ICI suppression schemes.

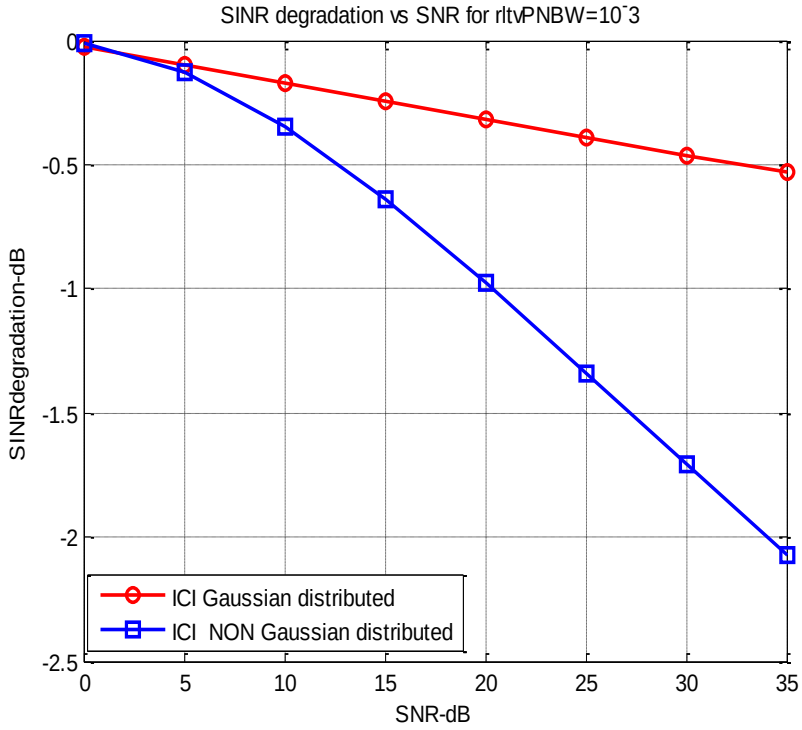

Figure 5.16 Comparison of SINR Degradation as a Function of SNR for $\Delta_{PN} = 10^{-3}$.

Further, if we compare the SINR degradation in an OFDMA system for $\Delta_{PN} = 10^{-3}$, i.e., non Gaussian distributed ICI area, with its peer value in OFDM system [31], where Gaussian distribution of ICI is assumed, we observe that heavier tails of limit distribution tend to produce higher degradation as shown in Figure 5.16. This also corresponds with the result proved in [33] that for AWGN channels the performance of the system with "real" PHN is much worse than for the Gaussian noise model.

In addition, to design the system parameters, we take the standard based on the IEEE 802.11a like system, where the frequency band is 5 GHz and transmission bandwidth is 20 MHz with 64 subcarriers. All users are working with same power, noise and PHN levels and channel is AWGN. With the SNR ranging between 0–30 dB, if we require that the SINR degradation cannot be larger than 2 dB, especially for high SNR levels, we obtain$\Delta_{PN} \leq 1.21 \times 10^{-3}$, in terms of Equation (5.11). In other words, the PHN Bandwidth must be less than 378 Hz.

5.9 Characterization of Multi User Interference

In this section all the formulation results are verified with respective simulation results in Figures 5.17 to 5.21, where each simulation point is conducted using 10,000 OFDMA symbols in MATLAB. Simulation model is based on IEEE 802.11a like system with parameters given in Table 5.2.

F_s	20 MHz
f_c	5GHz
N	64
Active sub-carriers	52
Users	4 (With Equal Resource)
FFT Size	64
N_g	16 Samples
Mapping	16-QAM

Table 5.2 OFDMA Modeling Parameters.

The DC carrier as well the carriers at the spectral edges are not modulated and are virtual carriers. OFDMA Symbols are generated using 16-QAM and 64-point IFFT, and then prepended by CP of length 16 samples.

Finally transmitter PHN is modeled before transmitting over the AWGN channel. The combined received signal from all four users is then OFDMA demodulated with 64-

point FFT after receiver PHN modeling followed by CP removal. Each user is following the above described operation separately so that power and 2(PHN 3-dB BW) can differ specifically, if applicable.

In Figure 5.17, SINR of four OFDMA users with contiguous subcarrier mapping is depicted corresponding to their subcarrier index where user-2 have 5dB more power than the other users and all users as well receiver 2 (PHN 3-dB BW) is 200 Hz.

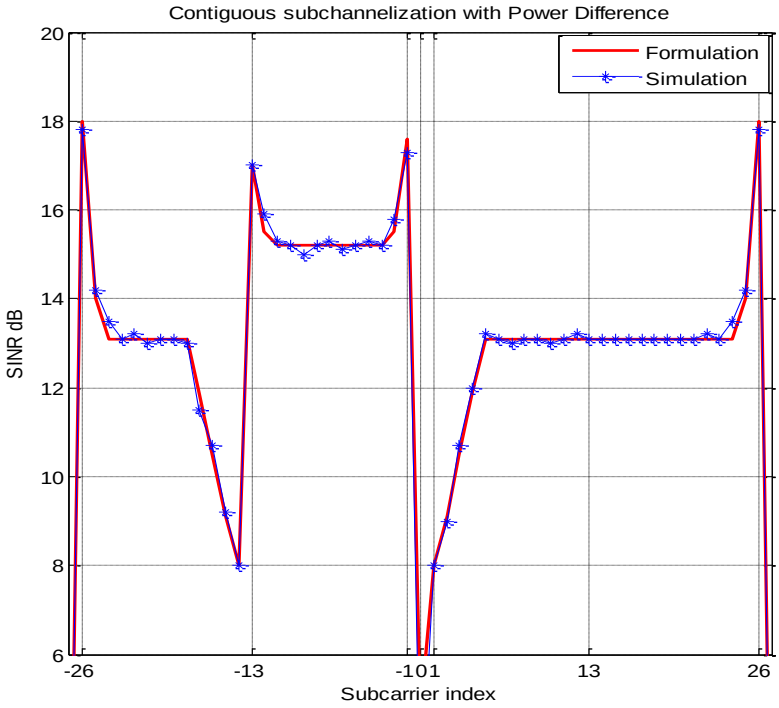

Figure 5.17 Subcarrier wise Effect of MUI on SINR Performance for Contiguous Mapping with Power Difference while 2(PHN 3-dB BW)=200Hz.

From the Figure 5.17, it can be observed that adjacent subcarriers to user-2 are experiencing very heavy SINR degradation because of ‘out-of-band’ (MUI) effect whereas the ‘in-band’ (SI) effect is relaxed because of high subcarriers’ power.

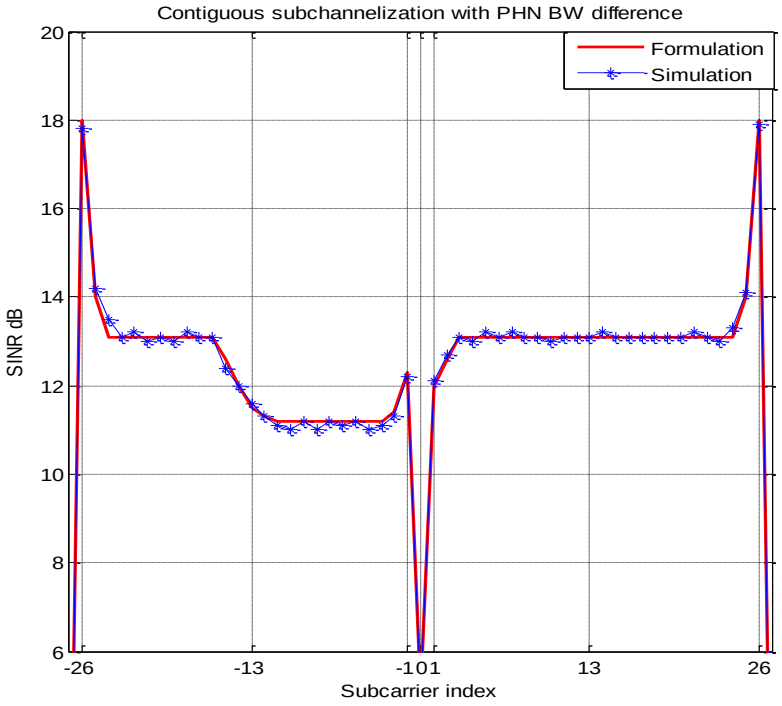

Figure 5.18 Subcarrier wise Effect of MUI on SINR performance for Contiguous Mapping with 2 (PHN 3-dB BW) Difference while SNR=20dB.

As shown in Figure 5.18, when user-2 have 400 Hz, 2(PHN 3-dB BW), but all the other users as well receiver have 200 Hz of 2(PHN 3-dB BW), again the adjacent subcarriers are facing severe 'out-of-band (MUI)' effect but this time the 'in-band' effect is stronger as high PHN of user-2 is resulting higher SI than the other users with lesser PHN. By comparing the results of Figure 5.17 and Figure 5.18, it can be also observed that severity of MUI is more serious in case of power difference.

In Figure 5.19, SINR of four OFDMA users with interleaved subcarrier mapping is depicted corresponding to their subcarrier index where user-2 have 400 Hz, 2(PHN 3-dB BW), but all the other users as well receiver have 200 Hz of 2(PHN 3 dB BW).

Subcarriers of user-2 are marked with vertical dashed lines. In this case the average MUI to the adjacent users is around to contiguous mapping but the instantaneous effect is moderate as in case of interleaved mapping MUI impact is also distributed.

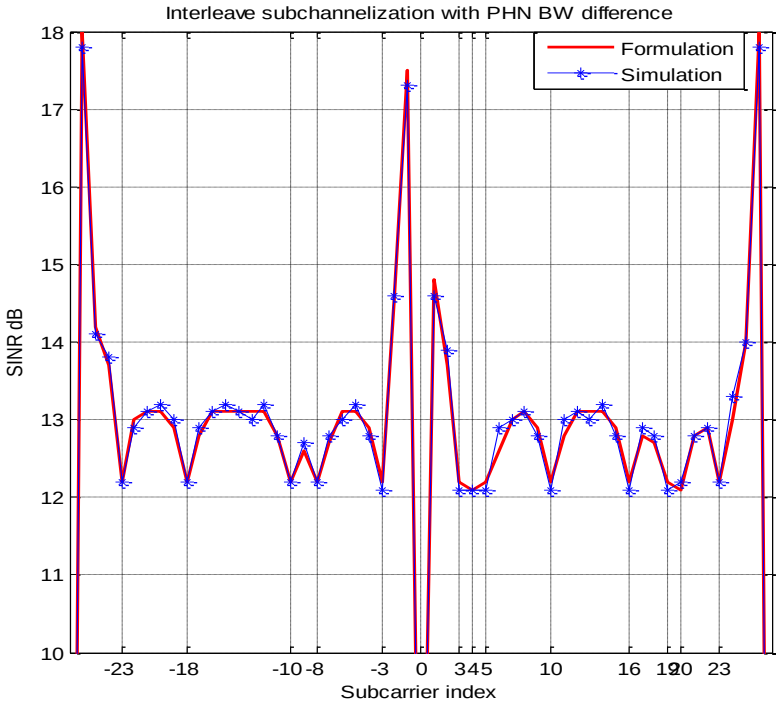

Figure 5.19 Subcarrier wise Effect of MUI on SINR Performance for Interleave Mapping with 2 (PHN 3-dB BW) Difference while SNR=20dB.

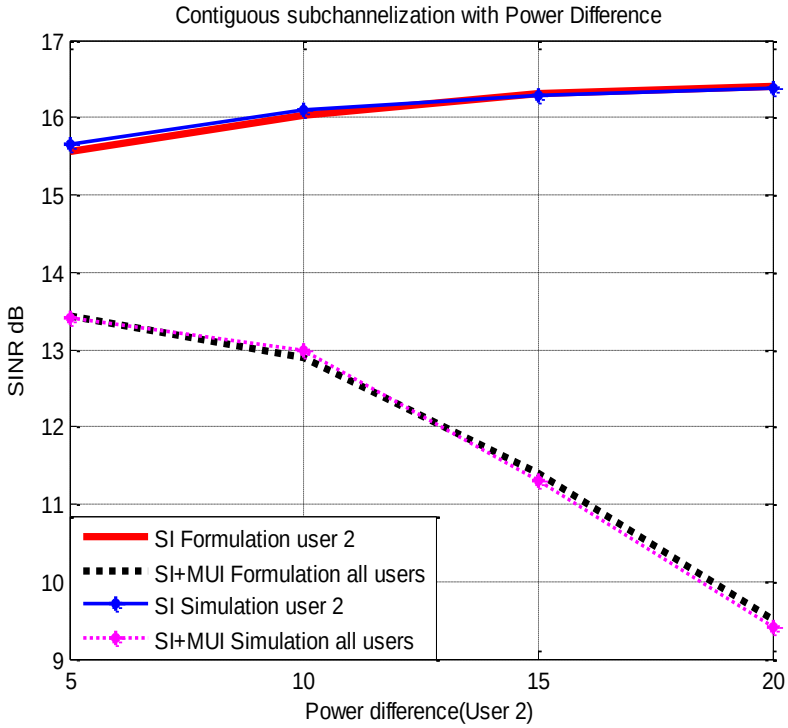

Figure 5.20 Effect of SI and MUI on Average SINR Performance for Contiguous Mapping with Power Difference while 2(PHN 3-dB BW) =200Hz.

In Figure 5.20 average SINR for four users and average SINR of user-2 is simulated for contiguous mapping, where user 2's subcarriers have 5dB to 20 dB more power than the other users'subcarriers and all users as well receiver 2(PHN 3-dB BW) is 200 Hz.

As user-2 gets power hike on the subcarriers, 'in-band (SI)' effect is limited, but power increment does not limit PHN effect when it reaches to high SNR region, as systems with high SNR are more sensitive to PHN. At the same time, since user-2 is producing more and more MUI, average SINR of all the users get degraded and this degradation is higher for higher SNR regions because of above stated reason.

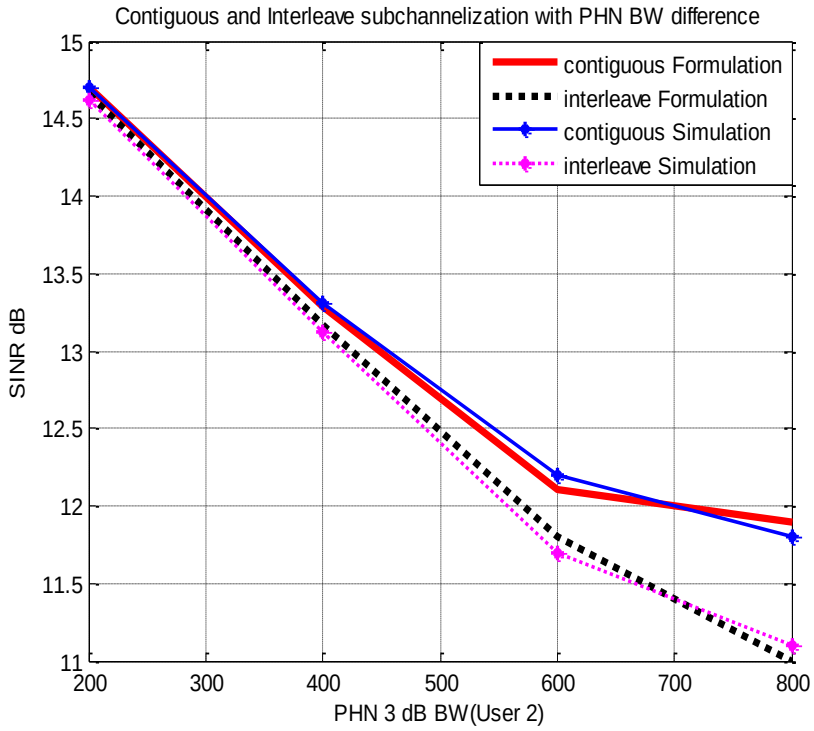

Figure 5.21 Comparison of Average SINR performance for Contiguous and Interleave Mapping with 2(PHN 3-dB BW) Difference while SNR=20dB.

Figure 5.21 shows the comparison of average SINR performance in case of Contiguous and Interleave mapping for four users, where all users as well receiver have 200 Hz of 2(PHN 3 dB BW) excluding user -2, who has variation of 2 (PHN 3-dB BW) from 200 to 800Hz, while all users' SNR is 20 dB.

At 200 Hz the values of SINR coincides but as it is increased, Interleave mapping clearly shows the lower SINR performance than Contiguous mapping as in case of interleave mapping MUI is evenly distributed around the OFDMA symbol. As we increase the 2(PHN 3-dB BW) difference, degradation in SINR performance shows that with high PHN level, MUI is catastrophic.

5.10 Conclusion

Being effective in mitigating the hostile channel selectivity with adaptive sub channelization and resource allocation, the OFDMA technique has gained much more interest in recent years. With transceiver PHN in OFDMA, CPE and in-band ICI are not the only sources of interference like OFDM but the multiplexing of several users introduces out-of-band interference from one user on another known as MUI. A unified PHN corrupted OFDMA uplink signal model, which can characterize any subcarrier assignment (Contiguous and Interleave) scheme, is derived where each OFDMA user suffers from the transmitter PHN and receiver PHN as well. A closed form expression for the SINR is derived without the restriction of complex Gaussian distributed ICI and MUI. The derived expression is analyzed as a function of different critical system parameters. This contribution is published in **[P4]**. Further the SINR is characterized in terms of SI and MUI for in-band and out-of-band effects of transceiver PHN. The analytical results are verified with the simulation results for arbitrary subcarrier mapping with different powers and PHN levels for different users in AWGN channel. This contribution is published in **[P3]**.

6. Estimation of Channel Transfer Function and Phase Noise in OFDM

OFDM, operating at high data rates and high spectral efficiency for a wireless multimedia service needs to estimate and track a time varying channel for a reliable estimation of channel and transmitted symbols. Although the use of non coherent detection of differential phase shift keying (DPSK) does not necessitate the tracking, however, it limits the arbitrary choice of signal constellation and number of bit per symbol, as compared to coherent phase shift keying (PSK) and its logical extension QAM.

In general, the channel estimation methods can be divided into two categories, blind channel estimation and pilot-based channel estimation. In blind channel estimation the correlation between the information transmitted and received is the criteria to estimate the channel, without knowing the information of the transmitted data. The pilot- based channel estimation methods are using pilots, which are the reference signals to be used at either transmitter or receiver side. These reference signals are carrying the information, known to both transmitter and receiver [96-97].

In case of pilot-based estimation methods, the spectral efficiency of the transmitted symbol gets lower as the pilot symbols are occupying the bandwidth without carrying the information. The power requirements get also rise or the power utilisation gets lower. Even with these two drawbacks the pilot-based channel estimations are more suitable for multipath fading channel. This is because even with higher spectral and power efficiencies, blind channel estimation needs many of the data's to analyse with complex analysis.

A quick response to the channel variation can be estimated with pilot-based channel estimation whereas the blind channel estimation is only suitable for very slow varying channel [98]. Thus the pilot based channel estimation with maintaining a good trade off between spectral efficiency & power utilization and channel tracking performance, is always preferred method in case of wireless channel estimation and with the same we are proceeding towards pilot-based channel estimation only.

6.1 Channel Estimation in Multipath Fading

As the multipath fading channel of OFDM system is viewed as a two dimensional (2D) signal in time and frequency domain, the channel estimator in terms of giving the minimum mean-square error should also be based on both the time and frequency dimension. Figure 6.1 is showing one such type of arrangement of pilots in transmitted OFDM frame, located along both the time and frequency grid for **2D channel estimation**. The 2D channel estimation is completed in two steps: first the initial estimate of the channel at pilot symbols' positions are obtained by dividing the received pilot symbol by the originally transmitted pilot symbol. In the second step, two dimensional interpolations or filtering is performed to have the final estimates of the complete channel belonging to the intended OFDM frame. 2D Wiener filter interpolation with orthogonality principle is the optimal filter to give the minimum mean square error in the estimation. Unfortunately, such a 2D estimator structure and interpolation/filtering is too complex for practical implementation.

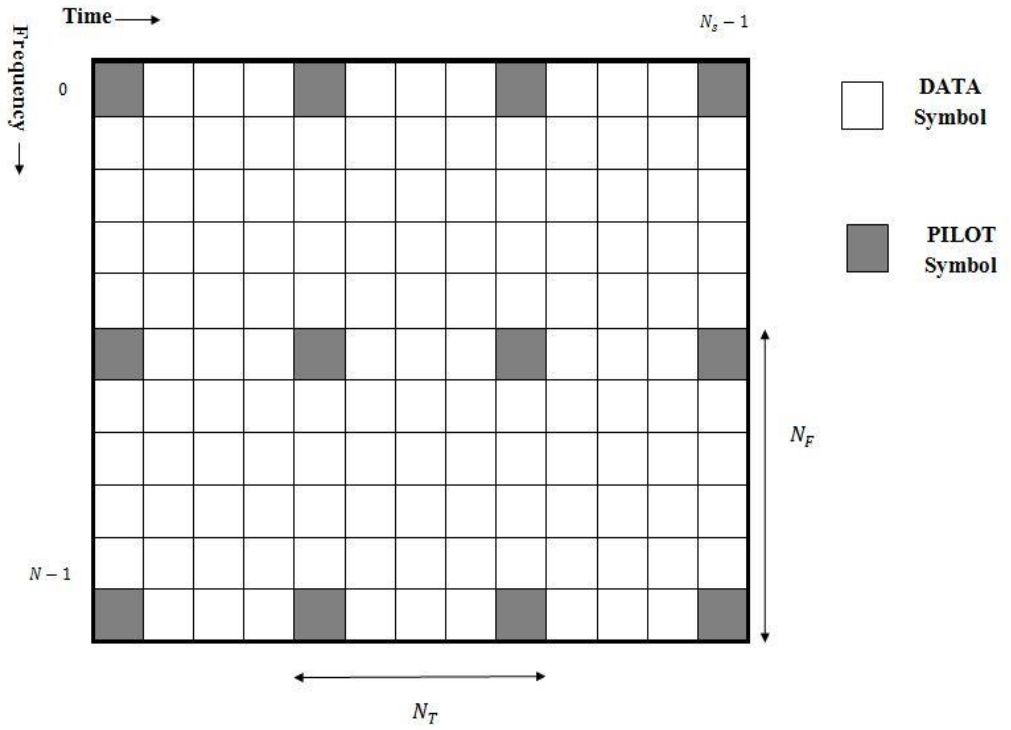

Figure 6.1 Pilot Symbol Grids for Two-Dimensional Channel Estimation.

The **one-dimensional (1D) channel estimations** are optimal in OFDM systems while maintaining the trade-off between computational complexity and performance accuracy. Pilot-based 1D channel estimation methods mainly face two challenges to design the channel estimator. The first challenge is to arrange the pilot information within the transmitted symbols with optimum use of bandwidth. The second challenge is the designing of estimator which tracks the channel with minimum error and has low computational complexity.

The design of a pilot pattern determines where to put the pilot and how closely. A suitable way of inserting these is based on frame structure and speed of the mobile terminal with occupying the minimum bandwidth [99]. As the multipath fading channel is viewed as 2D, the 2D sampling rate should be decided according to the Nyquist sampling theorem to avoid the distortion. As per the Nyquist theorem the span of time domain (N_T) and frequency domain (N_F) in between the pilots along time and frequency grid is given by:

$$f_D . T_S . N_T \leq 1/2 \quad \text{and} \quad \tau_{max} . \Delta f . N_F \leq 1/2 \tag{6.1}$$

where f_D is maximum Doppler frequency. But for practical implementation the oversampling is used with:

$$f_D . T_S . N_T \approx 1/4 \quad \text{and} \quad \tau_{max} . \Delta f . N_F \approx 1/4 \tag{6.2}$$

The two basic 1D pilot-based channel estimations are block-type pilot channel estimation and comb-type pilot channel estimation, in which the pilots are inserted in the frequency direction and in the time direction, respectively as shown in Figure 6.2.

In case of block type channel estimation, for a specific period in time, pilots are inserted in to all the subcarriers of OFDM (Figure 6.2 (a)). So the whole OFDM symbol is reference symbol and also known as training symbol. The next training symbol is inserted with the gap of at least N_T OFDM symbols. In case of comb type channel estimation, for a specific frequency span in frequency grid, pilots are inserted in to all the OFDM symbols (Figure 6.2 (b)). So a particular sub carrier is pilot in each OFDM symbol. The gap between two such pilot subcarriers will be at least N_F OFDM subcarriers.

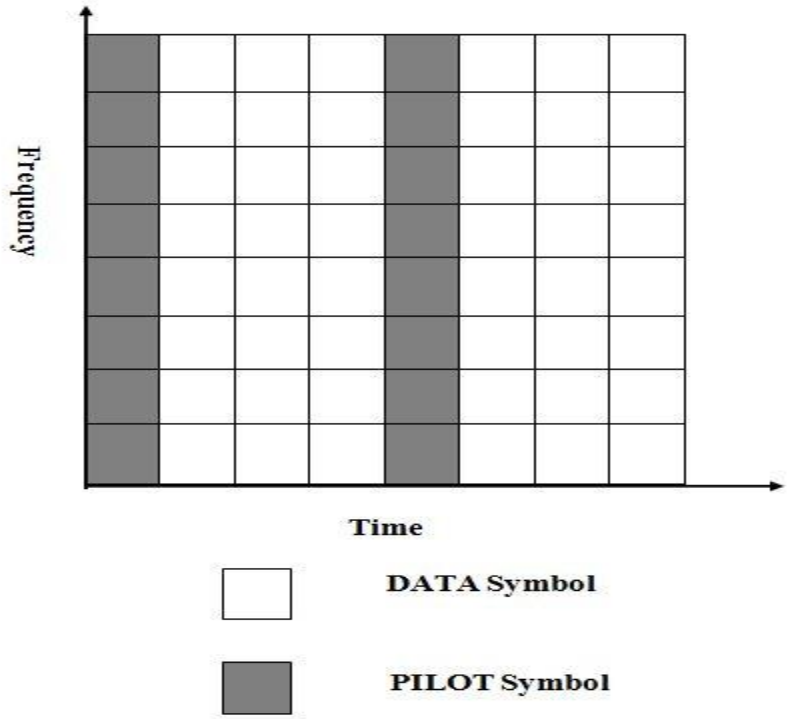

(a)

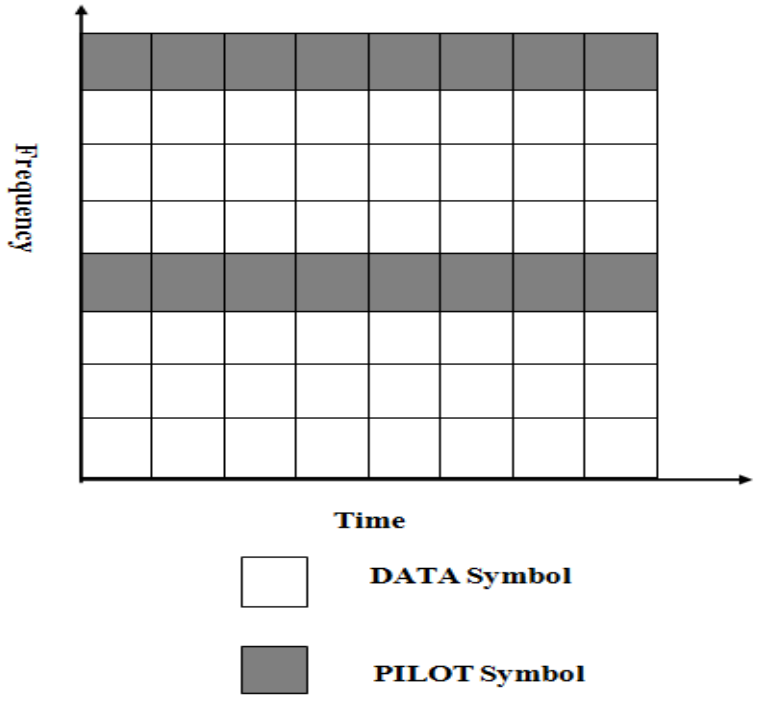

(b)

Figure 6.2 Pilot Symbol Grids for (a) Block Type Pilot (b) Comb Type Pilot Channel Estimation.

As the training symbol is covering all the subcarriers, block type pilot channel estimation is more effective for frequency selective fading environment [100] but at the same time very sensitive for the fast fading of the channel. Thus the block type pilot channel estimation is implemented with the assumption of slow fading channel. In case of comb type pilot channel estimation the interpolation is done to estimate the conditions of all the data sub carriers. The comb type pilot channel estimation satisfies the need for equalization when the channel changes even from one OFDM block to the next one [101].

6.1.1 Block Type Pilot Channel Estimation

In case of block type pilot channel estimation the task is to estimate the **g** or **h** given that the $\mathbf{Y}^m$ and $\mathbf{D}^m$ are known in Equation (4.11) and (4.13) respectively. The estimation can be based on LS or MMSE depending upon without or with use of certain channel statistical knowledge respectively.

For the **LS estimation** of the channel no noise and no ICI is considered. This technique minimizes the $(\mathbf{Y}^m - \mathbf{D}^m\mathbf{h})^H(\mathbf{Y}^m - \mathbf{D}^m\mathbf{h})$ and the LS estimate is given as:

$$\hat{\mathbf{g}}_{\mathrm{LS}} = \mathbf{F}^{-1}\mathbf{D}^{m\,-1}\mathbf{Y}^m \tag{6.3}$$

or

$$\hat{\mathbf{h}}_{\mathrm{LS}} = \mathbf{D}^{m\,-1}\mathbf{Y}^m = \left[\frac{y_0^m}{X_0^m}\ \frac{y_1^m}{X_1^m}\ \ldots\ \frac{y_{N-1}^m}{X_{n-1}^m}\right]^T . \tag{6.4}$$

The LS estimators are very low computationally complex but suffers with very high MSE.

To minimize the MSE, the **MMSE estimator** employs the second-order statistics of the channel conditions and minimise the $\{(\mathbf{h} - \hat{\mathbf{h}})(\mathbf{h} - \hat{\mathbf{h}})^H\}$. The MMSE estimate of the channel is given by:

$$\hat{\mathbf{h}}_{\mathrm{MMSE}} = \mathbf{R}_{\mathrm{hY}}\,\mathbf{R}_{\mathrm{YY}}{}^{-1}\mathbf{Y}^m \tag{6.5}$$

where $\mathbf{R}_{\mathrm{hY}}$ is cross covariance matrix of h *and* Y and $\mathbf{R}_{\mathrm{YY}}$ is auto covariance matrix of Y. These can be calculated with:

$$\mathbf{R}_{\mathrm{hY}} = \mathbf{R}_{\mathrm{hh}}\mathbf{D}^{m\,H} \tag{6.6}$$

and

$$\mathbf{R}_{\mathrm{YY}} = \mathbf{D}^{m}\mathbf{R}_{\mathrm{hh}}\mathbf{D}^{mH} + 2\sigma_{\omega}^{2}\mathbf{I} \tag{6.7}$$

where $\mathbf{R}_{\mathrm{hh}}$ is auto covariance matrix of the channel (h). So if $\mathbf{R}_{\mathrm{hh}}$ and $2\sigma_{\omega}^{2}$ are known at the receiver side the MMSE estimate can be calculated as:

$$\hat{\mathbf{h}}_{\mathrm{MMSE}} = \mathbf{R}_{\mathrm{hh}}(\mathbf{R}_{\mathrm{hh}} + 2\sigma_{\omega}^{2}(\mathbf{D}^{mH}\mathbf{D}^{m})^{-\mathbf{1}})^{-\mathbf{1}}\mathbf{Y}^{m} \tag{6.8}$$

The performance of MMSE estimator could gain 10-15 dB more of performance than LS estimator, precisely in lower SNR regions [97]. However, because of the matrix inversions, the computation complexity increases with the number of subcarriers of OFDM system. To reduce the computational complexity many modified variants of this technique are available in the literature including linear MMSE (LMMSE), optimal low rank MMSE (OLR-MMSE) and singular value decomposition MMSE (SVD MMSE) [98-99]. Further note that MSE is not minimum if channel is not Gaussian.

In block type pilot channel estimation, the estimation is performed once in a block but to further improve the estimate a **decision feedback equalizer** can be additionally used with each subcarrier after the initial estimation, done with the training symbol. If $\hat{\mathbf{h}}$ is the channel estimate (LS or MMSE):

$$\hat{\mathbf{h}} = \{\hat{\mathrm{h}}_{k}\}\ k = 0,1,2 \ldots N-1 \tag{6.9}$$

for the training symbol, than for the next symbol in the OFDM block X_{k}^{m+1} is calculated as:

$$\hat{X}_{k}^{m+1} = y_{k}^{m+1}/\hat{\mathrm{h}}_{k}\ \ k = 0,1,2 \ldots N-1. \tag{6.10}$$

The $\{\hat{X}_{k}^{m+1}\}\ k = 0,1,2 \ldots N-1$ is mapped to the binary data through the demodulation according to the signal de-mapper and then obtained back through signal mapper as $\{\check{X}_{k}^{m+1}\}\ k = 0,1,2 \ldots N-1$. The estimated channel $\hat{\mathrm{h}}_{k}$ is updated to:

$$\hat{\mathrm{h}}_{k} = y_{k}^{m+1}/\check{X}_{k}^{m+1}\ k = 0,1,2 \ldots N-1. \tag{6.11}$$

At each next OFDM symbol this updating is performed till next training symbol. As here we are assuming that the decision at each level is correct the fast fading channel can destroy the estimation accuracy very badly. The estimation technique for such fast fading channels is comb type pilot channel estimation.

6.1.2 Comb Type Pilot Channel Estimation

In comb type pilot channel estimation N_P pilot subcarriers are inserted uniformly in to the OFDM symbol with $N_F = N/N_P$ subcarriers apart from each other. As the receiver side knows the location of the pilot's subcarrier as well the pilot data, the LS estimate of the channel on the pilot subcarrier can be given as:

$$\hat{h}_k^P = \frac{y_{kN_F}^{mP}}{X_{kN_F}^{mP}}, k = 0,1,2 \dots N_P - 1. \tag{6.12}$$

After estimating the $\hat{h}_k^P,\ k = 0,1,2 \dots N_P - 1$, interpolation in frequency domain is used to get the channel estimation $\hat{\mathbf{h}} = \{\hat{\mathrm{h}}_k\}\ k = 0,1,2 \dots N - 1$. Many of the interpolation methods are described in the literature with different complexity and accuracy including piecewise constant interpolation, linear interpolation, second order interpolation, cubic spline interpolation, low-pass interpolation and time domain interpolation [98-99]. Some other methods can be ML estimator [98] and parametric channel modelling-based (PCMB) estimator [98].

6.2 Statistically Optimal Channel Estimation

To take a statistically optimal decision we need four elements. First we need a set of hypothesis that describes the possible true state of decision. Then a test through which the data are obtained. The truth is inferred from this data according to the decision rule for which a criterion of optimality is required.

In context of communication system the possible hypothesis is a finite set of signals, like in case of M-ary signaling there are M hypotheses available to describe the possible true states. The test to obtain the data is here the likelihood ratio test depending on the Bayes' theorem. The optimality criterion which we are operating on is to minimize the probability of making a decision with error. The decision rule which is applied on the test while comparing the measurement of received signal and the threshold can be maximum a posterior (MAP) or maximum likelihood (ML) criterion [66].

6.2.1 Maximum A Posteriori Criterion

According to the Bayes' theorem:

$$\Pr(s_i|z_j) = \frac{\Pr(z_j|s_i)\Pr(s_i)}{\Pr(z_j)} \quad i = 1,2,\dots M \; and \; j = 1,2,\dots \tag{6.13}$$

Here while examining the received sample, z_j, we need to find a statistical measure of the likelihood that z_j belongs to transmitted signal class s_i from the conditional PDF, $\Pr(z_j|s_i)$. The $\Pr(s_i)$ is a prior probability (before the experiment) of occurrence of the i^{th} transmitted signal class. After the experiment we improve over this a prior probability which is known as a posterior probability, $\Pr(s_i|z_j)$. $\Pr(z_j)$ is the probability of the received signal over the whole space of signal class such that:

$$\Pr(z_j) = \sum_{i=1}^{M} \Pr(z_j|s_i)\Pr(s_i) \tag{6.14}$$

and is taken as a scaling factor only.

For most of the wireless communication applications, the possible values of the received samples are continuous in range thus to understand the likelihood test we are taking continuous valued PDF. The threshold decision rule in this case is:

$$\hat{s} = s_i \text{ if } \Pr(s_i|z) > \Pr(s_k|z) \quad \forall\, k \neq i,\; k = 1,2 \dots M,\; i = 1,2 \dots M \tag{6.15}$$

From Equation (6.13):

$$\hat{s} = s_i \text{ if } \Pr(z|s_i)\Pr(s_i) > \Pr(z|s_k)\Pr(s_k) \;\; \forall\, k \neq i,$$
$$k = 1,2 \dots M,\; i = 1,2 \dots M \tag{6.16}$$

This gives the form of decision rule in terms of likelihoods:

$$\hat{s} = s_i \text{ if } \frac{\Pr(z|s_i)}{\Pr(z|s_k)} > \frac{\Pr(s_k)}{\Pr(s_i)} \forall\, k \neq i, k = 1,2 \dots M,\; i = 1,2 \dots M \tag{6.17}$$

The left hand side of $>$ in Equation (6.17) is known as likelihood ratio and the Equation (6.17) is known as likelihood ratio test. As we are making the decision on choosing the signal class with maximum a posteriori probability the decision criterion is known as MAP criterion. For the Gaussian probabilities this criterion is also called the MMSE criterion.

6.2.2 Maximum Likelihood Criterion

In communication systems, there may be non availability of a prior probability, $\Pr(s_i)$. Sometimes the availability is also not trusted as per the marked accuracy. In such cases an assumption of equally likely of signal classes is made and in this scenario the decision criterion with likelihood ratio test becomes maximum likelihood criterion. This gives the form of decision rule in terms of likelihoods:

$$\hat{s} = s_i \text{ if } \frac{\Pr(z|s_i)}{\Pr(z|s_k)} > 1 \ \forall\, k \neq i, k = 1,2 \ldots M,\ i = 1,2 \ldots M \tag{6.18}$$

6.3 Channel Estimation in OFDM System

The conventional OFDM channel estimator, without attending the substantial effect of PHN as CPE and ICI, severely degrades the wireless link quality because of channel estimation inaccuracy and this degradation gets more pronounced in the systems, with high carrier frequency and dense constellations. A reliable estimation of channel and transmitted symbols incorporate the functionality of PHN estimation either in isolation or joint.

As shown in Figure 6.3 (a), the independent function of channel estimation, PHN estimation and symbol estimation, in case of isolated approach, will result in poor channel estimate as well symbol estimates because in case of isolated estimation approaches, the channel and data is estimated using techniques that assume there is no PHN in the system. Semi joint approach of Figure 6.3 (b) probably will produce inaccurate symbol estimates. In the joint approach, Figure 6.3 (c), statistically optimal estimates are obtained by combining the PHN estimation simultaneously with both channel estimation and symbol estimation.

Most of the presented methods in the literature for the channel estimation in presence of PHN belong to either approach of isolated or fully joint. Previous one, developed in the initial stage of the research could not be very popular because of non optimal results [30-32], whereas the later one, with statistically optimal solutions, has become the necessary function of the OFDM receivers [47-52, 59-60].

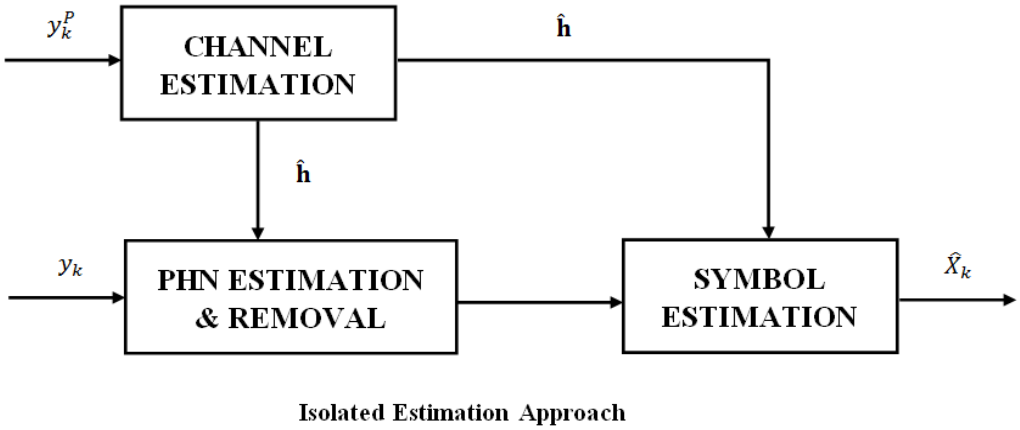

Isolated Estimation Approach

(a)

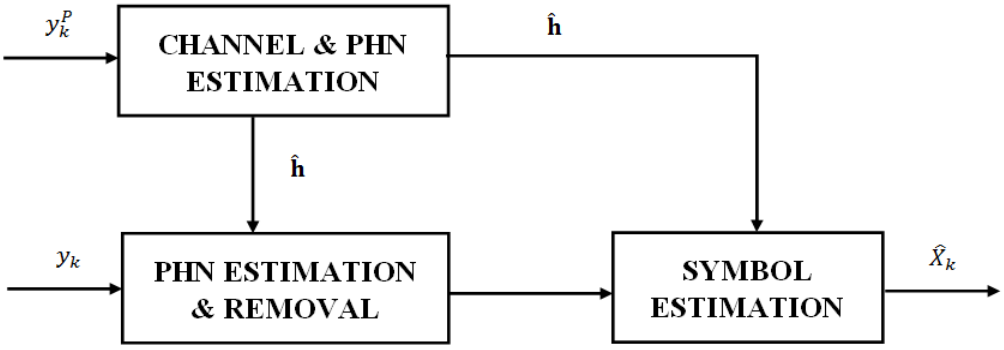

Semi-Joint Estimation Approach

(b)

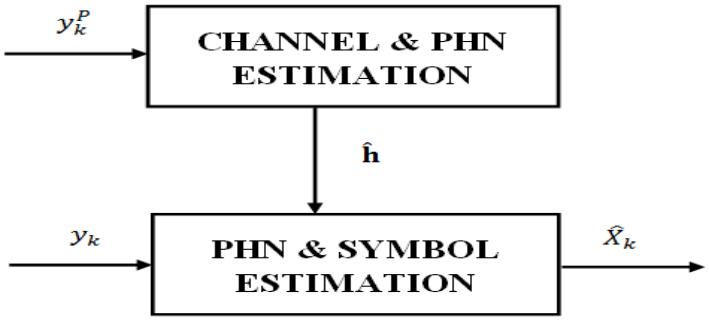

Joint Estimation Approach

(c)

Figure 6.3 Channel, PHN and Symbol Estimation Approach (a) Isolated (b) Semi-Joint (c) Joint.

6.4 Proposed Joint MAP Estimator

To estimate the channel, full pilot symbols are used, where the symbol vector is known to the receiver. We refer this phase of transmission as the channel estimation phase. The data transmission phase consists of regular transmission of symbols, and the task of the receiver is to recover symbol vector using the estimate of the channel obtained from the channel estimation phase.

This is a transmission method on the assumption of a quasi-static fading channel, where the channel is assumed to be static for a block length of the channel estimation and data transmission phase (Figure 4.17).

The PHN is present in both the channel estimation and data transmission phase. The known full pilot symbols are used to jointly estimate the PHN and channel as the data is known. In the data transmission phase also the pilots are inserted within each OFDM data symbol and are used to estimate PHN.

As the PHN is time varying it needs to be estimated over each OFDM symbol in case of data transmission phase whereas for quasi static channel the channel estimation is done once over a block of OFDM symbols for which channel is assumed to be static. In this chapter we are dealing with the channel estimation phase only and the data transmission phase will be discussed in the next chapter.

The statistically optimal channel estimation for OFDM systems in presence of PHN is presented here by deriving MAP cost function for the joint estimation of CTF and PHN in frequency domain by utilizing the prior statistical knowledge of PHN spectral components without the restriction of small PHN. The frequency domain estimation of unknown frequency selective fading makes the method simpler compared with the estimation of CIR in time domain.

Further a statistically optimal solution of the joint estimate is produced with the proposed cyclic gradient descent optimization algorithm for minimization of cost function globally. The MSE of the channel estimation is compared to the CRLB for an OFDM channel estimator without PHN.

6.4.1 PHN Modelling

If the samples of PHN (θ_n) are modelled as a discrete-time Wiener process and P^m defines a vector of the DFT coefficients of one realization of $e^{j\theta_n}$ during m^{th} OFDM symbol then the correlation matrix $\mathbf{R}_{\mathrm{P}^m}(a,b)$ is given as [32]:

$$\mathbf{R}_{\mathrm{P}^m}(a,b) = \frac{1}{N^2}\sum_{u=0}^{N-1}\sum_{v=0}^{N-1} e^{\frac{-j2\pi(au-bv)}{N}} \quad -\frac{N}{2} \le a,b \le \frac{N}{2}-1. \tag{6.19}$$

As the cumulative PHN increment between two samples of the received signal is a Gaussian random variable, for θ_n modelled as Wiener process, P^m is complex Gaussian distributed, $\Pr(\mathrm{P}^m) = \mathcal{CN}(0, \boldsymbol{\Theta})$ with mean zero and covariance matrix, $\boldsymbol{\Theta} = \mathbf{R}_{\mathrm{P}^m}(a,b)$. Since the power spectral density (PSD) of PHN tappers off rapidly beyond the loop bandwidth, PHN process can be sufficiently characterized by few lower order spectral components, containing most of the energy of a PHN sequence. These lower order spectral components of PHN are given by ${p_0}^m, {p_1}^m, {p_{-1}}^m, {p_2}^m, {p_{-2}}^m$ etc. Here we define a variable Q, as an approximation order for which $2Q+1$ elements of the vector $\mathrm{P}^m, i.e.\ p_{-Q}^m, \dots, p_0^m, \dots, p_Q^m$ can well approximate the PHN process.

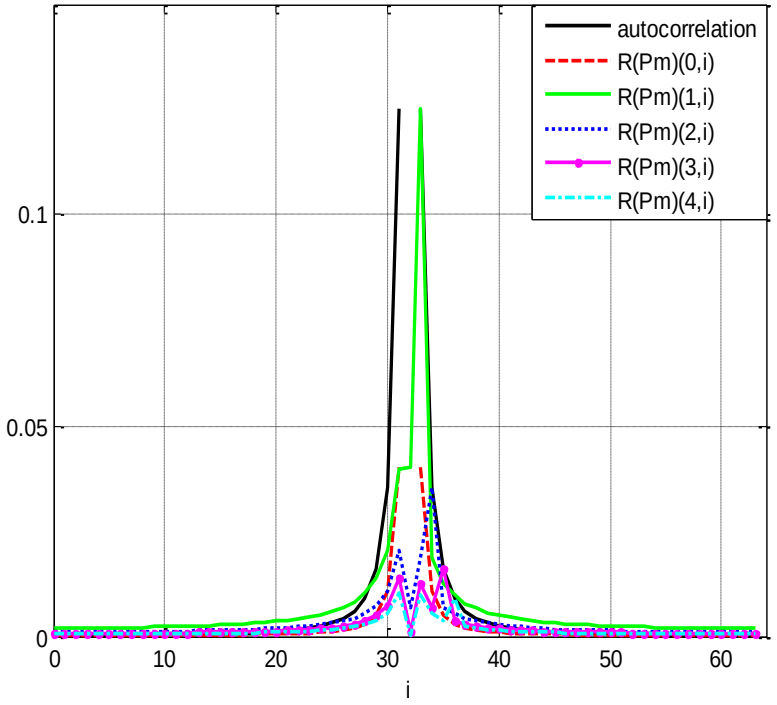

Figure 6.4 Correlation Properties of PHN Spectral Components.

Results for the matrix $\mathbf{\Theta}$ are evaluated and presented in Figure 6.4, corresponding to IEEE 802.11g like system with 64 subcarriers, 20 MHz baseband sampling frequency and 200 kHz, 2(PHN 3-dB BW). It can be observed from the Figure 6.4 that, although the cross correlation terms are significant for some lower order PHN spectral components only, the cross correlation of these PHN spectral components cannot be neglected when compared with auto correlation terms.

6.4.2 Joint MAP Estimation

In this section we will form a MAP estimate of the CTF ($\mathbf{h}$) and the PHN spectral components ($\mathbf{P}^m$) jointly, given that $\mathbf{Y}^m$ is observed for the OFDM signal model given in Equation 4.22. As a posterior distribution $\Pr(\mathbf{h}, \mathbf{P}^m|\mathbf{Y}^m)$ is proportional to the "complete likelihood function", $\Pr(\mathbf{Y}^m, \mathbf{h}, \mathbf{P}^m)$, by using Bayes' rule we can write:

$$\Pr(\mathbf{Y}^m, \mathbf{h}, \mathbf{P}^m) = \Pr(\mathbf{Y}^m|\mathbf{h}, \mathbf{P}^m)\Pr(\mathbf{h})\Pr(\mathbf{P}^m). \quad (6.20)$$

With the assumption of no prior knowledge of $\mathbf{h}$, $\Pr(\mathbf{h})$ is constant and with Wiener PHN model presented in Chapter 3 and Sub-section 6.4.1, the prior distribution of $\mathbf{P}^m$ is $\Pr(\mathbf{P}^m) = \mathcal{CN}(0, \mathbf{\Theta})$:

$$\Pr(\mathbf{P}^m) = \frac{1}{\pi^N|\mathbf{\Theta}|}\exp\left(-\mathbf{P}^{mH}\mathbf{\Theta}^{-1}\mathbf{P}^m\right) \quad (6.21)$$

where $\mathbf{\Theta}$ is known. It is equivalent to minimize the "complete negative log-likelihood function" than maximising the "complete likelihood function" in Equation (6.20). This yield:

$$\hat{\mathbf{h}}, \widehat{\mathbf{P}}^m = \arg\min_{\mathbf{h},\mathbf{P}^m}\{-\log[\Pr(\mathbf{Y}^m|\mathbf{h}, \mathbf{P}^m)] - \log[\Pr(\mathbf{P}^m)]\} \quad (6.22)$$

Given the signal model in Equation (4.22) and the AWGN density in Equation (4.12), the conditional density can be written as:

$$\Pr(\mathbf{Y}^m|\mathbf{h}, \mathbf{P}^m) = \frac{1}{(2\pi)^N\sigma_\omega^{2N}}\exp\{\frac{-1}{2\sigma_\omega^2}(\mathbf{Y}^m - \mathbf{H}^m\mathbf{P}^m)^H(\mathbf{Y}^m - \mathbf{H}^m\mathbf{P}^m)\}. \quad (6.23)$$

Using Equation (6.21), (6.22) and (6.23), the joint MAP estimate can be given as:

$$\hat{\mathbf{h}}, \widehat{\mathbf{P}}^m = \arg\min_{\mathbf{h},\mathbf{P}^m}\{\mathcal{L}(\mathbf{h}, \mathbf{P}^m)\} \quad (6.24)$$

where:

$$\mathcal{L}(\mathbf{h}, \mathbf{P}^m) = \frac{1}{2\sigma_\omega^2}(\mathbf{Y}^m - \mathbf{H}^m\mathbf{P}^m)^H(\mathbf{Y}^m - \mathbf{H}^m\mathbf{P}^m) + \mathbf{P}^{mH}\boldsymbol{\Theta}^{-1}\mathbf{P}^m \quad (6.25)$$

defines the joint MAP cost function, which is to be minimized simultaneously, for statistically optimal solution of $\widehat{\mathbf{h}}$ and $\widehat{\mathbf{P}}^m$ with respect to $\mathbf{h}$ and $\mathbf{P}^m$.

6.4.3 Cyclic Gradient Descent optimization

The problem of cost function minimization is challenging and is solved in this section with cyclic gradient descent optimization algorithm. For a frequency selective fading environment, Equation (6.25) is not easily differentiable with respect to $\mathbf{h}$, whereas with a fixed $\mathbf{P}^m$, by searching over a finite set of feasible CTF, we can minimize the Equation (6.25) with respect to $\mathbf{h}$. Now, as $\boldsymbol{\Theta}$ is a non-singular covariance matrix, $\boldsymbol{\Theta}^{-1}$ is possible and is positive semi definite matrix, which makes Equation (6.25) a quadratic function in $\mathbf{P}^m$.

Further note that for a possible solution of Equation (6.24) with respect to $\mathbf{P}^m$, Equation (6.25) should be holomorphic, means analytic in complex vector $\mathbf{P}^m$. Thus if $\mathbf{h}$ is fixed, cost function in Equation (6.25) can be minimized by taking its conjugate gradient with respect to $\mathbf{P}^m$ and equate it to zero. We begin the optimization with some initial estimate of PHN spectral components, $\widehat{\mathbf{P}}^{m\,0}$. This estimate can be obtained by least square (LS) estimation of [36] or minimum mean square error (MMSE) estimation of [35]. At i^{th} iteration, the estimate of CTF can be calculated as:

$$\hat{\mathbf{h}}^i = \arg\min_{\mathbf{h}}\{\left(\mathbf{Y}^m - \mathbf{H}^m\widehat{\mathbf{P}}^{m\,i}\right)^H\left(\mathbf{Y}^m - \mathbf{H}^m\widehat{\mathbf{P}}^{m\,i}\right)\} \quad (6.26)$$

To find the minimiser of Equation (6.26), an exhaustive grid search over a range of possible values of $\mathbf{h}$ can be used, however it is important to begin with the best estimate of $\mathbf{P}^m$ possible to avoid local minima.

In particular, random search method has been found to be more effective in high dimensional spaces [102] than potentially expensive exhaustive grid search method, which suffers from the "curse of dimensionality". To update the PHN spectral components estimate, we compute the conjugate gradient of the MAP cost function with respect to the vector $\mathbf{P}^m$. This gradient is given by:

$$\nabla_{\mathbf{P}^{m*}}\mathcal{L}(\mathbf{h},\mathbf{P}^m)=\frac{1}{\sigma_\omega^2}\left(\mathbf{H}^{mH}\mathbf{H}^m\mathbf{P}^m-\mathbf{H}^{mH}\mathbf{Y}^m\right)+2\boldsymbol{\Theta}^{-1}\mathbf{P}^m \tag{6.27}$$

where:

$$\nabla_{\mathbf{P}^{m*}}\mathcal{L}(\mathbf{h},\mathbf{P}^m)=\begin{bmatrix}\frac{\partial\mathcal{L}(\mathbf{h},\mathbf{P}^m)}{\partial p_0^{m*}}\\ \frac{\partial\mathcal{L}(\mathbf{h},\mathbf{P}^m)}{\partial p_1^{m*}}\\ \vdots\\ \frac{\partial\mathcal{L}(\mathbf{h},\mathbf{P}^m)}{\partial p_{N-1}^{m\ *}}\end{bmatrix}. \tag{6.28}$$

At iteration i, we fix the CTF in Equation (6.27) such that $\mathbf{h}=\hat{\mathbf{h}}^i$. Then by setting $\nabla_{\mathbf{P}^{m*}}\mathcal{L}(\mathbf{h},\mathbf{P}^m)\big|_{\mathbf{h}=\hat{\mathbf{h}}^i}$ equal to zero and solving for $\mathbf{P}^m$ we obtain the next PHN spectral components estimate:

$$\widehat{\mathbf{P}}^{m\,i+1}=[\widehat{\mathbf{H}}^{m\,i^H}\widehat{\mathbf{H}}^{m\,i}+2\sigma_\omega^2\boldsymbol{\Theta}^{-1}]^{-1}\widehat{\mathbf{H}}^{m\,i^H}\mathbf{Y}^m. \tag{6.29}$$

This updating procedure for the CTF and PHN spectral components continues for $i=0,1,2,3$ .... till $\mathcal{L}(\hat{\mathbf{h}},\widehat{\mathbf{P}}^m)$ get stabilized with $\|\hat{\mathbf{h}}^{i+1}-\hat{\mathbf{h}}^i\|/\|\hat{\mathbf{h}}^i\|<\varepsilon$ (preset threshold) or a number of iteration is reached.

6.4.4 Computational Complexity

The computational complexity is a critical issue for an OFDM receiver design and is addressed by the aid of FFT implementation with complexity order of $\mathcal{O}(NlogN)$. The frequency domain analysis maintains its original motivation of easy single tap equalization and linear receiver design. In case of PHN estimation, the frequency domain approach is always preferred over time domain as it allows the estimation of only few lower order PHN spectral components to mitigate nearly 100% of interference. Estimating the CTF in a frequency selective fading environment rather than CIR facilitates the proposed algorithm with the advantage of correlated subcarriers channel frequency responses (CFR) being associated with dominant PHN spectral components.

The computational complexity for the proposed joint MAP algorithm rest over evaluating Equation (6.26) and (6.29). In Equation (6.26), $\mathbf{Y}^m$ and $\widehat{\mathbf{P}}^m$ are vectors while $\mathbf{H}^m$ is a circulant matrix. Thus each matrix-vector computation has complexity

order of $\mathcal{O}(N)$. The applied random search method is computationally compact with majority of addition and subtraction with few multiplication and no divisions [102]. The PHN estimation step of Equation (6.29) is more critical as it involves inversion of a matrix with complexity order of $\mathcal{O}(N^3)$. However, in the frequency domain analysis of proposed joint MAP algorithm, all the matrices in Equation (6.29) are reduced in the size of $2Q+1 \times 2Q+1$, resulting in the complexity order of $\mathcal{O}(i(2Q+1)^3)$, where $Q \ll N$. The empirical values and dependency of estimation accuracy on $i \; and \; Q$ are further simulated in the next section.

6.4.5 Performance Analysis: Mean Square Error

Performance of the proposed algorithm is simulated in this Section for various system parameters, where each simulation point is conducted using 1,000 OFDM symbols in MATLAB. Simulation model is based on IEEE 802.11g like system with parameters given in Table 4.1. OFDM symbols are generated using 16-QAM and 64-point IFFT, and then prepended by CP of length 16 samples before transmitting over the channel.

The discrete sampled CIR is modelled as 10 tapped delay lines having an exponentially decreasing PDP as given in Equation (4.14). The 64-point FFT of the received signal is taken after receiver PHN modelling followed by CP removal. The receiver PHN, modelled as Wiener process with $\beta = 200KHz$, is simulated by passing independent identically distributed samples of a Gaussian process through one pole low pass filter. The initial estimate of $\mathbf{P}^m, i.e. \widehat{\mathbf{P}}^{m^0}$ is obtained by LS estimation [36] using different order of approximation (Q) where channel is estimated with CPE correction [30]. For CPE estimation, channel has been LS estimated [97], while ignoring the PHN. An MMSE approach can also be used, instead of LS estimation which is chosen here because of its computational simplicity. The random search algorithm [102] is applied to find the minimiser of Equation (6.26).

We now simulate the channel estimation performance for the proposed joint MAP algorithm in presence of receiver PHN. To illustrate the convergence behaviour of the algorithm, the cost function, Equation (6.25), is plotted in Figure 6.5 as a function of iteration numbers (i) for different order of approximation (Q) with signal to noise ratio (SNR) =25dB. Figure 6.5 shows that, higher the order of approximation: faster and better is the convergence.

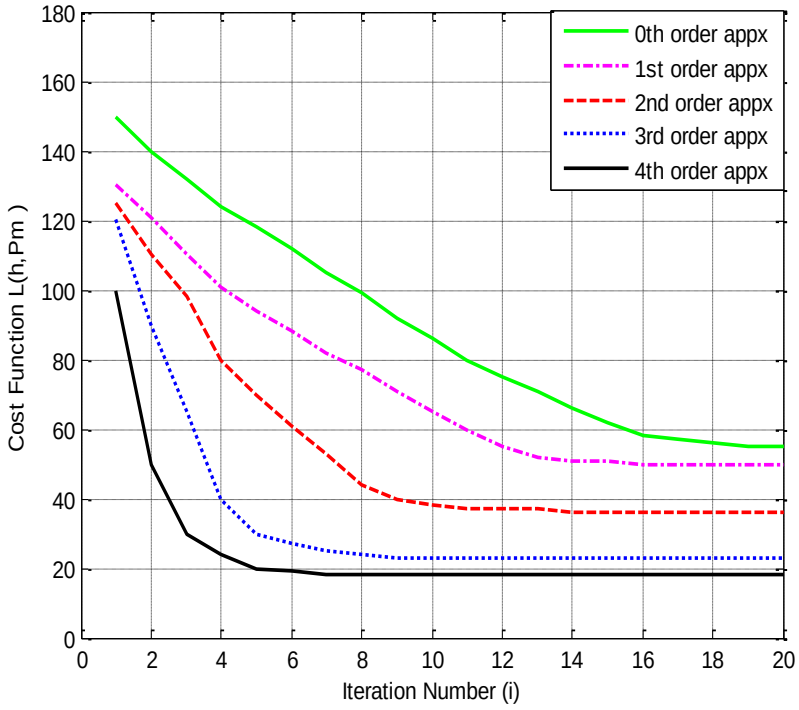

Figure 6.5 Cost Function Minimization with Cyclic Gradient Descent Optimization.

In Figure 6.6 the MSE of the proposed channel estimation for estimating normalised CTF against system SNR for $i = 6$ and $Q = 4$, is compared with the posterior CRLB for an OFDM channel estimator without PHN distortion. MSE performance curves for the channel estimation with CPE correction only and non iterative ML joint estimation of [50] are also simulated and presented in Figure 6.6.

For an OFDM system, operating in a frequency selective channel, discrete composite CIRs are uncorrelated whereas the subcarriers CFRs, which are DFTs of CIRs, are correlated. Thus for the proposed joint MAP estimator, we cannot calculate the CRLB of the MSE for the estimation of CTF directly. Instead, we derive the CRLB of the MSE for the estimation of CIR ($CRLB_{\mathrm{g}}$), and use the fact [100]:

$$CRLB_{\mathrm{h}} = N.CRLB_{\mathrm{g}}. \tag{6.30}$$

The received frequency domain signal, for an OFDM system without PHN distortion can be written as Equation (4.11) and thus:

$$\Pr(\mathbf{Y}^m|\mathbf{g}) = \mathcal{CN}(\mathbf{D}^m\mathbf{F}\mathbf{g}, 2\sigma_\omega^2\mathbf{I}). \tag{6.31}$$

or similarly:

$$\log\left[\Pr(\mathbf{Y}^m|\mathbf{g})\right] = \frac{-1}{2\sigma_\omega^2}(\mathbf{D}^m\mathbf{F}\mathbf{g} - \mathbf{Y}^m)^H(\mathbf{D}^m\mathbf{F}\mathbf{g} - \mathbf{Y}^m). \quad (6.32)$$

By taking the conjugate derivative with respect to **g**:

$$\frac{\partial}{\partial \mathbf{g}^*}\{\log\left[\Pr(\mathbf{Y}^m|\mathbf{g})\right]\} = \frac{-1}{2\sigma_\omega^2}\mathbf{F}^H\mathbf{D}^{mH}(\mathbf{D}^m\mathbf{F}\mathbf{g} - \mathbf{Y}^m)$$

$$= \frac{-1}{2\sigma_\omega^2}\mathbf{F}^H\mathbf{D}^{mH}\mathbf{W}^m. \quad (6.33)$$

The Fisher information matrix [47, 49] can be calculated as:

$$FIM(\mathbf{g}) = E\left\{\left[\frac{\partial}{\partial \mathbf{g}^*}(\log[\Pr(\mathbf{Y}^m|\mathbf{g})])\right][\frac{\partial}{\partial \mathbf{g}^*}(\log[\Pr(\mathbf{Y}^m|\mathbf{g})])]^H\right\}$$

$$= E\{\frac{1}{(2\sigma_\omega^2)^2}\mathbf{F}^H\mathbf{D}^{mH}\mathbf{W}^m\mathbf{W}^{mH}\mathbf{D}^m\mathbf{F}\}$$

$$= \frac{1}{(2\sigma_\omega^2)^2}\mathbf{F}^H\mathbf{D}^{mH}E\{\mathbf{W}^m\mathbf{W}^{mH}\}\mathbf{D}^m\mathbf{F}$$

$$= \frac{1}{2\sigma_\omega^2}\mathbf{F}^H\mathbf{D}^{mH}\mathbf{D}^m\mathbf{F}\,. \quad (6.34)$$

For a constant modulus modulation, $\mathbf{D}^{mH}\mathbf{D}^m = 2\rho^2\mathbf{I}$, where, $2\rho^2 = E_s$ is the symbol energy per subcarrier. Thus:

$$FIM(\mathbf{g}) = \frac{2\rho^2}{2\sigma_\omega^2}\mathbf{F}^H\mathbf{F}$$

$$= \frac{\rho^2}{\sigma_\omega^2}N\mathbf{I}. \quad (6.35)$$

Therefore the $CRLB_{\mathrm{g}}$ is given by:

$$CRLB_{\mathrm{g}} = Tr[FIM^{-1}(\mathbf{g})]$$

$$= \frac{L\sigma_\omega^2}{N\rho^2}$$

$$= \frac{L}{N\times SNR} \quad (6.36)$$

where $SNR = {E_s}/{\mathrm{N}_0} = \frac{2\rho^2}{2\sigma_\omega^2}$.

From Equation (6.30) the posterior CRLB for estimating the CTF, ($CRLB_{\mathrm{h}}$), is calculated as:

$$CRLB_{\mathrm{h}} = \frac{L}{SNR}. \quad (6.37)$$

The MSE is obtained as:

$$MSE = \frac{1}{MN}\sum_{m=1}^{M}\sum_{n=0}^{N-1}\left(h_n^m - \hat{h}_n^m\right)^2 \tag{6.38}$$

where M represents the number of simulated OFDM symbols.

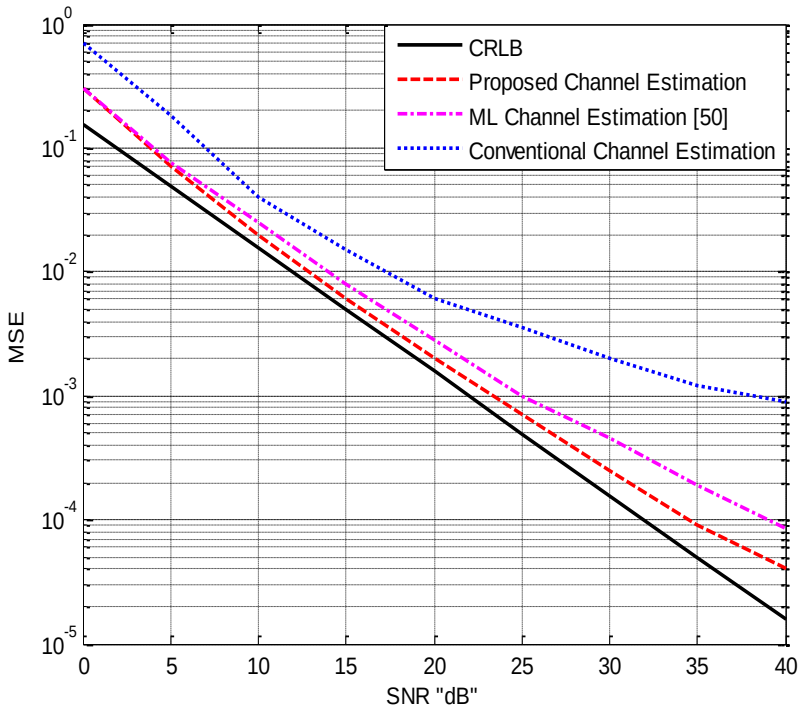

Figure 6.6 MSE Performance of CTF Estimation as a Function of SNR.

It can be observed from Figure 6.6 that for a wide range of SNR, the proposed joint MAP algorithm performs almost optimal with cancelling the effect of PHN distortion completely. Whereas, the performance of conventional channel estimator with CPE correction only is much inferior than proposed joint MAP estimation and this performance gap increases with SNR. This happens because, for large values of SNR, random ICI dominates over CPE, which produces significant SNR degradation in the channel estimation and creates an error floor. Although the conventional method is having very small computational complexity of order $\mathcal{O}(N)$ to estimate the CPE only but the MSE performance comparison proves that the proposed algorithm is quite cost effective to use for performance up gradation.

It can also be observed from Figure 6.6 that in comparison to the non iterative ML joint estimator [50], the proposed joint MAP algorithm results in better

improvements. This happens because of the performed optimization before each iteration, which combat the sever sensitivity towards high PHN level. Applying the statistical knowledge of the PHN spectral components for the optimization without small PHN approximation, even adds over the performance improvements. Though the order of computational complexity of proposed algorithm and of non iterative ML joint estimator [50] is comparable, the proposed algorithm has a higher computational time precisely.

The number of iterations (i) and the order of approximation (Q), are the two critical factors to decide about the complexity of the proposed joint MAP estimator. Thus the Figures 6.7 and 6.8 demonstrate the performance of the channel estimation as a function of i and Q respectively, at $SNR = 15, 25, and\ 35\ dB$.

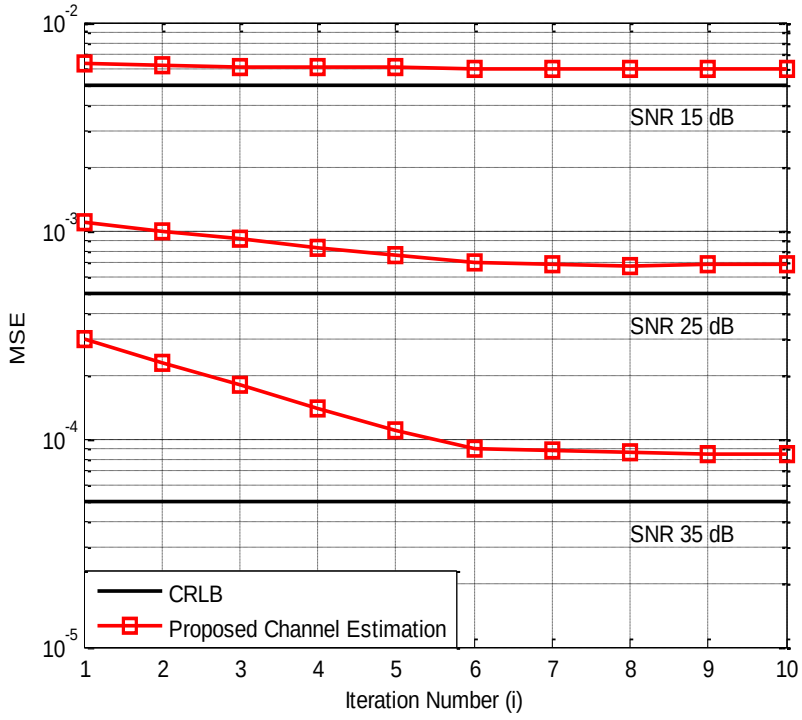

Figure 6.7 MSE Performance of CTF Estimation as a Function of Iteration Number.

It can be observed from Figure 6.7, that the cyclic gradient descent optimization improves the estimation for any SNR value, whereas a negligibly slow, performance improvement in very low SNR range can be explained with CPE dominating region which improves with SNR only. The slow improvement of very high SNR range is

there because of the sensitivity to PHN modelling error, which needs more iteration to get compensated.

Figure 6.8 shows that at any SNR value, increasing the order of approximation produces similar performance improvement for the CTF estimation. It can also be observed from Figure 6.8 that beyond $Q = 4$, increasing the approximation order does not produce significant improvement. This happens because of frequency selective nature of the channel which shapes the PHN spectrum. However, increasing the approximation order excludes the trapping of random search algorithm in local minima [102] and speeds up the convergence.

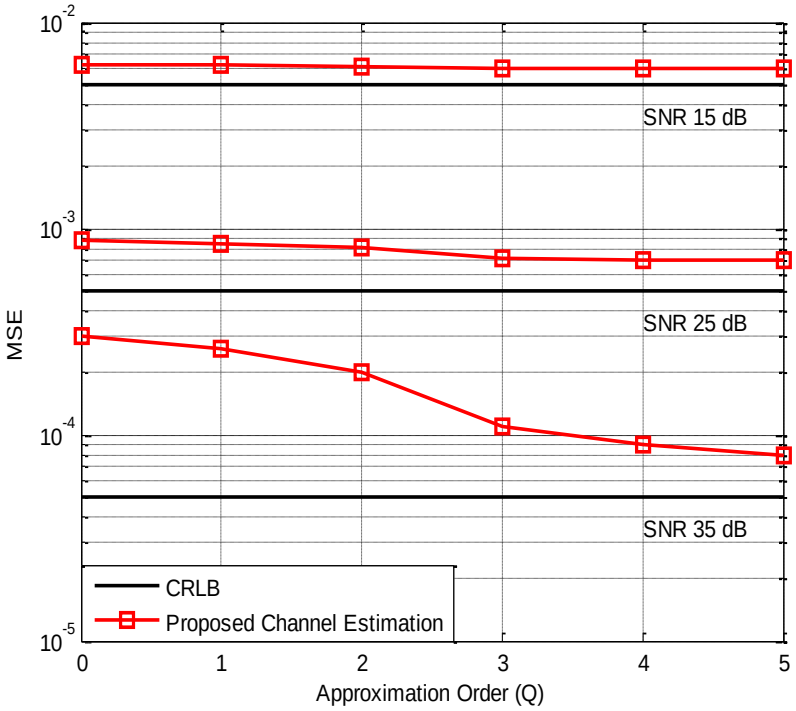

Figure 6.8 MSE Performance of CTF Estimation as a Function of Approximation Order.

6.5 Conclusion

The coherent receiver necessitates the joint channel tracking with PHN estimation for OFDM system. A 1D, block type pilot channel estimation approach with the optimum MAP criterion is proposed here. The joint estimation is performed in frequency domain with the proposed iterative cyclic gradient descent optimization algorithm.

The applied optimization including the random search method shows the fast and better convergence with increasing iteration number and approximation order. The proposed joint MAP algorithm shows better performance improvement over conventional method and ML joint estimator [50] and approaches to CRLB. This contribution is published in **[P2]**.

7. Cost Function Optimization for Joint MAP Detection in OFDM

A reliable detection of transmitted symbols incorporates the functionality of PHN estimation in joint. With the quasi-static fading channel, the channel is assumed to be static for a block length of OFDM symbols with the channel estimation and data transmission phase (Figure 4.17). As described in the last chapter, the known full pilot symbols are used to jointly estimate the PHN and channel in the channel estimation phase. The pay load is transmitted in the data transmission phase, in which data and pilot subcarriers are multiplexed together. As the PHN is time varying it needs to be estimated over each OFDM symbol in case of data transmission phase whereas for quasi static channel the channel estimation is done, once over a block of OFDM symbols. In this chapter we are dealing with the data transmission phase only and assume that channel is already known with channel estimation phase.

The conventional OFDM receivers, without attending the substantial effect of PHN in joint with data detection, severely degrade the SER performance of the system [30-32, 35-36]. Thus a reliable detection of data incorporates the functionality of PHN estimation in joint [53-58, 61-62].

A new approach to derive the MAP cost function for the joint data detection and PHN estimation in frequency domain is introduced in this chapter. The proposed joint MAP detector utilizes the prior statistical knowledge of PHN spectral components without the restriction of small PHN. Further a statistically optimal and computationally compact solution of the joint detection is produced with proposed cyclic gradient descent optimization algorithm for minimization of cost function. The proposed iterative receiver focuses on more enhanced PHN model as O-U process [78-79], as well on most studied model in literature [74-77] as Wiener process.

7.1 Phase Noise Modeling

For the samples of PHN (θ_n), P^m defines a vector of the DFT coefficients of one realization of $e^{j\theta_n}$ during m^{th} OFDM symbol, then the correlation matrices for FRO and PLL VCO are given as [32, 35]:

$$\mathbf{R}_{\mathrm{P}^m}(a,b) = \frac{1}{N^2}\sum_{u=0}^{N-1}\sum_{v=0}^{N-1} e^{\frac{-|u-v|\sigma_\phi^2}{2}} e^{\frac{-j2\pi(au-bv)}{N}}, -\frac{N}{2} \le a,b \le \frac{N}{2}-1 \quad (7.1)$$

and

$$\mathbf{R}_{\mathrm{P}^m}(a,b)_{PLL} = \frac{1}{N^2}\sum_{u=0}^{N-1}\sum_{v=0}^{N-1} e^{\frac{-j2\pi(au-bv)}{N}} \; e^{-4\pi^2 {f_c}^2\left(C_{in}\frac{|u-v|\,T_s}{N}+2\sum_{i=1}^{2}(\xi_i+\zeta_i)\left(1-e^{-\lambda_i\frac{|u-v|T_s}{N}}\right)\right)}$$

$$-\frac{N}{2} \le a,b \le \frac{N}{2}-1. \quad (7.2)$$

As the cumulative PHN increment between two samples of the received signal is a Gaussian random variable, for θ_n modelled as Wiener process and asymptotically Gaussian random variable for θ_n modelled as celebrated O-U process, P^m is complex Gaussian distributed, $\Pr(\mathrm{P}^m) = \mathcal{CN}(0, \boldsymbol{\Theta})$, with mean zero and covariance matrix, $\boldsymbol{\Theta} = \mathbf{R}_{\mathrm{P}^m}(a,b)$for FRO and $\boldsymbol{\Theta} = \mathbf{R}_{\mathrm{P}^m}(a,b)_{PLL}$ for PLL VCO.

Since the PSD of PHN tappers off rapidly beyond the loop bandwidth, PHN process can be sufficiently characterized by few lower order spectral components, containing most of the energy of a PHN sequence. These lower order spectral components of PHN are given by ${p_0}^m, {p_1}^m, {p_{-1}}^m, {p_2}^m, {p_{-2}}^m$ etc.

Here we define a variable Q, as an approximation order for which $2Q+1$ elements of the vector $\mathrm{P}^m, i.e.\ p_{-Q}^m, \ldots, p_0^m, \ldots, p_Q^m$ can well approximate the PHN process. Results for the matrix $\boldsymbol{\Theta}$ are evaluated and presented in Figure 7.1 (a) and 7.1 (b) for FRO and PLL VCO respectively, corresponding to IEEE 802.11g like system with parameters given in Table 4.1. The parameters of PHN from FRO and PLL VCO are described in Table 3.2.

By comparing Figure 7.1(a) and 7.1(b), it can be observed that PLL VCO tends to reduce the overall PHN as well the near carrier PHN significantly.

It can also be concluded from the Figure 7.1 (a) and 7.1 (b) that, although the cross correlation terms are significant for some lower order PHN spectral components only, the cross correlation of these PHN spectral components cannot be neglected when compared with auto correlation terms.

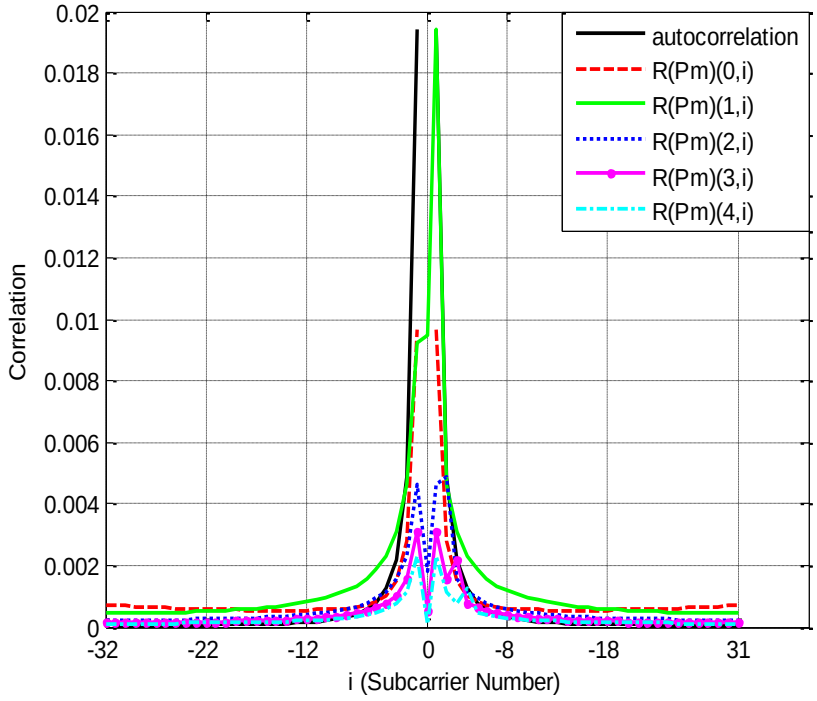

(a)

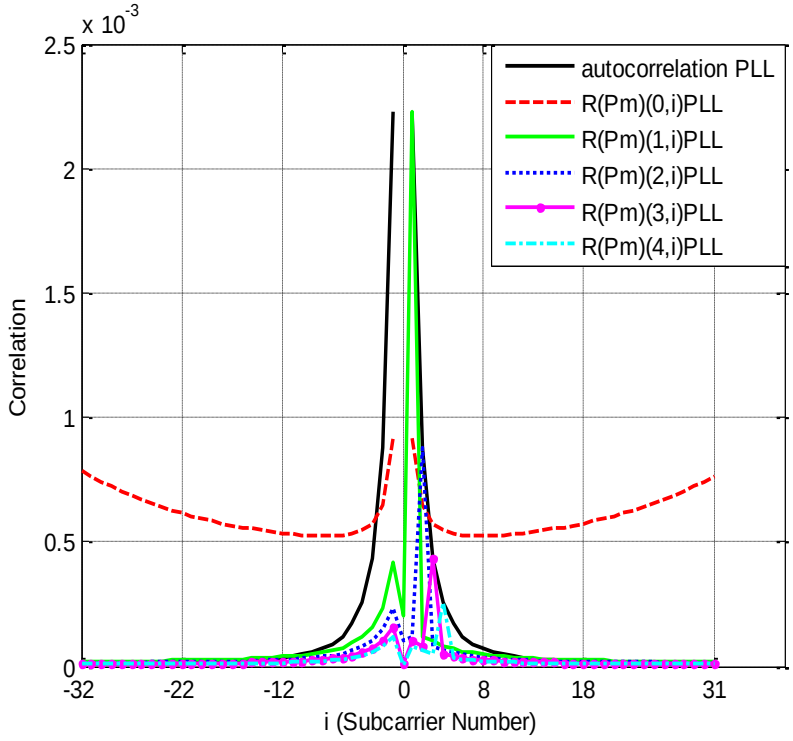

(b)

Figure 7.1 Correlation Property of PHN spectral components (a) FRO (b) PLL VCO.

7.2 OFDM Modeling

The frequency domain received signal on the k^{th} subcarrier of the m^{th} symbol after taking the FFT of r_n^m is given in Equation (4.21), and is represented in the matrix form as:

$$\mathbf{Y}^m = \mathbf{Z}^m\mathbf{P}^m + \mathbf{W}^m \tag{7.3}$$

where $\mathbf{Y}^m = [y_0^m, y_1^m, \dots, y_{N-1}^m]^T$, $\mathbf{P}^m = [p_0^m, p_1^m, \dots, p_{N-1}^m]^T$, $\mathbf{h} = [h_0, h_1, h_2, \dots, h_{N-1}]^T$, $\mathbf{X}^m = [X_0^m, X_1^m, \dots, X_{N-1}^m]^T$ and $\mathbf{Z}^m$ is a column wise circulant matrix whose first column is vector $[h_0X_0^m, h_1X_1^m, \dots, h_{N-1}X_{N-1}^m]^T$. $\mathbf{W}^m = [W_0^m, W_1^m, \dots, W_{N-1}^m]^T$, is an uncorrelated white noise vector distributed as, $\Pr(\mathbf{W}^m) = \mathcal{CN}(0, 2\sigma_\omega^2\mathbf{I})$(Equation 4.12).

7.3 Joint MAP Detector

In this section we will form a MAP estimate of the symbol vector ($\mathbf{X}^m$) and the PHN spectral components ($\mathbf{P}^m$) jointly, given that $\mathbf{Y}^m$ is observed and $\mathbf{h}$ is known. As a posterior distribution, $\Pr(\mathbf{X}^m, \mathbf{P}^m|\mathbf{Y}^m)$ is proportional to the "complete likelihood function", $\Pr(\mathbf{Y}^m, \mathbf{X}^m, \mathbf{P}^m)$, so by using Bayes' rule we can write:

$$\Pr(\mathbf{Y}^m, \mathbf{X}^m, \mathbf{P}^m) = \Pr(\mathbf{Y}^m|\mathbf{X}^m, \mathbf{P}^m)\Pr(\mathbf{X}^m)\Pr(\mathbf{P}^m). \tag{7.4}$$

With no prior knowledge of $\mathbf{X}^m$, $\Pr(\mathbf{X}^m)$ is constant and with PHN model presented in Chapter 3 and Section 7.1, the prior distribution of $\mathbf{P}^m$ is, $\Pr(\mathbf{P}^m) = \mathcal{CN}(0, \boldsymbol{\Theta})$, which says:

$$\Pr(\mathbf{P}^m) = \frac{1}{\pi^N|\boldsymbol{\Theta}|}exp\left(-\mathbf{P}^{mH}\boldsymbol{\Theta}^{-1}\mathbf{P}^m\right) \tag{7.5}$$

where $\boldsymbol{\Theta}$ is known. As it is equivalent to minimize the "complete negative log-likelihood function" and maximise the "complete likelihood function" in Equation (7.4), so:

$$\widehat{\mathbf{X}}^m, \widehat{\mathbf{P}}^m = \underset{\mathbf{X}^m, \mathbf{P}^m}{arg\,min} \{-log[\Pr(\mathbf{Y}^m|\mathbf{X}^m, \mathbf{P}^m)]] - log[\Pr(\mathbf{P}^m)]\}. \tag{7.6}$$

Given the signal model in Equation (7.3) and the AWGN density in Equation (4.12), the conditional density can be written as:

$$\Pr(\mathbf{Y}^m|\mathbf{X}^m,\mathbf{P}^m) = \frac{1}{(2\pi)^N\sigma_\omega^{2N}} exp\{\frac{-1}{2\sigma_\omega^2}(\mathbf{Y}^m - \mathbf{Z}^m\mathbf{P}^m)^H(\mathbf{Y}^m - \mathbf{Z}^m\mathbf{P}^m)\}. \quad (7.7)$$

Using Equation (7.5), (7.6) and (7.7), the joint MAP estimate can be given as:

$$\widehat{\mathbf{X}}^m, \widehat{\mathbf{P}}^m = arg\, min_{\mathbf{X}^m,\mathbf{P}^m}\{\mathcal{L}(\mathbf{X}^m,\mathbf{P}^m)\} \quad (7.8)$$

where:

$$\mathcal{L}(\mathbf{X}^m,\mathbf{P}^m) = \frac{1}{2\sigma_\omega^2}(\mathbf{Y}^m - \mathbf{Z}^m\mathbf{P}^m)^H(\mathbf{Y}^m - \mathbf{Z}^m\mathbf{P}^m) + \mathbf{P}^{mH}\boldsymbol{\Theta}^{-1}\mathbf{P}^m \quad (7.9)$$

defines the joint MAP cost function, which is to be minimized simultaneously, for statistically optimal solution of $\widehat{\mathbf{X}}^m$ and $\widehat{\mathbf{P}}^m$ with respect to $\mathbf{X}^m$ and $\mathbf{P}^m$.

7.4 Cost Function Optimization

The problem of cost function minimization is challenging and is solved in this section with the cyclic gradient descent optimization algorithm proposed in the last chapter. We begin the optimization with some initial estimate of PHN spectral components, $\widehat{\mathbf{P}}^{m^0}$. At i^{th} iteration, the estimate of symbol vector can be calculated as:

$$\widehat{\mathbf{X}}^{m^i} = arg\, min_{\mathbf{X}^m} \{\left(\mathbf{Y}^m - \mathbf{Z}^m\widehat{\mathbf{P}}^{m^i}\right)^H \left(\mathbf{Y}^m - \mathbf{Z}^m\widehat{\mathbf{P}}^{m^i}\right)\}. \quad (7.10)$$

To find the minimiser of Equation (7.10), an exhaustive grid search or a random search method over a range of possible values of $\mathbf{X}^m$ can be used with the best estimate of $\mathbf{P}^m$, to avoid the local minima. To update the PHN spectral components estimate, we compute the conjugate gradient of the MAP cost function with respect to the vector $\mathbf{P}^m$. This gradient is given by:

$$\nabla_{\mathbf{P}^{m^*}}\mathcal{L}(\mathbf{X}^m,\mathbf{P}^m) = \frac{1}{\sigma_\omega^2}\left(\mathbf{Z}^{mH}\mathbf{Z}^m\mathbf{P}^m - \mathbf{Z}^{mH}\mathbf{Y}^m\right) + 2\boldsymbol{\Theta}^{-1}\mathbf{P}^m \quad (7.11)$$

where:

$$\nabla_{\mathbf{P}^{m^*}}\mathcal{L}(\mathbf{X}^m,\mathbf{P}^m) = \begin{bmatrix} \frac{\partial\mathcal{L}(\mathbf{X}^m,\mathbf{P}^m)}{\partial p_0^{m^*}} \\ \frac{\partial\mathcal{L}(\mathbf{X}^m,\mathbf{P}^m)}{\partial p_1^{m^*}} \\ \vdots \\ \frac{\partial\mathcal{L}(\mathbf{X}^m,\mathbf{P}^m)}{\partial p_{N-1}^{m^*}} \end{bmatrix}. \quad (7.12)$$

At iteration i, we fix the symbol vector in Equation (7.11) such that $\mathbf{X}^m = \widehat{\mathbf{X}}^{m^i}$. Then by setting $\nabla_{\mathbf{P}^{m*}} \mathcal{L}(\mathbf{X}^m, \mathbf{P}^m)\big|_{\mathbf{X}^m = \widehat{\mathbf{X}}^{m^i}}$ equal to zero and solving for $\mathbf{P}^m$ we obtain the next PHN spectral components estimate:

$$\widehat{\mathbf{P}}^{m^{i+1}} = [\hat{\mathbf{Z}}^{m^{i^H}} \hat{\mathbf{Z}}^{m^i} + 2\sigma_\omega^2 \mathbf{\Theta}^{-1}]^{-1} \hat{\mathbf{Z}}^{m^{i^H}} \mathbf{Y}^m. \tag{7.13}$$

This updating procedure for the symbol vector and PHN spectral components continues for $i = 0,1,2,3$ .... till $\mathcal{L}(\widehat{\mathbf{X}}^m, \widehat{\mathbf{P}}^m)$ get stabilized with $\left\|\widehat{\mathbf{X}}^{m^{i+1}} - \widehat{\mathbf{X}}^{m^i}\right\| / \left\|\widehat{\mathbf{X}}^{m^i}\right\| < \varepsilon$ (preset threshold) or a number of iteration is reached.

7.5 Performance Analysis: Symbol Error Rate

Performance of the proposed joint MAP algorithm is simulated in this Section for various system parameters, where each simulation point is conducted using 10,000 OFDM symbols in MATLAB. Simulation model is based on IEEE 802.11g like system with parameters given in Table 7.1.

F_s	20 MHz
N	64
Active Sub-Carriers	56
N_P	10
FFT Size	64
N_g	16 Samples
Mapping	16-QAM

Table 7.1 OFDM Modeling Parameters for Data Detection.

OFDM symbols are generated using 16-QAM and 64-point IFFT, and then prepended by CP of length 16 samples before transmitting over the channel. The channel is AWGN or multipath channel (Equation (4.14)) as applicable.

The 64-point FFT of the received signal is taken after receiver PHN modelling followed by CP removal. The receiver PHN is modelled as Wiener process and celebrated O-U process for FRO and PLL VCO respectively as described in Table 3.2 and shown in Figure 3.12. The PHN effect is estimated and then jointly optimized with data detection by using proposed joint MAP algorithm. The initial estimate of $\mathbf{P}^m$, i. e. $\widehat{\mathbf{P}}^{m^0}$ is obtained by LS estimation [36] using order of approximation (Q) equals to 4. The random search algorithm [102] is applied to find the minimiser of Equation (7.10).

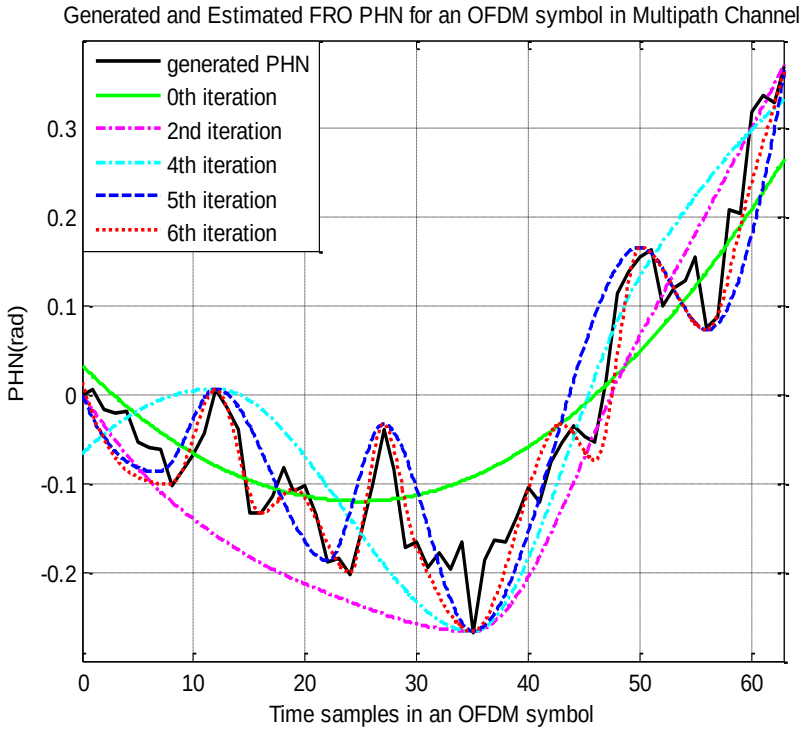

Figure 7.2 FRO PHN Estimation with Proposed Joint MAP Algorithm for Multipath Channel.

We now simulate the performance of proposed joint MAP algorithm in presence of applicable receiver PHN model and channel type. To illustrate the estimation accuracy and convergence behaviour of the algorithm, the generated PHN samples for FRO over one OFDM symbol are compared with estimated PHN samples in multipath channel for different no. of iterations (i) with SNR=30 dB and $Q = 4$. Figure 7.2 shows that estimation approaches to the actual PHN with $i = 5$ whereas with $i = 6$, it is very accurate.

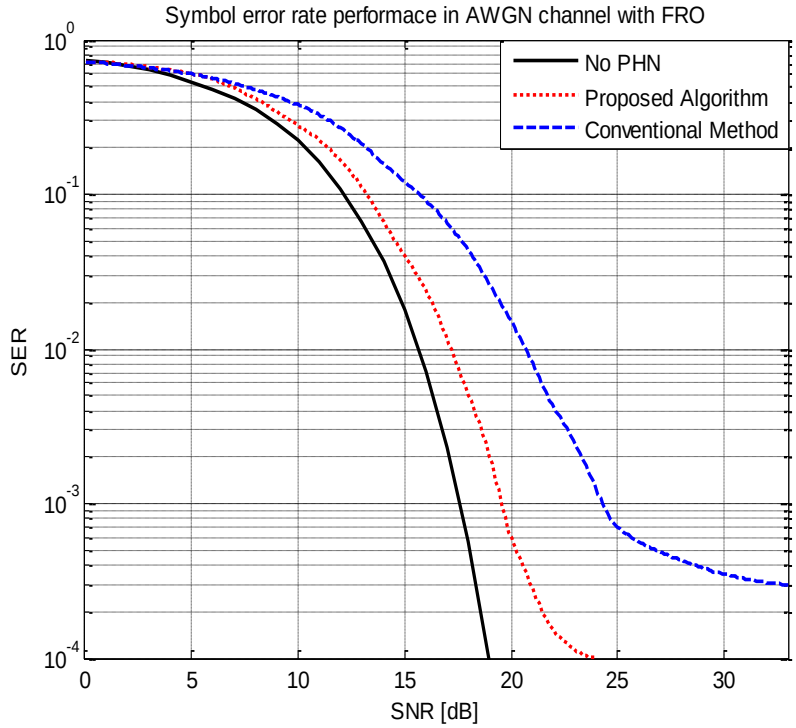

Figure 7.3 SER Performance Comparison between the Conventional Method and Proposed Algorithm for AWGN Channel in case of FRO.

In Figure 7.3 the SER performance of the proposed joint MAP algorithm is compared with the "No PHN" scenario, for $i = 6$ and $Q = 4$, against system SNR in AWGN channel in case of FRO. The corresponding SER performance of the conventional method [35-36] is also simulated and presented in Figure 7.3.

It can be observed from Figure 7.3 that proposed joint MAP algorithm achieves near "No PHN" performance whereas the conventional method shows an error floor at higher SNR values. This happens because the inaccurate detection of symbols led to less accurate PHN spectral components estimation and this error propagation at higher SNR values deteriorate the SER performance, which is compensated in the proposed algorithm with joint MAP optimization before next iteration. Although the conventional method is having lesser computational complexity than the proposed algorithm but the SER performance comparison proves that the proposed algorithm is quite cost effective to use for performance up gradation.

In Figure 7.4 the SER performance of the proposed joint MAP algorithm is compared with the "No PHN" scenario and conventional method of [35-36], for $i = 6$ and $Q = 4$, against system SNR in AWGN channel in case of PLL VCO. It can be observed from Figure 7.4 that as the PLL VCO limits the single direction drift of PHN process, it reduces the overall PHN floor and so the CPE significantly. Simultaneously the high frequency components of PHN are also suppressed with PLL VCO.

This double advantage can be observed in the SER performance of Figure 7.4, which is showing 1dB improvement at SER=10^{-3} and 4 dB improvement at SER=10^{-4}, as compared to FRO case of Figure 7.3. It can be also observed from Figure 7.4 that the conventional method also works significantly well in case of PLL VCO because with less CPE and reduced high frequency components of PHN, the probability of inaccurate detection of symbols reduces and so the error floor.

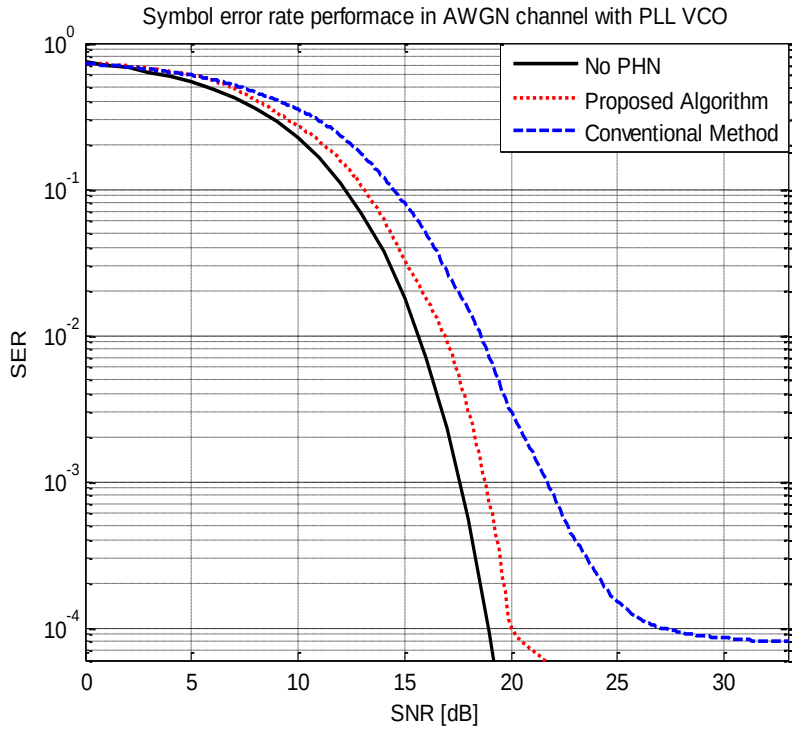

Figure 7.4 SER performance comparison between the conventional method and proposed algorithm for AWGN channel in case of PLL VCO.

In Figure 7.5 the SER performance of the proposed joint MAP algorithm is compared with the "No PHN" scenario, for $i = 6$ and $Q = 4$, against system SNR in multipath channel in case of FRO. The corresponding SER performance of the conventional method [35-36] is also simulated and presented. It can be observed from Figure 7.5 that presented joint MAP estimator with proposed optimization closely follows the "No PHN" curve even in multipath channel whereas the conventional method underperforms over the entire range of SNR and needs higher order of approximation to combat the severe sensitivity towards PHN modelling error, because of deep fade scenario.

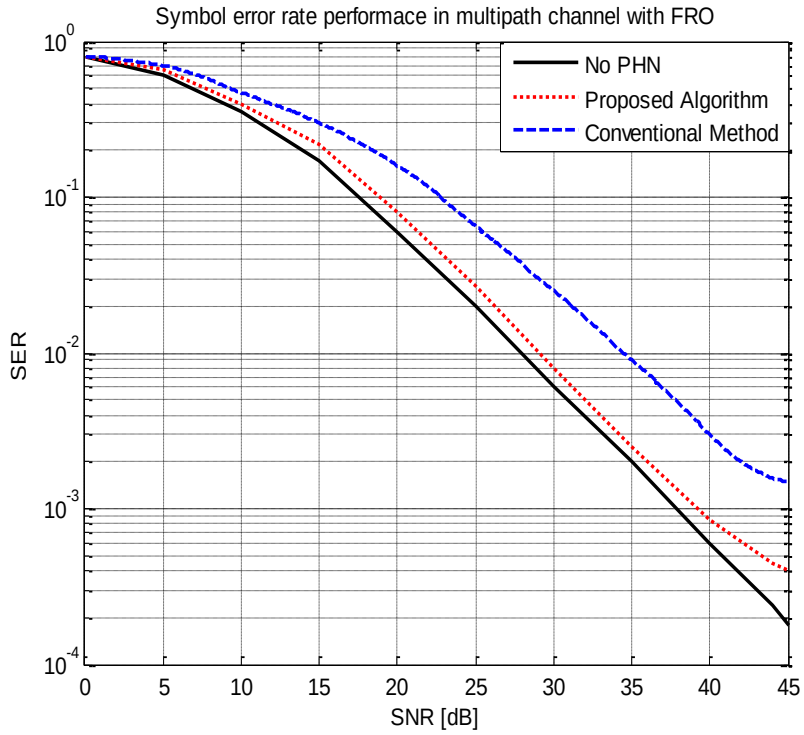

Figure 7.5 SER performance Comparison between the Conventional Method and Proposed Algorithm for Multipath Channel in case of FRO.

In Figure 7.6 the SER performance of the proposed joint MAP algorithm in case of FRO is compared with the case of PLL VCO, for $i = 6$ and $Q = 4$, against relative PHN bandwidth, Δ_{PN},with system SNR=30dB, in multipath channel. With the double advantage of PLL VCO, SER of the proposed algorithm shows the noticeable increment at very large Δ_{PN}, whereas it rises early at very small Δ_{PN} for FRO

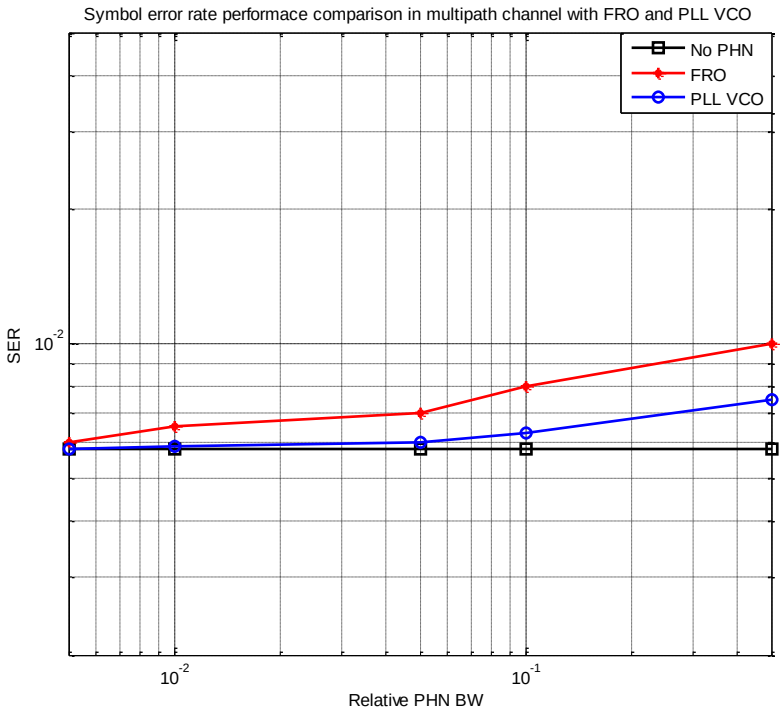

Figure 7.6 SER Performance Comparison between the FRO and PLL VCO for Proposed Algorithm in Multipath Channel.

7.6 Conclusion

Because of the time varying nature we need to estimate the PHN over each OFDM symbol in joint with data detection for data transmission phase. A 1D, comb type pilot data detection approach with the optimum MAP criterion is proposed here with cyclic gradient descent optimization algorithm. Simulation results demonstrate that the proposed joint MAP detection algorithm shows better performance improvement over conventional method for both the PHN models, i.e. Wiener and O-U process. The SER approaches to “No PHN” performance for both the channel models, i.e. AWGN and multipath channel. This contribution is published in **[P1].**

8. Conclusion and Future Scope

With great potential for high data rate even in multipath fading channel, OFDM have gained ample interest to be deployed worldwide. Multiuser extension of the technique, i.e. OFDMA, further adds the potential of high spectral efficiency to the system. This chapter highlights the contribution of our research work done in the area of OFDM/OFDMA systems with PHN. The chapter also presents the opportunities to extend the research in future.

8.1 Discussion over Contributions

Designing an OFDM/OFDMA-based communication system demands an accurate prediction of the tolerable PHN which can allow the system and RF engineers to relax the specifications. In single carrier systems, the PHN merely causes simple rotation in the symbol constellation, whereas in OFDM systems, in addition to the rotational effect called CPE, PHN also causes ICI. Moreover the PHN in OFDMA system heavily degrades the performance as it creates MUI also because of multiple access technique. Incorporating both the transmitter, accompanied with power and PHN level differences between the users, and receiver PHN induced spread in OFDMA uplink system, further produces the performance degradation for users with low signal powers.

In this thesis an improved evaluation of OFDMA system performance is studied in terms of SINR, which is derived here to extend the state of art results while relaxing the assumption of complex Gaussian distributed ICI and MUI. The analysis is proven with simulation results to have an insight of PHN effect on the actual system as a function of critical system parameters. This efficient analysis will allow the design of oscillators to meet the necessary PHN requirements and hence ensures satisfactory performance of the overall system. This contribution is published in **[P4]**.

Further the characterization of MUI, in the SINR, as a function of power level and PHN level differences among the users is done with both type of sub channelization (Contiguous and Interleave). The simulation verifies the analysis results and also proves that non Gaussian distributed ICI and MUI produces serious degradation in the

system performance even with small 2(PHN 3-dB BW). This accurate characterization tends to improve the performances of algorithms, designed to perform sub channelization and resource allocation in OFDMA systems with PHN. This contribution is published in **[P3]**.

To improve the system performance even in the presence of PHN, designing the baseband algorithm to estimate and mitigate the PHN effect is always preferred over incorporating the highly complex and costly accurate RF devices. Computational complexity of the algorithm is also the critical parameter to prove the competence of the derived algorithm along the system performance improvement. Thus a near optimum channel estimation for OFDM system in presence of receiver PHN, using joint MAP criterion is proposed in this thesis. With the proposed iterative cyclic gradient descent algorithm for optimization, the MSE of the channel estimation achieves near CRLB performance even with lower computational complexity.

Estimated PHN spectral components analysis without the assumption of small PHN improves over the cost function minimization and joint MAP estimation. Simulation results prove the performance improvement over state of art results and also show that the estimator improves with order of approximations and number of iterations. The performance of the conventional channel estimator with CPE correction only is much inferior to proposed joint MAP estimation and this performance gap increases with SNR because for high PHN levels, with large values of SNR, random ICI dominates over CPE, which produces significant SNR degradation in the channel estimation and creates an error floor.

In comparison to the non iterative ML joint estimator [50], the proposed joint MAP algorithm results in better improvements because of the performed optimization before each iteration, which combat the sever sensitivity towards high PHN level. This contribution is published in **[P2]**.

With the proposed iterative cyclic gradient descent optimization algorithm a new alternative of near optimum data detection for OFDM system in presence of PHN is also proposed in this thesis. Simulation results show that by using joint MAP criterion, SER achieves near “No PHN” performance whereas the conventional method shows an error floor at higher SNR values. This happens because the inaccurate detection of symbols led to less accurate PHN spectral components estimation and this error

propagation at higher SNR values deteriorate the SER performance, which is compensated in the proposed algorithm with joint MAP optimization before next iteration.

Results also show that presented joint MAP detector with proposed optimization closely follows the "No PHN" curve even in multipath channel whereas the conventional method underperforms over the entire range of SNR and needs higher order of approximation to combat the severe sensitivity towards PHN modelling error, because of deep fade scenario. This contribution is published in **[P1]**.

8.2 Suggestions for Future Work

A research can be completed but never ends, as there is always a scope to extend the current outcomes. Some directions for the future extension of the presented work can be:

- While characterizing the MUI in OFDMA uplink system, the transmitter AFE is always more critical than receiver AFE in context of PHN production. This factor has been proved in the presented work with simulation results. To incorporate the effect of as many PHN sequences as there are users, not only the non Gaussian distribution of MUI but also the additional degradation due to the acyclic nature of the transmitted signal can be considered. This calls for a more complex analysis as one need to deal with diverse PHN parameter's set.
- In the proposed joint MAP channel estimator, to derive the joint MAP cost function of CTF and PHN spectral components, $\Pr(\mathbf{h})$ is taken constant which represents that $\Pr(\mathbf{h})$ is non informative prior which usually happens when channel is blind. This generalized approach can be extended while incorporating the fading statistics for different channel modeling. This calls for deriving the cost function with known statistical channel state information (CSI) without knowing the instantaneous CSI. Further this will be limited by the choice of fast and slow fading channel. The achievable techniques can be: exploiting the diversity (spatial dimension) as in MIMO-OFDM or relaxing the blind channel with known fading distribution and line of sight component.

- In the proposed joint MAP data detection algorithm the aid of channel coding, as in Coded OFDM, can be the next state to enhance the system performance. This plausible enhancement in the performance calls for a more careful insight in the field of channel coding and detection algorithms. The achievable technique can be the aid of soft extrinsic information in case of Turbo Codes or some complex pruning algorithm in case of Low Density Parity Check Codes.

References

[1] B. Saltzberg, "Performance of an Efficient Parallel Data Transmission System", *IEEE Transactions on Communication Technology*, vol. 15, no. 6, pp. 805-811, 1967.

[2] R. W. Chang and R. Gibby, "A theoretical Study of Performance of an Orthogonal Multiplexing Data Transmission Scheme", *IEEE Transactions on Communication Technology*, vol. 16, no. 4, pp. 529-540, 1968.

[3] R.W. Chang, "*Orthogonal Frequency Division Multiplexing*", U.S. Patent 3,488,445, 1970.

[4] S. Weinstein and P. Ebert. "Data Transmission by Frequency-Division Multiplexing using the Discrete Fourier Transforms", *IEEE Transactions on Communication Technology*, vol. 19, no. 5, pp. 628-634, 1971.

[5] A. Peled and A. Ruiz, "Frequency Domain Data Transmission Using Reduced Computational Complexity Algorithms", *IEEE International Conference on Acoustics, Speech, and Signal Processing*, vol. 5, DOI: 10.1109/ICASSP. 1980.1171076, 1980

[6] L. J. Cimini, "Analysis and Simulation of a Digital Mobile Channel using Orthogonal Frequency Division Multplexing", *IEEE Transactions on Communications*, vol. COM-33, pp. 665-675, 1985.

[7] J. A. C. Bingham, "Multicarrier Modulation for Data Transmission: An Idea Whose Time has Come", *IEEE Communications Magazine*, vol. 28, no. 5, pp. 5-14, 1990.

[8] Y. Wu and W. Y. Zou, "Orthogonal Frequency Division Multiplexing: A Multi-Carrier Modulation Scheme", *IEEE Transactions on Consumer Electronics*, vol. 41, no. 3, pp. 392-399, 1995.

[9] K. Fazel and S. Kaiser, "*Multicarrier and Spread Spectrum Systems*", A John Wiley and Sons, Limited, Publication, Second Edition, 2008.

[10] H. J. Taha and M. F. M. Salleh, "Multi-carrier Transmission Techniques for Wireless Communication Systems: A Survey", *WSEAS Transactions on Communications*, vol. 8, no. 5, pp. 457-472, 2009.

[11] R. Saxena and H. D. Joshi, "OFDM and its Major Concerns: A Study with Way Out", *IETE Journal of Education*, vol. 54, no. 1, pp. 26-49, 2013.

[12] C. Y. Wong, R. S. Cheng, K. B. Lataief and R. D. Murch, "Multiuser OFDM with Adaptive Sub- carrier, Bit and Power Allocation", *IEEE Journal on Selected Areas in Communications*, vol. 17, no. 10, pp. 1747-1758, 1999.

[13] S. Srikanth, V. Kumaran, C. Manikandan and Murugesapandian, "Orthogonal Frequency Division Multiple Access: Is it the Multiple Access System of the Future?", *AU-KBC Research Center*, Anna University, India, 2006.

[14] H. H. Chen, X. Zhang and W. Xu, "Next-generation CDMA vs. OFDMA for 4G wireless Applications", *IEEE Wireless Communications*, Guest Editorial, 2007.

[15] P. H. Lehne and F. Bøhagen, "OFDM (A) for Wireless Communication", *R&I Research Report*, Telnor, 2008.

[16] D. T. C. Wong, P. Y. Kong, Y. C. Liang, K. C. Chua and J. W. Mark, "*Wireless Broadband Networks*", A John Wiley & Sons, Incorporated, Publication, 2009.

[17] A. Maeder and N. Zein, "OFDMA in the Field: Current and Future Challenges", *ACM SIGCOMM Computer Communication Review*, vol. 40, no. 5, pp. 71-76, 2010.

[18] M. Krondorf and G. Fettweis, "OFDM Link Performance Analysis under Various Receiver Impairments" *EURASIP Journal on Wireless Communications and Networking*, DOI: org/10.1155/2008/145279, 2008.

[19] P. H. Moose. "A Technique for Orthogonal Frequency Division Multiplexing Frequency Offset Correction", *IEEE Transactions on Communications*, vol. 42, pp. 2908-2914, 1994.

[20] Z. Zhang, W. Jiang, H. Zhou, Y. Liu, and J. Gao, "High Accuracy Frequency Offset Correction with Adjustable Acquisition Range in OFDM Systems", *IEEE Transactions on Wireless Communications*, vol. 4, no. 1, pp. 228-237, 2005.

[21] D, Huang and K. B. Letaief, "An Interference-Cancellation Scheme for Carrier Frequency Offsets Correction in OFDMA Systems", *IEEE Transactions on Communications*, vol. 53, no. 7, pp. 1155-1165, 2005.

[22] Z. Zhang and C. Tellambura, “The Effect of Imperfect Carrier Frequency Offset Estimation on an OFDMA Uplink”, *IEEE transactions on Communications*, vol. 57, no. 4, pp. 1025-1030, 2009.

[23] A. Tarighat, R. Bagheri and A. H. Sayed, “Compensation Schemes and Performance Analysis of IQ Imbalances in OFDM Receivers”, *IEEE Transactions on Signal Processing*, vol. 53, no. 8, pp. 3257-3268, 2005.

[24] J. Tubbax, B. Come, L. V. Perre, S. Donnay, M. Engels, H. D. Man and M. Moonen, “Compensation of IQ Imbalance and Phase Noise in OFDM Systems”, *IEEE Transactions on Wireless Communications*, vol. 4, no. 3, pp. 872-877, 2005.

[25] Q. Zou, A. Tarighat and A. H. Sayed, “Joint Compensation of IQ Imbalance and Phase Noise in OFDM Wireless Systems” *IEEE Transactions On Communications*, vol. 57, no. 2, pp. 404-414, 2009.

[26] P. Robertson and S. Kaiser, “Analysis of the Effects of Phase Noise in Orthogonal Frequency Division Multiplex (OFDM) Systems”, in *Proc. IEEE ICC’95*, vol. 3, pp. 1652-1657, Seattle, WA, 1995.

[27] A. Armada and M. Calvo, “Phase Noise and Sub-Carrier Spacing Effects on the Performance of an OFDM Communication System”, *IEEE Communication Letters*, vol. 2, no. 1, pp. 11 –13, 1998.

[28] A. Armada, “Understanding the Effects of Phase Noise in Orthogonal Frequency Division Multiplexing (OFDM)”, *IEEE Transactions on Broadcast*ing, vol. 47, no. 2, pp. 153 –159, 2001.

[29] S. Wu and Y. Bar-Ness, “Performance Analysis on the Effect of Phase Noise in OFDM Systems”, in *Proc. IEEE Seventh International Symposium on Spread Spectrum Techniques and Applications*, Prague, Czech Republic, 2002.

[30] S. Wu and Y. Bar-Ness, “A Phase Noise Suppression Algorithm for OFDM based WLANs”, *IEEE Communication Letters*, vol. 6, no. 12, pp. 535-537, 2002.

[31] S. Wu and Y. Bar-Ness, “OFDM Systems in the Presence of Phase Noise: Consequences and Solutions”, *IEEE Transactions on Communications*, vol. 52, no. 11, pp. 1988-1997, 2004.

[32] D. Petrovic, W. Rave and G. Fettweis, “Intercarrier Interference due to Phase Noise in OFDM - Estimation and Suppression”, in *Proc. IEEE Vehicular Technology Conference Fall,* vol. 3, pp. 2191 – 2195, 2004.

[33] D. Petrovic, W. Rave and G. Fettweis, “Properties of the Intercarrier Interference due to Phase Noise in OFDM”, in *Proc. IEEE International conference on Communications,* Seoul, 2005.

[34] T. C. W. Schenk, R. W. V. Hofstad, E. R. Fledderus and P. F. M. Smulders, “Distribution of the ICI term in Phase Noise impaired OFDM systems”, *IEEE Transactions on Wireless Communications*, vol. 6, no. 4, pp. 1488 – 1500, 2007.

[35] D. Petrovic, W. Rave and G. Fettweis, “Effect of Phase Noise on OFDM Systems with and without PLL: Characterization and Compensation”, *IEEE Transactions on Communications,* vol. 55, no. 8, pp. 1607-1616, 2007.

[36] V. Syrjälä, M. Valkama, N. Tchamov and J. Rinne, “Phase Noise Modelling and Mitigation Techniques in OFDM Communications Systems”, in *Proc. Wireless Telecommunications Symposium,* pp. 1–7, 2009.

[37] U. Rohde and J. Whitaker, “*Communications Receivers: DSP, Software Radios, and Design”*, McGraw-Hill Professional, 3rd Edition, 2000.

[38] T. C.W. Schenk, X. J. Tao, P. F. M. Smulders and E. R. Fledderus, “Influence and Suppression of Phase Noise in Multi-Antenna OFDM” in *Proc. IEEE Vehicular Technology Conference (Fall),* pp. 1443-1447, Los Angeles, 2004.

[39] T. C. W. Schenk and X. J. Tao, “On the Influence of Phase Noise Induced ICI in MIMO OFDM Systems”, *IEEE Communications Letters,* vol. 9, no. 8, pp. 682-684, 2005.

[40] T. C. W. Schenk, “*RF Impairments in Multiple Antenna OFDM: Influence and Mitigation*”, PhD Dissertation, Technische Universiteit Eindhoven, ISBN-13: 978-90-386-1913-2, 2006.

[41] B. Razavi, “Design Considerations for Direct-Conversion Receivers”, *IEEE Transactions on Circuits and Systems – II: Analog and Digital Signal Processing,* vol. 44, no. 6, pp. 428-435, 1997.

[42] Y.-C. Liao and K.-C. Chen, “Multiuser Common Phase Error Estimation for Uplink OFDMA Communications”, in *Proc. Wireless Communications and Networking Conference*, Kowloon, China, 2007.

[43] V. Syrjälä and M. Valkama, “Flexible Adjacent Channel Interference and Phase Noise Suppression in Energy-Efficient OFDMA Receivers”, in *Proc. IEEE 17th CAMAD*, Barcelona, Spain, 2012.

[44] V. Syrjälä, “Accurate Characterization of Oscillator Phase-Noise Corrupted OFDMA-Link”, *IEEE Communications Letters*, vol. 17, no. 10, pp. 1968-1971, 2013.

[45] G. Sridharan and T. J. Link, “Performance Analysis of SC-FDMA and OFDMA in the Presence of Receiver Phase Noise” *IEEE Transactions on Communications*, vol. 60, no. 12, pp. 3876-3885, 2013.

[46] L. Samara, V. Syrjälä, R. Hamila and M. Valkama, “Phase Noise Mitigation in OFDMA Uplink”, in *Proc. 6th International Symposium on Communications, Control and Signal Processing*, Athens, Greece, 2014.

[47] D. D. Lin, R. A. Pacheco, T. J. Lim and D. Hatzinakos, “Joint estimation of Channel Response, Frequency Offset, and Phase Noise in OFDM”, *IEEE Transactions on Signal Processing*, vol. 54, no. 9, pp. 3542-3554, 2006.

[48] F. Munier, T. Eriksson and A. Svensson, “An ICI Reduction Scheme for OFDM System with Phase Noise over Fading Channels”, *IEEE Transactions on Communications*, vol. 56, no. 7, pp. 1119–1126, 2008.

[49] J. Tao, J. Wu and C. Xiao, “Estimation of Channel Transfer Function and Carrier Frequency Offset for OFDM Systems with Phase Noise”, *IEEE Transactions on Vehicular Technology*, vol. 58, no. 8, pp. 4380-4387, 2009.

[50] P. Rabiei, W. Namgoong and N. Al-Dhahir, “A Non-Iterative Technique for Phase Noise ICI Mitigation in Packet-Based OFDM Systems”, *IEEE Transactions on Signal Processing*, vol. 58, no. 11, pp. 5945–5950, 2010.

[51] F. Septier, Y. Delignon, A. M. Rivenq and C. Garnieret, “OFDM channel Estimation in the Presence of Phase Noise and Frequency Offset by Particle Filtering”, in *Proc. IEEE International Conference on Acoustics, Speech and Signal Processing*, Honolulu, HI, USA, 2007.

[52] O. H. Salim, A. A. Nasir, H. Mehrpouyan, W. Xiang, S. Durrani and R. A. Kennedy, “Channel, Phase Noise, and Frequency Offset in OFDM Systems: Joint Estimation, Data detection, and Hybrid Cramer-Rao Lower Bound”, *IEEE Transactions on Communications*, vol. 62, no. 9, pp. 3311–3325, 2014.

[53] D. D. Lin and T. J. Lim, “The Variational Inference Approach to Joint Data Detection and Phase Noise Estimation in OFDM”, *IEEE Transactions on Signal Processing*, vol. 55, no. 5, 2007.

[54] S. Stefanatos and A. K. Katsaggelos, “Joint Data Detection and Channel Tracking for OFDM Systems With Phase Noise” *IEEE Transactions On Signal Processing*, vol. 56, no. 9, pp. 4230-4243, 2008.

[55] Y. Gong and X. Hong, “OFDM Joint Data Detection and Phase Noise Cancellation for Constant Modulus Modulations”, *IEEE Transactions on Signal Processing*, vol. 57, no. 7, pp. 2864-2868, 2009.

[56] M. K. Lee, S. C. Lim and K. Yang, “Blind Compensation for Phase Noise in OFDM Systems over Constant Modulus Modulation”, *IEEE Transactions on Communications*, vol. 60, no. 3, pp. 620-625, 2012.

[57] S. Negusse, P. Zetterberg and P. Händel, “Phase-Noise Mitigation in OFDM by Best Match Trajectories”, *IEEE Transactions on Communications*, vol. 63, no. 5, pp. 1712 – 1725, 2015.

[58] R. Wang, H. Mehrpouyan, M. Tao and Y. Hua, “Channel Estimation, Carrier Recovery, and Data Detection in the Presence of Phase Noise in OFDM Relay Systems”, *IEEE Transactions on Wireless Communications*, vol. 15 no. 2, pp. 1186-1205, 2016.

[59] V. N. D. Nhat, T. B. T. Minh, C. T. Tan, V. N. Q. Baat and H. Nguyen-Le, “Joint Phase Noise and Doubly Selective Channel Estimation in Full-Duplex MIMO-OFDM Systems”, in *Proc. of The International Conference on Advanced Technologies for Communications*, pp: 412-417, 2016.

[60] T. J. Lee and Y. C. Ko. “Channel Estimation and Data Detection in the Presence of Phase Noise in MIMO-OFDM Systems with Independent Oscillators”, *IEEE Access*, DOI: 10.1109/ACCESS.2017.2709325, 2017.

[61] A. Ishaque, and A. Gerd, “Efficient MAP-based Estimation and Compensation of Phase Noise in MIMO-OFDM Receivers”, AEU-International Journal of Electronics and Communications, vol. 67, no. 12, pp. 1096-1106, 2013.

[62] A. O. Isikman, H. Mehrpouyan, A. A. Nasir, A. G. Amat and R. A. Kennedy, “Joint Phase Noise Estimation and Data Detection in Coded Multi-Input–Multi-Output Systems”, *IET Communications*, vol. 8, no. 7, pp. 981-989, 2014.

[63] G. Li and H. Liu, “Downlink Radio Resource Allocation for Multi-Cell OFDMA System”, *IEEE Transactions on Wireless Communications*, vol. 5, no. 12, pp. 3451-3459, 2006.

[64] K. Gunaseelan, R. Venkateswari and A. Kandaswamy, “A Novel Efficient Resource Allocation Algorithm for Multiuser OFDM Systems”, *IETE Technical Review*, vol. 25, no. 4, pp. 201-208, 2008.

[65] D. W. K. Ng, E. S. Lo and R. Schober, “Energy-Efficient Resource Allocation in OFDMA Systems with Large Numbers of Base Station Antennas”, *IEEE Transactions on Wireless Communications*, vol. 11, no. 9, 2012.

[66] B. Skalar, “*Digital Communications: Fundamentals and Applications*”, Pearson Education, Incorporation, Publication, Second edition, 2006.

[67] S. H. Muller and J. B. Huber, “A Comparison of Peak Power Reduction Schemes for OFDM”, in *Proc. IEEE Global Telecommunications Conference*, vol. 1, 1997.

[68] A. D. S. Jayalath, C. Tellambura and H. Wu, “Reduced Complexity PTS and New Phase Sequences for SLM to reduce PAP of an OFDM signal” in *Proc. IEEE 51st Vehicular Technology Conference*, Tokyo, Japan, pp. 1914-1917, 2000.

[69] S. H. Han and J. H. Lee, “An Overview of Peak-To-Average Power Ratio Reduction Techniques for Multicarrier Transmission”, *IEEE Wireless Communications*, vol. 12, no. 2, pp. 56-65, 2005.

[70] T. Jiang and Y. Wu, “An Overview: Peak-to-Average Power Ratio Reduction Techniques for OFDM Signals,” IEEE Transactions on Broadcasting, vol. 54, no. 2, pp. 257-268, 2008.

[71] F. Herzel and B. Razavi, “A Study of Oscillator Jitter Due to Supply and Substrate Noise”, *IEEE Transactions on Circuits and Systems-II*, vol. 46, no. 1, pp. 56–62, 1999.

[72] A. Demir, “Phase Noise and Timing Jitter in Oscillators with Colored-Noise Sources” *IEEE Transactions on Circuits and Systems—I: Fundamental Theory and Applications*, vol. 49, no. 12, pp. 1782-1791, 2002.

[73] A. Demir, “Computing Timing Jitter from Phase Noise Spectra for Oscillators and Phase-Locked Loops with White and 1/*f* Noise,” *IEEE Transactions on Circuits Systems I,* vol. 53, no. 9, pp. 1869 –1884, 2006.

[74] A. Hajimiri and T. Lee, “A General Theory of Phase Noise in Electrical Oscillators”, *IEEE Journal of Solid-State Circuits*, vol. 33, no. 2, pp. 179 –194, 1998.

[75] A. Demir, “Phase Noise in Oscillators: DAEs and Colored Noise Sources”, *Bell Laboratories*, DOI: ACM 1-58113-008-2/98/0011.

[76] A. Demir, A. Mehrotra and J. Roychowdhury, “Phase Noise in Oscillators: A Unifying Theory and Numerical Methods for Characterization,” *IEEE Transactions on Circuits Systems I, Fundaental, Theory & Applications*, vol. 47, no. 5, pp. 655 – 674, 2000.

[77] A. Chorti and M. Brookes, “A Spectral Model for RF Oscillators with Power-Law Phase Noise”, *IEEE Transactions on Circuits and Systems—I: Regular Papers*, vol. 53, no. 9, pp. 1989-1999, 2006.

[78] A. Hajimiri, “Noise in Phase Locked Loops”, in *Proc. Southwest Symposium on Mixed-Signal Design*, pp. 1-6, Austin, TX, USA, USA 2001.

[79] A. Mehrotra, “Noise Analysis of Phase-Locked Loops”, *IEEE Transactions on Circuits and Systems-I: Fundamental Theory and Applications*, vol. 49, no. 9, pp. 1309, 2002.

[80] A. P. Ghosh, W. Qin and A. Roitershtein, “Discrete-Time Ornstein-Uhlenbeck Process in a Stationary Dynamic Environment”, *Journal of Interdisciplinary Mathematics*, vol. 19, no. 1, pp. 1–35, 2016.

[81] W. Kester, “Converting Oscillator Phase Noise to Time Jitter”, *Tutorial MT-008-Analog Devices*, 2009.

[82] T. S. Rappaport, “*Wireless Communications: Principles and Practice*”, Prentice Hall PTR, Publication, Second Edition, 2001.

[83] L. Hanzo, M. Munster, B.J. Choi and T. Keller, "*OFDM and MC-CDMA for broadband multi-user communications, WLANs and broadcasting*", John Wiley & Sons, Publications, 2005.

[84] L. Tomba, "On the Effect of Wiener Phase Noise in OFDM Systems", *IEEE Transactions on Communications*, vol. 46, no. 5, pp. 580-583, 1998.

[85] P. Mathecken, T. Riihonen, S. Werner and R. Wichman, "Performance Analysis of OFDM with Wiener Phase Noise and Frequency Selective Fading Channel", *IEEE Transactions on Communications*, vol. 59, no. 5, pp. 1321, 2011.

[86] V. Syrjala, M. Valkama, Y. Zou, N. N. Tchamov and J. Rinne, "On OFDM Link Performance under Receiver Phase Noise with Arbitrary Spectral Shape", in *Proc. Wireless Communications and Networking Conference*, Cancun, Mexico, 2011

[87] M.R. Khanzadi, D. Kuylenstierna, A. Panahi, T. Eriksson, and H. Zirath, "Calculation of the Performance of Communication Systems from Measured Oscillator Phase Noise", *IEEE Transactions on Circuits Systems I, Regular Papers*, vol. 61, no. 5, pp. 1553-1565, 2013.

[88] S. H. Song, G. L. Chen and K. B. Letaief, "Localized or Interleaved? A Trade off between Diversity and CFO Interference in Multipath Channels" *IEEE Transactions on Wireless Communications*, vol. 10, no. 9, pp. 2829-2834, 2011.

[89] H. G. Myung, "Introduction to Single Carrier FDMA", in *Proc. 15th European Signal Processing Conference*, Poznan, Poland, 2007.

[90] M. Melood, A. Abdased, M. Ismail and R. Nordin, "PAPR Performance Comparison between Localized and Distributed-Based SC-FDMA Techniques" in *Proc. of World Cong. on Multimedia and Computer Science*, DOI: 02.WCMCS.2013.1.5, 2013

[91] J. Zhang, C. Huang, G. Liu and P. Zhang, "Comparison of the Link Level Performance between OFDMA and SC-FDMA", *First International Conference on Communications and Networking*, China, 2006.

[92] S. Zhou, G. B. Giannakis and A. Scaglione, "Long Codes for Generalized FH-OFDMA through Unknown Multipath Channels", *IEEE Transactions on Communications*, vol. 49, no. 4, pp. 721-733, 2001.

[93] S. Zhou, G. B. Giannakis and A. Swami, “Frequency-Hopped Generalized MC-CDMA for Multipath and Interference Suppression”, in *Proc. MILCOM Conference*, pp. 22-25, Los Angeles, CA, 2000.

[94] S. Plass and S. Kaiser, “MC-CDMA versus OFDMA in Cellular Environments”, in *Proc. 13th European IEEE Signal Processing Conference*, Antalya, Turkey 2005.

[95] A. Persson, T. Ottosson and E. G. Ström, “A Unified Analysis for Coded DS-CDMA with Equal-Gain Chip Combining in the Downlink of OFDM systems”, *IEEE Transactions on Communications,* vol. 53, no. 2, pp.289 – 298, 2005.

[96] Ye (G.) Li, “Pilot-Symbol-Aided Channel Estimation for OFDM in Wireless Systems”, *IEEE Transactions on Vehicular Technology*, vol. 49, no. 4, pp. 1207-1215, 2000.

[97] S. Coleri, M. Ergen, A. Puri and A. Bahai, “Channel Estimation Techniques based on Pilot Arrangement in OFDM Systems”, *IEEE Transactions on Broadcasting*, vol. 48, no. 3, pp. 223-229, 2002.

[98] Y. Shen, and E. Martinez, “Channel Estimation in OFDM Systems” *Free Scale Semi Conductor Application Note*, pp. 1-15, 2006.

[99] F. Wang, “*Pilot-Based Channel Estimation in OFDM System*”, Theses and Dissertations, The University of Toledo, 2011.

[100] S. H. Liao, M. H. Ho, R. Y. Yen, and H. Y. Liu, “Maximum-Likelihood vs. Least Squares Schemes for OFDM Channel Estimation using Techniques of Repeated Training Blocks”, *Journal of Applied Science and Engineering*, vol. 16, no. 4, pp. 385-394, 2013.

[101] M.-H. Hsieh and C.-H. We, “Channel Estimation for OFDM Systems Based on Comb-Type Pilot Arrangement in Frequency Selective Fading Channels”, *IEEE Transactions on Consumer Electronic,* vol. 44, no. 1, pp. 217-225, 1998.

[102] J. A. Nelder, R. Mead, “A Simplex Method for Function Minimization”, *The Computer Journal*, vol. 7, no. 4, pp. 308–313, 1965.

Bio-Data

Kamayani Shrivastav received her B.E. degree from Rajasthan University, India, from the Department of Electronics and Communication Engineering in 2002. She completed her M. Tech dissertation work in the area of “Turbo Coding for Wireless Communication Systems” from MNIT, Jaipur. She worked as an Assistant/ Associate Professor for 12 years and now is doing research work as a Ph.D. scholar at MNIT, Jaipur, India. Her research area comprises, Error Control Codes, MIMO-OFDM/A, Mobile and Wireless Communication Systems, and Mobile Ad-hoc and Sensor Network.